

Master's Programme in Geoengineering

Mechanical properties of recycled materials in non-load bearing wall structure

Anssi Luoma

Master's Thesis
2023

Author Anssi Luoma

Title of thesis Mechanical properties of recycled materials in non-load bearing wall structure

Programme Master's Programme in Geoengineering

Thesis supervisor Prof. Leena Korkiala-Tanttu

Thesis advisor(s) DSc. Anoosheh Iravanian, MSc. Henry Gustavsson

Collaborative partner Kiertomaa Oy

Date 29.12.2023

Number of pages 90+59

Language English

Abstract

The use of recycled materials is the key component of sustainable development in the construction industry. This study examines the suitability of recycled materials obtained from the Turku region for non-load bearing wall structure using both rammed earth and casting methods.

The traditional method of rammed earth involves methodically compacting damp natural soil inside a mould. The mould may be removed immediately after compacting the soil, leaving behind well-structured compacted earth. Casting technique was specifically studied focusing on precast interlocking concrete blocks. With these it is possible to create interlocking blocks that allow convenient and efficient construction. Using both techniques, the objective was to create an environmentally friendly construction material from recycled materials. The compressive strength is the most important property for both construction methods and the created construction material.

The materials used as binders in this research were bio-based fly ash and bottom ash, blast furnace slag and CEM III/B. Crushed concrete and quarry fines have been used as aggregates. Nominal quantities of cement have been utilized solely as an activator in the masses, constituting between 3,33-5,00% by weight of the dry mass.

Laboratory tests were conducted to assess the properties and suitability of recycled materials for specific construction methods. The study focused on the compressive strength of the materials, employing ultrasonic pulse velocity and unconfined compression tests. Freeze-thaw cycles were also examined for their impact on material properties. Six samples were tested for each set, with three undergoing freeze-thaw cycles and three undergoing immediate unconfined compression testing. The rammed earth method exhibited higher compressive strengths compared to the casting technique when utilizing recycled materials. After 28 days of curing, rammed earth samples achieved 3,1-18,1 MPa compressive strengths, while casting method samples varied from 0,8-11,2 MPa. Freeze-thaw cycles had minimal impact on rammed earth samples, and using Stora Enso fly ash as a binder increased the maximum compressive strength after freeze-thaw cycles. Conversely, casting method samples experienced an average 37% decrease in compressive strength when exposed to freeze-thaw cycles.

Using recycled materials, both precast and rammed earth methods are best suited to simple, non-load bearing structures that do not require high structural properties such as high compressive, tensile or shear strength. The main advantage of using recycled materials is the low carbon footprint compared to for example using traditional concrete.

Keywords rammed earth, precast interlocking concrete block, recycled materials, fly ash, bottom ash, blast furnace slag, crushed concrete, quarry fines, environmental impact

Tekijä Anssi Luoma

Työn nimi Kierrätysmateriaalien mekaaniset ominaisuudet ei-kantavassa muurirakenteessa

Koulutusohjelma Master's Programme in Geoen지니어ing

Vastuuopettaja/valvoja Prof. Leena Korkiala-Tanttu

Työn ohjaaja(t) TkT Anoosheh Iravanian, DI Henry Gustavsson

Yhteistyötaho Kiertomaa Oy

Päivämäärä 29.12.2023

Sivumäärä 90+59

Kieli Englanti

Tiivistelmä

Kierrätysmateriaalien käyttö on keskeinen osa kestävästä kehitystä rakennusallalla. Tässä tutkimuksessa tarkastellaan Turun seudulta saatujen kierrätysmateriaalien soveltuvuutta sulloin maan- sekä valumenetelmällä rakennetussa ei-kantavassa muurirakenteessa.

Perinteisessä sulloin maan menetelmässä kostea luonnonmaata tiivistetään muotin sisään. Muotti voidaan poistaa välittömästi maan tiivistämisen jälkeen, jolloin jäljelle jää tiivistetystä maasta muodostuva rakenne. Valumenetelmää tutkittiin keskittyen erityisesti esivalettuihin lukkiutuviin betonielementteihin. Niiden avulla voidaan valmistaa yhteen liitettäviä elementtejä, jotka mahdollistavat tehokkaan rakentamisen. Molempia tekniikoita käyttäen tavoitteena oli luoda kierrätysmateriaaleista ympäristöystävällinen rakennusmateriaali. Molempien rakennustapojen sekä luodun materiaalin tärkein ominaisuus on puristuslujuus.

Tässä tutkimuksessa sideaineina käytettiin biopohjaista lento- ja pohjatuhkaa, masuunikuonaa ja CEM III/B:tä. Kiviaineksena on käytetty betonimurskettä ja kivituhkaa. Sementtiä on käytetty pieninä määrinä massojen aktivaattorina, jolloin sen kokonaispitoisuus oli 3,33–5,00 massaprosenttia materiaalien kuivamassasta.

Kierrätysmateriaalien ominaisuuksia ja soveltuvuutta tutkittuihin rakennusmenetelmiin arvioitiin laboratoriokokeilla. Tutkimuksessa keskityttiin materiaalien puristuslujuuden määrittämiseen käyttämällä ultraäänipulsseja sekä yksiaksiaalista puristuskoea. Myös jäätymis-sulamissykliin vaikutusta materiaalien ominaisuuksiin tutkittiin. Kustakin sarjasta testattiin kuusi näytettä, joista kolme altistettiin jäätymis-sulamissykliin ja kolme testattiin ilman altistumista jäätymis-sulamissykleille. Kierrätysmateriaaleja käytettäessä sulloin maan menetelmällä saavutettiin korkeammat puristuslujuudet kuin valumenetelmällä. Kun sulloin maan näytteet olivat kovettuneet 28 päivää, niiden puristuslujuudet vaihtelivat 3,1–18,1 MPa:n välillä. Kun taas valumenetelmällä valmistettujen näytteiden puristuslujuudet vaihtelivat välillä 0,8–11,2 MPa. Jäätymis-sulamissykliin vaikutus sulloin maan tekniikalla valmistettuihin näytteisiin oli lähes merkityksetön ja Stora Enson lentotuhkaa käytettäessä, näytteiden maksimaalinen puristuslujuus oli korkeampi jäätymis-sulamissykliin jälkeen. Sitä vastoin valumenetelmällä valmistettujen näytteiden puristuslujuus laski keskimäärin 37 %, kun ne altistettiin jäätymis-sulamissykleille.

Kierrätysmateriaalien käyttö sekä valamis- että sulloin maan menetelmällä soveltuvat parhaiten yksinkertaisiin, ei-kantaviin rakenteisiin, jotka eivät vaadi korkeita rakenteellisia ominaisuuksia, kuten suurta puristus-, veto-, tai leikkauslujuutta. Kierrätysmateriaalien käytön suurin etu on niiden pieni hiilijalanjälki verrattuna esimerkiksi perinteiseen betoniin.

Avainsanat sulloin maa, rammed earth, precast interlocking concrete block, uusiomateriaalit, lentotuhka, pohjatuhka, betonimurske, kivituhka, ympäristövaikutus

Table of Contents

1	Introduction.....	9
2	Earth construction	11
2.1	History	11
2.2	Construction method of rammed earth technique	13
2.3	Properties of rammed earth	14
2.3.1	Strength	14
2.3.2	Freeze-thaw resistance	17
2.3.3	Environmental impact.....	18
2.4	Suitable materials for rammed earth method.....	20
3	Precast interlocking concrete blocks	24
3.1	History	24
3.2	Constructing method of precast interlocking concrete blocks	26
3.3	Properties of precast interlocking concrete blocks	28
3.4	Environmental impact.....	30
3.5	Suitable materials for precast interlocking concrete blocks.....	31
3.5.1	Case study (Attri et al., 2022).....	31
3.5.2	Case study (Uygunoglu et al., 2012).....	32
4	Researched materials and methods	35
4.1	Aggregate materials	35
4.1.1	Crushed concrete	37
4.1.2	Quarry fines	38
4.1.3	Mixture of quarry fines and crushed concrete	38
4.2	Binder materials	39
4.2.1	CEM I	39
4.2.2	Blast furnace slag.....	40
4.2.3	CEM III/B	40
4.2.4	Naantali bio-based fly ash and bottom ash.....	41
4.2.5	Stora Enso Varkaus bio-based fly ash	42
5	Laboratory tests	43
5.1	Water content	43
5.2	Sieving	43
5.3	Specific gravity.....	44
5.4	Modified Proctor test.....	45

5.5	pH-values.....	45
5.6	Preparing of test samples	45
5.6.1	Casting of the binder samples	46
5.6.2	Intensive compaction tester	47
5.6.3	VTT compaction hammer	50
5.6.4	Casting	52
5.7	Ultrasonic pulse velocity	53
5.8	Unconfined compression test.....	54
5.9	Freeze-thaw test	55
6	Results of laboratory tests	57
6.1	Index-tests	57
6.1.1	Water content	57
6.1.2	Sieving.....	57
6.1.3	Specific gravity.....	58
6.1.4	Modified Proctor test.....	60
6.1.5	pH-values.....	60
6.2	Ultrasonic pulse velocity	61
6.3	Unconfined compression test.....	63
6.3.1	Binder samples	63
6.3.2	ICT compacted samples.....	64
6.3.3	Samples made with VTT hammer (ramming)	66
6.3.4	Samples made by casting.....	68
7	Analysis of the research results	70
7.1	Relationship of UPV and UCS.....	70
7.2	Ramming vs. casting	73
7.3	Effects of freeze-thaw cycles.....	77
7.4	Comparison with previous research	78
7.5	Aggregates	80
7.6	Binders.....	80
8	Conclusions and recommendations for further research	83
	References	85
	Attachments	90

Preface

Over the past few years, Aalto University has been researching how to enhance the utilization of recycled materials in civil engineering. These studies have aimed to encourage the incorporation of recycled materials in construction projects and to promote the commercialization of such materials. The overarching objective is to establish carbon sinks in infrastructure through the effective use of recycled materials. Given the positive outcomes observed in prior research, there is an interest in expanding the studies to explore various construction methods and the effect of the freeze-thaw effect. This thesis has been commissioned by Kiertomaa Oy.

I would like to thank Professor Leena Korkiala-Tanttu for acquiring the topic for this thesis, and for providing guidance, and feedback throughout the process. Additionally, I extend my appreciation to advisors Anoosheh Iravanian and Henry Gustavsson for their advice and assistance. I would also like to thank the laboratory staff at the Department of Civil Engineering in Aalto University, for their assistance in conducting the laboratory experiments. I would also like to acknowledge Antti Kuosmanen, the Managing Director of Kiertomaa Oy, for his contributions.

A special acknowledgement is reserved for my wife, Sofia, whose encouragement, and support have been essential not only in this thesis but also in other aspects of my life.

Espoo 29.12.2023
Anssi Luoma

Symbols and abbreviations

Symbols

F	[kN]	Force, compressive and flexural
V	[m/s]	Velocity
L	[mm]	Length
T	[μ s]	Time
m-%	[%]	Dry mass percentage
s	[kPa]	Apparent cohesion
u_a	[kPa]	Pore air pressure
u_w	[kPa]	Pore water pressure
τ_u	[kPa]	Shear strength of PICB joint
τ_o	[kPa]	Shear strength at zero pre-compression stress
μ		Actual friction coefficient in joint interface
σ_n	[kPa]	Normal stress from pre-compression load
Vol-%	[%]	Volume percentage
E_{50}	[MPa]	Young's modulus

Abbreviations

BA	Bottom ash
BFS	Blast furnace slag
CC	Crushed concrete
CE	Circular economy
CEB	Compressed earth blocks
CEM I	Portlandcement, CEM I 42,5 R
CEM III/B	Blast furnace slag cement, CEM III/B 42,5 L – LH/SR
CSS	Crushed sandstone
CW	Concrete waste
FA	Fly ash
F-T	Freeze-thaw
ICT	Intensive compactor tester
ISSB	Interlocking stabilized soil block
MW	Marble waste
OWC	Optimal water content
PICB	Precast interlocking concrete block
RE	Rammed earth
SRE	Stabilized rammed earth
UCT	Unconfined compression test
UPV	Ultrasonic pulse velocity
VTT	Technical research centre of Finland
QF	Quarry fines

1 Introduction

Sustainable development and urbanization have historically constituted prominent research focal points. The imperative for heightened construction activities has surged in tandem with the escalating urban influx, thereby augmenting the requisition for construction materials to accommodate the burgeoning urban population through city expansion and densification. Simultaneously, the depletion of finite resources has precipitated the necessity for innovative alternatives to conventional materials. Consequently, the emergence of the circular economy is supplanting the erstwhile linear economic model, renowned for its inefficiencies and inherent inadequacies in addressing the exigencies of contemporary society.

The construction industry is by far the largest emitter of greenhouse gases worldwide. In addition, the construction industry is the largest consumer of virgin materials and fresh water. High-volume consumption of the concrete makes its main binder, ordinary Portland cement (OPC), contributes about 8 % to the carbon emissions of the world and uses about 3 % of the energy consumed in the world. (United Nations Environment Programme, 2020; Sivakrishna et al., 2020).

The primary objective of this research was to systemically assess and contrast the viability of recycled materials for the construction of wall structure, employing two distinctive methodologies: rammed earth and precast interlocking concrete blocks. The research of materials and construction methods was restricted to their suitability for non-load bearing wall structure. This investigation encompassed a comprehensive approach, combining a meticulous review of existing literature with a series of comprehensive laboratory experiments.

The core purpose of the laboratory experiments was to conduct a detailed analysis of the properties inherent in the recycled materials utilized within this study. This analytical process was aimed at meticulous formulation of an optimal recipe and construction procedure, specifically tailored for the subsequent construction phase of the wall. The binder and aggregate materials in this study are recycled, excluding cement. Since the focus in this thesis was to minimize the carbon footprint of the resulting structure, the amount of cement was kept as low as possible, representing only 3,33-5,00% of the mass of the final structure. Notably, the final structure comprises 95-96,7% recycled materials. Cement is utilized as an activator in the mixture to enhance reactivity, which is a crucial factor in material strengthening. In the context of non-load bearing wall structures, the load primarily comprises the self-weight of the structure. In Finnish conditions, the assumed maximum design load of the structure is influenced by variations in weather conditions, such as rainfall and freeze-thaw cycles, rather than the inherent weight of the structure. In addition, the study entailed an extensive review of pertinent literature, focusing on the operational methodologies, design principles, and fundamental physical phenomena associated with the utilization of rammed earth and precast interlocking concrete blocks in construction.

This research aligns closely with Kiertomaa Oy's visionary goals, as all the researched aggregates were exclusively sourced from their Saramäki site. The research considered various binding agents, including ashes derived from bio-based waste incineration and blast furnace slag produced during steel manufacturing. In this research the primary focus was on the

analysis of locally available binding agents within Turku region. In addition to these regional alternatives two other binding agents were also studied: bio-based fly ash from Stora Enso, Varkaus and environmentally sustainable CEM III/B which was included in the research as an only commercially available product.

2 Earth construction

Earth is one of the simplest construction materials and all earth buildings have the same basic constituent parts: soil from the ground and water. (Jaquin, 2012). This chapter is dedicated to comprehensive exploration of the construction methodologies and historical development of earth construction techniques, concentrating on rammed earth technique. It also entails an in-depth analysis of the physical determinants that influence the structural strength and long-term resilience of these earth building techniques. Additionally, the chapter explores the future potential of rammed earth technique as an ecologically sustainable construction technique.

When utilized as a construction material, soil is scientifically referred as loam. Loam is essentially a composite mixture encompassing clay, silt, sand, and occasionally larger aggregates like gravel or stones. In the context of handmade, unbaked bricks, the designations mud bricks or adobes are conventionally employed, while compressed, unbaked bricks are often referred to as soil blocks or compressed earth blocks (CEB). When this earth material is compacted within a formwork, it is denoted as rammed earth. (Minke, 2006).

2.1 History

Soil stands as one of the most ancient construction materials, and it remains prevalent, particularly in regions characterized by warm and arid climates, notably within developing nations. Building using subsoil is one of the oldest construction techniques, providing simple shelter using freely available material. Buildings made from soil are found in many parts of the world, in different forms, sometimes mixed with other traditional construction materials such as timber or stone, or with more modern inventions such as cement and steel. (Jaquin, 2012; Minke, 2006).

Earth construction techniques likely emerged independently in various regions of the world and disseminated as populations migrated. The advent of settled agriculture marked a pivotal moment in the evolution of permanent shelter construction, as it afforded the luxury of dedicating more time and effort to building the shelters. Notably, agriculture initially took root in fertile river valleys, where the presence of silt and clays offered exceptional raw materials for earth construction. In the early stages of earth construction, on-site methods like the rammed earth technique were employed. The transition to unit construction likely occurred subsequently, with the initial formation of units being accomplished by manual means, and later with the aid of formwork. These blocks, upon drying, became transportable, enabling the separation of material production from the construction site. This breakthrough facilitated the utilization of suitable earth sourced from the river valleys prone to flooding for the construction of buildings at elevated locations, mitigating the risk associated with flooding. (Jaquin et al., 2012).

Earth construction techniques have a history spanning over 9000 years. Remarkable findings, such as mud brick (adobe) houses dating back to 8000-6000 BC in Russian Turkestan, exemplify the enduring legacy of earth-based construction. In Assyria, foundations crafted with rammed earth technique, dating approximately to 5000 BC, serve as further testament

to the early utilization of earth as a construction material. This practice extended beyond residential structures, as earth played a pivotal role in constructing religious edifices in diverse ancient cultures. Notably, the vaults in the Temple of Ramses II in Gourn, Egypt, stands as a testament to the use of mud bricks, a construction method employed over 3200 years ago. Additionally, the citadel of Bam in Iran (figure 2.1), some portions of which are around 2500 years old, highlights the continued prominence of earth construction across different eras. Even the iconic Great Wall of China, dating back 4000 years, was initially constructed entirely from rammed earth, with subsequent layers of stones and bricks giving it the appearance of a stone wall. (Minke, 2006).



Figure 2.1 – The citadel of Bam (Iran) before and after 2003 earthquake (Langenbach, 2005).

Across Mexico, Central America, and South America, adobe buildings were prominent in various pre-Columbian cultures, while the rammed earth technique was known in many regions, sometimes introduced by Spanish conquerors. A 250-year-old rammed earth finca in the state of São Paulo, Brazil, provides a tangible example of this practice. (Minke, 2006).

During the Medieval period (13th to 17th centuries), earth continued to play a vital role in Central European construction. It served as infill in timber framed structures and was applied to straw roofs to enhance their fire resistance. In France the rammed earth technique increased from the 15th to the 19th centuries. Furthermore, Europe is home to the tallest house with solid earth walls, situated in Weilburg, Germany, and completed in 1828, showcasing the enduring durability of earth-based construction. All ceilings and the entire roof structure rest on solid rammed earth walls that are 750 mm thick at the bottom and 400 mm thick at the top floor and where the compressive force at the bottom of the wall reaches approximately 0,75 MPa. (Minke, 2006).

Structures constructed from earth as a construction material can be observed on a global scale, with some of these structures enduring for centuries. In recent times, the surging global environmental consciousness has rekindled interest in earth-based construction practices in Western countries. CEBs and Rammed earth has been explored as a potential alternative to concrete, however, it does not attain the same level of structural strength as a concrete. Efforts have been made to enhance the structural robustness of these techniques by introducing binders into the mixture, with cement and various ashes emerging as the most prevalent choices. For rammed earth this fortified form augmented with a binder, is

referred to as “stabilized rammed earth”. Today, both rammed earth and CEB construction is celebrated for its sustainability, natural beauty, and ability to regulate indoor temperatures. It has found a place in eco-friendly and sustainable building practices, and contemporary architects and builders continue to explore its potential for modern construction. (Kariyawasam et al., 2016).

2.2 Construction method of rammed earth technique

Rammed earth technology as a construction method entails the meticulous integration of soil with an appropriate quantity of water, followed by the compaction of the resulting mixture within a predefined mold. The precise amount of water introduced into the soil mass plays a significant role in the preparation process, exerting a profound influence on the final surface quality of the completed structure. This water content serves the dual purpose of rendering the paste amenable to compaction while also facilitating optimal material densification. In the unstabilized rammed soil technique, most of the water mixed into the mass evaporates after compaction. The residual water subsequently forms interstitial bonds between the individual soil particles, constituting a fundamental component for enhancing the structural integrity of the material compared to completely dry or fully saturated soil conditions. In the stabilized rammed earth technique, the binder interacts with the available water, initiating a hydraulic binding process that contributes to the structural cohesion of the material. (Jaquin, 2012).

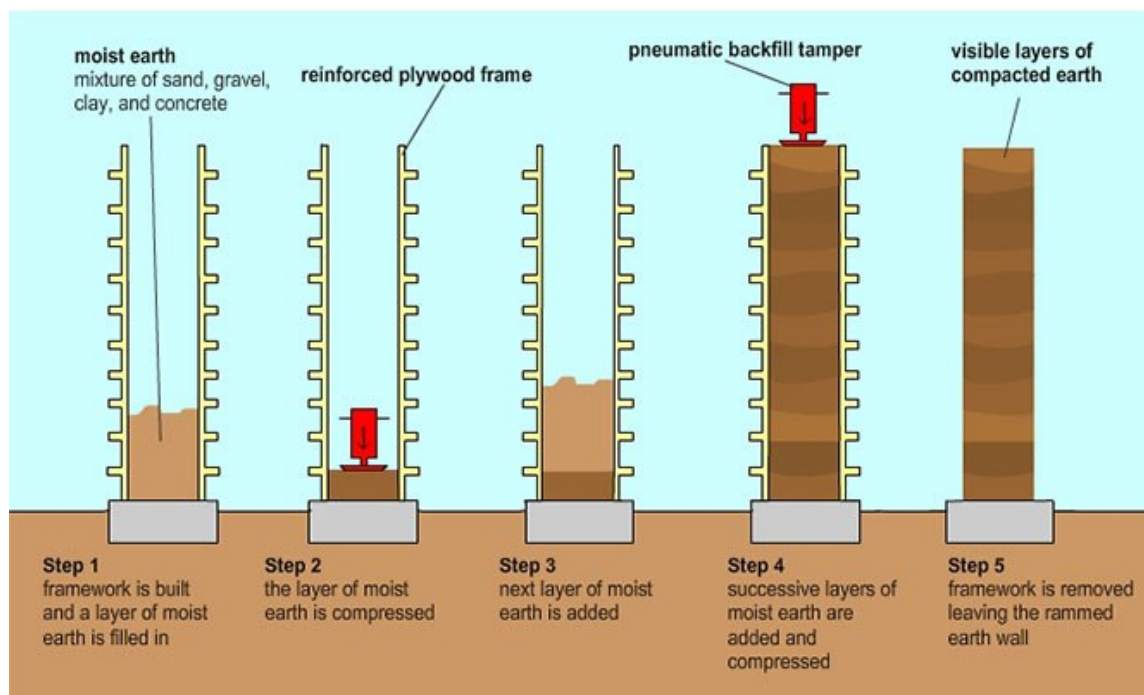


Figure 2.2 – Construction method of rammed earth technique (Greenspec, 2023).

The construction of an infilled soil wall entails the layer-by-layer filling of a mold with soil and water. Compaction can be achieved through manual or mechanical means. While a variety of manual compacting tools such as different types of compaction hammers are available, contemporary rammed earth technology often favors the application of pneumatic or electric hammers for soil compaction. In figure 2.2 is presented the main steps of rammed

earth construction technique. In general, the mold can be disassembled immediately upon molding completion, reducing the quantity of molding material required in comparison to casting processes. Apertures within rammed earth structures are established through the introduction of void forms or by the insertion of lintels between two distinct sections of rammed earth walls. (Jaquin, 2012).

It is demonstrated that density serves as a prominent predictor of attainable strength and longevity when constructing with rammed earth technique. To attain an optimal strength and durability, soil compaction should be carried out at the moisture content corresponding to the maximum dry density. This scenario results in the highest attainable structure density, which in turn leads to enhanced durability. However, the design of compressive strength for compacted soil poses a complex challenge, as it is contingent upon a various variable. These variables encompass the compaction method, density, porosity, grain size distribution of the aggregates, mineral structure of the aggregates, quantity and type of binder and moisture content of the mixture during compaction. (Narloch et al., 2020).

In the rammed earth construction method, the structural constituents comprise the aggregates, binder, and water. These constituents' attributes and quantities wield a substantial influence over the ultimate outcome's quality. Notably, the grain size distribution of the aggregates exerts a significant impact on the resultant wall's durability. It is imperative that the base material encompasses a range of 45-80 % gravel fraction (with grain size exceeding 2 mm), complemented by 10-30 % silt fraction and a 5-20 % clay fraction (with grain sizes less than 0,063 mm). The inclusion of a sufficiently ample gravel fraction within the aggregate material guarantees the attainment of adequate compressive strength, while the finer components assume a significant role in establishing the desired pore structure. (Walker et al., 2005).

2.3 Properties of rammed earth

One of the foremost attributes of rammed earth resides in the compressive strength of its structural composition. The compressive strength, along with various other characteristics of rammed earth, is substantially influenced by factors such as soil type, grain size distribution, density, water content, and the energy applied during the compaction process. The existing body of literature and empirical investigations collectively attest to the marked variability in the compressive strength of rammed earth. This variance is attributable in part to the fact that not all underlying phenomena dictating the strength of rammed earth have been comprehensively elucidated. Additionally, the employed operational techniques and compaction apparatus further contribute to the nuanced extent of achievable compressive strength. Furthermore, disparities in the type of soil utilized are evident across diverse studies, even when the grain size distribution is seemingly analogous. (Ávila et al., 2021).

2.3.1 Strength

The evaluation of the strength and behavior of rammed earth involves the application of soil mechanics theory. When employing the rammed earth technique, the structural strength is frequently assessed through the measurement of uniaxial compressive strength (UCS).

Numerous studies on the rammed earth technique highlight the influence of water content on the final strength of the structure. UCS achieved through the rammed earth technique typically span from 0,5 to 4 MPa. Conversely, the stabilized rammed earth technique can yield strengths exceeding 10 MPa even after 7 days of curing, depending on used aggregates and binders. For strength determination, test cylinders are prepared either in laboratory setting or on-site. These specimens typically undergo curing in the controlled conditions. The anticipated compressive strengths must account for the highest conceivable humidity levels to which the structure may be exposed under the design load. Given the substantial time required for the structure to attain its ultimate water content, it is estimated that the measured compressive strength of damp rammed earth structures is generally at least 50 % lower than the ultimate compressive strength achieved by the structure. Consequently, the completed structure experiences gradual strengthening, and strengths measured immediately post-construction may not provide a realistic presentation. (Jaquin et al., 2009; Walker et al., 2005).

The tensile strength of rammed earth registers at a mere 10 % of its compressive strength, approximately ranging from 0,1 to 0,35 MPa. Consequently, designing tensile stresses within the rammed earth structure is impractical. However, instances of fracture due to tensile stress, such as seismic events, are exceedingly rare. To mitigate the absence of tensile strength, reinforcement measures involve the incorporation of materials like straw or other natural fibers into the mass. (Ávila et al., 2021).

Similarly, shear strength in rammed earth structures is presumed to be negligible or close to zero. In accordance with the Mohr-Coulomb theory, soil shear strength is characterized by cohesion, friction angle, and normal stress. Consequently, the shear strength of rammed earth can be leveraged to deduce the material's friction angle and cohesion when the relationship between shear stress and normal stress is established. Determination of shear and normal stress typically involves conducting triaxial or radial shear tests. (Ávila et al., 2021).

Conventionally, soil classifications distinguish between cohesive and frictional soil types. In cohesive soil, intergranular friction is the primary cohesive force, while in frictional soil, cohesive forces are predominantly attributable to electrochemical particle forces within the structure. Beyond inherent cohesion, there exists apparent cohesion, a manifestation arising from pore water pressure within the structure. The terrestrial substrate comprises three phases, encompassing solid particles, along with air- and water-filled pores. The internal pressure of the soil is contingent upon the stress experienced by it. When the pore water pressure is negative, the strength of the soil increases, signifying the presence of apparent cohesion. (Jaquin et al., 2012).

The apparent cohesion in rammed earth is also contingent upon the pore structure of the material. In the context of an unsaturated soil, a negative pore water pressure operates within, facilitated by the coexistence of water and air. Surface tension between water and air fosters the forces within the pores, contributing to the observed apparent cohesion. The magnitude of apparent cohesion is contingent upon the water content, with suction pressure (i.e., negative pore water pressure) increasing as water content decreases. The internal suction pressure of infiltrated soil peaks between fully saturated soil and complete desiccation.

In the figure 2.1 is shown the simple model of an unsaturated soil structure. (Jaquin et al., 2012).

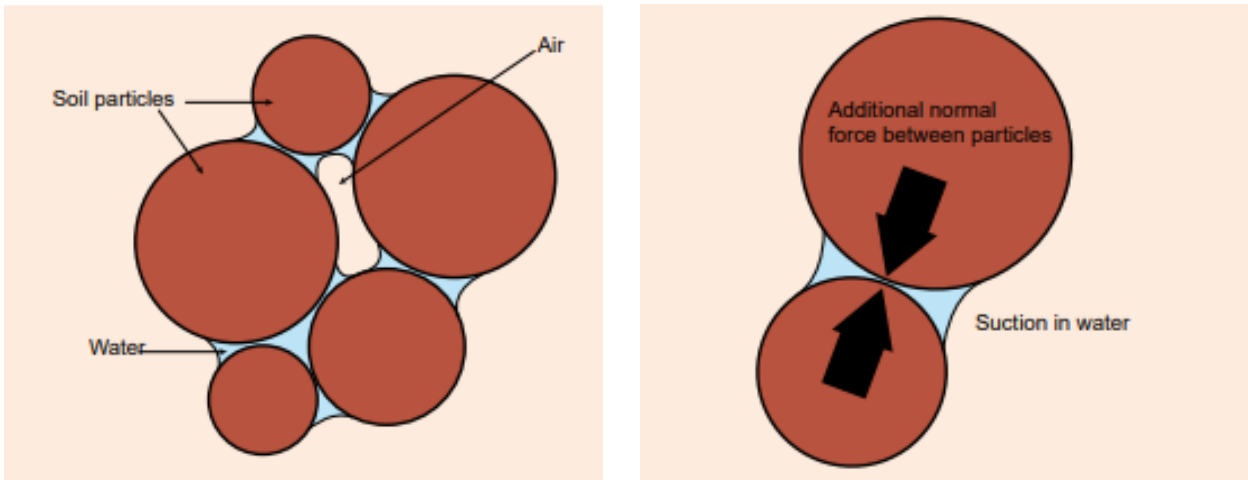


Figure 2.3. Simple model of an unsaturated soil. Water bridges are causing suction that strengthens the structure. (Jaquin et al. 2012).

From a geomechanical perspective, the configuration of rammed earth can be conceptualized as a consolidation of compacted soil. The desiccated rammed earth is characterized by partial saturation with water and air. In accordance with the principles of soil mechanics, the strength of partially water- and air-saturated soils encompasses a component arising from internal vacuum conditions, specifically suction forces. This internal force, denoted as apparent cohesion, is computable through the application of equation (2.1). (Jaquin et al., 2012).

$$s = u_a + u_w \quad (2.1)$$

where

s = apparent cohesion (suction force)

u_a = pore air pressure

u_w = pore water pressure

In earth construction, materials are formulated through a process of compaction, resulting in material of increased density. Techniques such as rammed earth and compressed earth blocks employ mechanical force on the soil mixture to attain this densification. The compaction process significantly influences the establishment of pore size distribution, consequently impacting the material's overall strength. (Jaquin et al., 2012).

Compaction is a procedural reduction in the volume of soil, leading to the expulsion of air from the pore spaces, thereby augmenting soil density and degree of saturation. The quantification of soil compaction is characterized by the measurement of dry density, representing the mass of solids per unit volume of the soil. This parameter is contingent upon the initial water content and the energy input during compaction, referred to as compaction energy. For a given soil and compaction energy, there exists an optimal water content (OWC)

at which maximum compaction and, consequently, dry density is achieved – an optimal state. (Jaquin et al., 2012).

Excessive soil moisture results in predominantly water-filled pores, wherein compaction energy essentially compresses the incompressible water phase. Consequently, a notable increase in density becomes unattainable. Various standardized laboratory tests, such as the standard or heavy Proctor tests and the vibrating-hammer test, are employed to ascertain the OWC for the compaction of a sample. The peak of the compaction curve of the sample denotes the OWC for the specific soil under consideration, utilizing the designated compaction procedure. (Jaquin et al., 2012).

The moisture content in stabilized rammed earth deviates slightly from that in unstabilized rammed earth. In concrete technology, it is widely acknowledged that an increase in the water-cement ratio leads to a decrease in the compressive strength of the material. In unstabilized rammed earth, attaining the highest compressive strength does not necessarily hinge on minimizing the water content to bind the material together but rather involves adhering to the OWC of the material or closely approximating it. Notably, investigations have often revealed higher OWC values for recycled materials compared to natural soils of analogous granularity. In the context of stabilized rammed earth, achieving the OWC of the material may present a conflict with both the OWC of the material and the objective of minimizing the water-cement ratio. It is observed that in a 5 % cementitious paste produced using the rammed earth technique, the highest compressive strengths were realized at water contents slightly lower than the OWC of the material. The incorporation of cement into a grouted mass introduces additional complexities, necessitating an examination of the OWC for the aggregate material contingent upon the type of aggregate used. (Beckett et al., 2014).

2.3.2 Freeze-thaw resistance

Freeze-thaw cycles are causing substantial effects, manifesting as infrastructure frost damage, ground surface heave, and intensified erosion in water-saturated soils. Frost heave encompasses phenomena arising from soil freezing or thawing. The primary mechanism behind frost heave involves the formation of ice lenses within the freezing zone, resulting in an expansion of the volume of the frozen soil. This volumetric increase is typically generating elevation in the surface of the soil structure, commonly known as frost heave. A soil material is classified as frost-susceptible when, under appropriate moisture and freezing conditions, substantial ice lens formation occurs. Ice lenses develop through the absorption of water from the molten soil at the frost line. Conversely, material that undergoes minimal ice lens formation during freezing is not frost-susceptible. In addition to the development of ice lenses, frost heave can also occur as in situ frost heave, which takes place when in situ pore water freezes. (Pylkkänen et al., 2015).

In the realm of construction, frost heave poses challenges to the stability of road and railway structures, as well as building foundations. Mitigation efforts involve constructing structures on layers impervious to frost. Clay and silt, characterized by a high content of fine aggregate, are highly frost-susceptible. Sands and gravels, with their coarse subsoil, generally exhibit resistance to frost heaving. The aggregate material of rammed earth is likely to be prone to frost heaving due to the presence of fines. The principal risk to rammed earth during pore water

freezing is an increase in water volume, leading to structural cracks and subsequent weakening. (Pylkkänen et al., 2015).

The impact of the freeze-thaw phenomenon on the durability of rammed earth has been the subject of various investigations. Bui et al. (2009) observed, over a 20-year duration, that erosion does not exhibit a direct correlation with time; instead, erosion rates were highest shortly after the construction phase. The non-linear trend may be attributed to the dissipation of compaction energy when in contact with the mold during the compaction process. This loss of compaction energy occurs due to friction between the material and the mold, resulting in weaker compaction at the edges of the mold surface and heightened erosion in those areas. Consequently, as the less compacted region succumbs to erosion, the remaining material erodes at a slower rate.

Contrastingly, Narloch and Woyciechowski (2020) observed that a wet sample exhibited significantly greater weight than a dry sample. Their freeze-thaw tests underscored the essential role of a binder, as the absence of it rendered the sample considerably more brittle. Additionally, the study emphasized the significance of water content in determining the longevity and durability of the structure. A vulnerability of the structure to damage increases when it becomes wet, as water absorption weakens cohesive forces, thereby diminishing strength. Rainfall contributes to surface erosion, while winter freezing exacerbates structural stress through repeated freeze-thaw cycles.

Aromaa (2021) investigated the influence of Finnish winter conditions on the noise barrier structure composed of recycled materials. In her study, test specimens were fabricated using the rammed earth technique, and the impact of freeze-thaw cycles and road salt on the structure was systematically examined. The primary findings indicate that the most pronounced effects of freeze-thaw cycles occur in situations where water accumulates on the structure's surface, leading to material erosion. The degradation of the structure is expedited by prior exposure to salt stress. Notably, the tests did not reveal any detrimental impact of freeze-thaw cycles on the compressive strength of the structure, provided that the structure remains free from contact with freezing water. Aromaa (2021) suggests that safeguarding the top and surface of a thawed soil structure from water and salt stress is crucial to prevent the structure from becoming friable due to freeze-thaw cycles. Recommended protective measures include the installation of a canopy on top of the structure, coupled with extended eaves, which would collectively shield both the top and wall surfaces of the structure.

2.3.3 Environmental impact

Sustainable development encompasses the dimensions of social, environmental, and economic sustainability. In the study of recycled materials, particular emphasis is placed on ecological sustainability, as the recycling of materials is strongly linked to the preservation of the carrying capacity of nature and ecosystems. The ecological potential of infilled soil, especially as an alternative to conventional concrete and bricks, renders it an intriguing focal point for research. Rammed earth, constructed through traditional methods, eliminates the need for material transportation over long distances and, optimally, utilizes soil already present at the site. The ready availability of essential raw materials concurrently diminishes

transport and procurement expenses. Furthermore, the production of rammed earth generates minimal waste. (Narloch et al., 2020).

The ecological performance of stabilized rammed earth is markedly influenced by the choice of binder, as the carbon footprint of the rammed earth and the energy expended in its manufacturing process are particularly contingent on the binder type. The consumption of energy and the emission of greenhouse gases exhibit a linear relationship with the cement content within the binder. Cement, commonly employed as a binder in rammed earth, is associated with substantial greenhouse gas emissions during its production. Consequently, the extent of cement utilization directly correlates with higher greenhouse gas emissions from the rammed earth. Nevertheless, in comparison to brick construction, the energy consumption associated with rammed earth is notably reduced. (Venkatarama Reddy et al., 2010).

The objective of incorporating a binder is to enhance control over material properties and achieve a material with predetermined characteristics. Traditionally, on-site soil has served as the primary material, but contemporary practices increasingly involve the use of pre-prepared soil engineered with an optimal blend of fines and coarser granules. Similarly, the conventional manual procedures for mixing and ramming are gradually being supplanted by mechanical methods. Consequently, these shifts contribute to increased construction efficiency, reduced reliance on manual labor, and heightened predictability and control over the final product's characteristics. However, it is noteworthy that the construction of rammed earth now necessitates a considerably higher energy input and results in elevated emissions. (Dahmen, 2015).

The production of recycled materials is typically characterized as having zero emissions, and it is commonly treated as emission-free at the point of use. Consequently, the emissions attributed to recycled materials only encompass those arising from their transportation. Utilizing recycled materials has the potential to mitigate carbon dioxide emissions during the construction phase of infrastructure projects. Frequently, the emissions associated with material installation are overlooked, yet they are comparatively minor compared to transportation emissions. Historically, the primary raw material for compacted earth, namely soil, has been sourced locally, resulting in minimal emissions associated with material transportation. However, the adoption of recycled materials introduces emissions related to transportation. Additionally, the preparation of stabilized soil into a structural element requires labor, and emissions from ramming activities should be duly estimated. Furthermore, the greenhouse gas emissions from stabilized soil are contingent on the type of binder employed. The use of cement-based binders substantially amplifies the carbon footprint, given the significant emissions generated during cement production. (Teittinen, 2019).

The environmental footprint of rammed earth constructed from renewable materials over its life cycle is primarily attributed to greenhouse gas emissions arising from transportation and the utilization of cementitious binders. When implemented judiciously, this approach exhibits the potential to serve as a durable solution necessitating minimal maintenance during usage and offering recyclability post-decommissioning. Nevertheless, a comprehensive life-cycle analysis of the landfill is imperative to ascertain the actual environmental impacts. (Aromaa 2021).

2.4 Suitable materials for rammed earth method

Initiating the identification of materials suitable for rammed earth technology often begins with the classification provided by geotechnical engineering, which offers a foundation based on known properties. Among these properties, the crucial determinant is the type of soil selected, defined by its granularity curve. Table 2.1 displays the soil types categorized by the range of grain sizes. The material designated for compaction must encompass a balance, featuring an ample quantity to enhance its strength, as well as a fine component facilitating pore formation through the generation of internal suction forces. The establishment of an appropriate pore structure, coupled with the utilization of the correct water content in the ramming operation, is imperative for the cohesion and attainment of the requisite density in the final structure. The spectrum of materials compatible with this methodology extends beyond purely compacted compositions, encompassing stabilized rammed earth where strength development is influenced by the physico-chemical properties of the soil. The associated phenomena deviate slightly from traditional rammed earth techniques. (Walker et al., 2005).

Table 2.1. Classification of soil according to particle size fractions (SFS-EN ISO 14688-1:2018). *RE-method=Rammed earth method.

Soil group	Particle size fractions	Range of particle sizes (mm)	Optimal composition for RE-method*
Coarse soil	Gravel	>2,0 to ≤63	45 to 80 m-%
	Sand	>0,063 to ≤2	
Fine soil	Silt	>0,002 to ≤0,063	10 to 30 m-%
	Clay	≤0,002	5 to 20 m-%

In contemporary applications, there exists a demand for exploring new uses for recyclable soil materials. When integrating rammed earth technology with recycled materials, the stabilized method proves more suitable for this purpose. Stabilization serves as an additional component augmenting the soil's quality, thereby providing a broader range of choices for aggregate materials in the context of the stabilized rammed earth method.

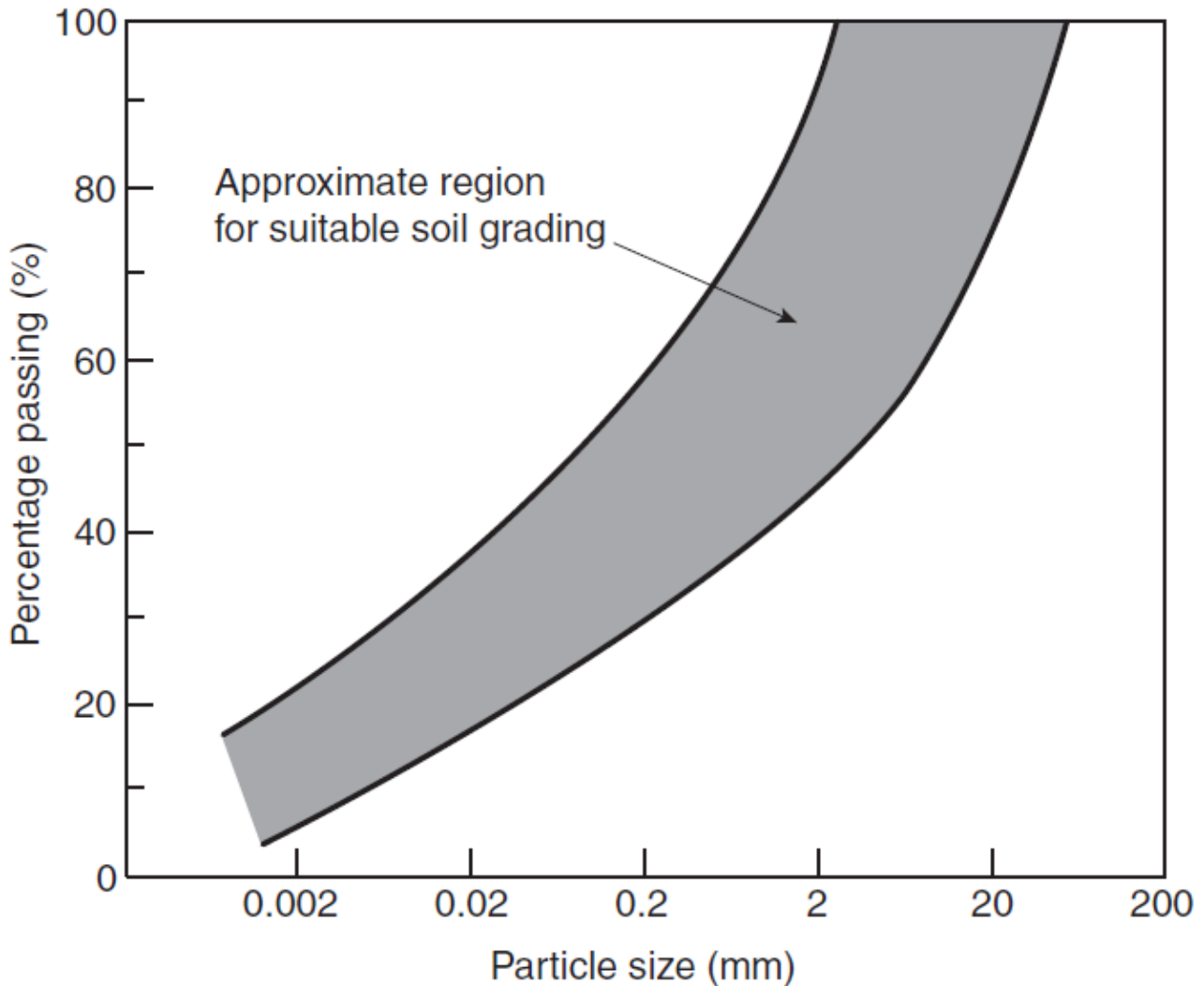


Figure 2.4. Indicative upper and lower limits of granularity curves for rammed earth materials. (Walker et al., 2005).

The robustness and modifiability of rammed earth are subject to alteration through the incorporation of diverse binding agents. Predominantly, cement, lime, and bitumen emerge as the most prevalent binders employed in rammed earth. The augmentation of these binders within rammed earth engenders what is conventionally referred to as stabilized rammed earth (SRE) or cement-stabilized rammed earth (CSRE). The enhanced strength exhibited by SRE in comparison to conventional rammed earth methodologies can be ascribed to the binding properties and chemical reactions, typically catalyzed by water. These chemical reactions facilitate the interparticle cohesion, thereby substantiating the term “bind” in binding the mass together. (Cristelo et al., 2012).

Arrigoni et al. (2018) investigated the applicability of crushed concrete in rammed earth techniques, an area with limited research despite the abundance of data of crushed concrete. The study focused on test specimens created using the stabilized rammed earth technique (SRE). Specimens comprised varying proportions (0 %, 25 %, 50 %, 75 % and 100 %) of crushed concrete mixed with natural soil. To optimize mass granularity, crushed concrete underwent sieving to eliminate particles smaller than 6 mm and larger than 19 mm. The

study employed cement as a binder, constituting 7 % of the dry matter weight. Additionally, sample cylinders were produced with crushed concrete as aggregate, exploring different binder combinations: CEM 7 %, CEM 10 %, and CEM 5 %/Fly ash 5 %. The experimental cylinders were manufactured at the optimal water content and subjected to a 28-day curing period under 96 % room humidity at an approximate temperature of 21 ° C before undergoing compression test.

The study results indicated that while an increased proportion of crushed concrete in the mixture often led to a reduction in compressive strength, a direct linear relationship between the proportion of crushed concrete and compressive strength was not observed. This phenomenon was attributed to the greater influence of grain size distribution and impurities in the crushed concrete on the compressive strength, which, in turn, negatively impacted the material and caused localized fractures during the compression test. Furthermore, the study identified a reduction in the carbon footprint of the structure with an increasing amount of added crushed concrete to the mass. The challenge emerged when incorporating crushed concrete led to a reduction in the compressive strength of the structure in comparison to natural aggregate, necessitating a higher cement content to compensate for this decline. The ultimate finding of the investigation determined that the optimal approach involves utilizing crushed concrete aggregate in conjunction with a binder comprising 5 % cement and 5 % fly ash of the total mass of the mixture. This composition resulted in a CO₂ savings compared to the use of solely natural aggregate and cement, all while maintaining the structural integrity of the material. (Arrigoni et al., 2018).

Limited research exists on the properties of quarry fines in relation to rammed earth technology. However, Zhang et al. (2019) investigated the mechanical properties of stabilized quarry fines, assessing its applicability in road construction. In this study, samples were prepared through two distinct methods. Mechanically compacted samples, measuring 50 mm in diameter and 100 mm in height, were compacted in three layers, achieving a density approximately 85 % of the theoretical maximum density. The optimal material mixtures were identified based on these samples. For the compression test, samples were prepared using a gyratory intensive compactor tester (ICT), achieving densities of up to 96 % of the theoretical maximum. The results from both sample preparation methods serve as indicative benchmarks for the rammed earth approach in this study. Subsequently, the experimental cylinders were cured at 100 % room humidity at 25° C for 7 and 28 days.

The study employed quarry fines as the aggregate with a grain size ranging from 0-4 mm. The binders utilized were Finnsementti's CEM I 42,5 R (CEM I), Ecolan Infra 80 (composed of coal ash, wood biomass, lime, and 20% cement) and fly ash from 100 % coal combustion residuals. CEM I was incorporated into samples representing 2,5 % and 4,5 % of the total mass. Ecolan 80 was introduced at concentrations of 4,5 % and 6,5 %. Fly ash was integrated into the samples at concentrations of 12 % and 15 %, with 1 % cement serving as the activator. The optimal water content was established at 9,26 %, and water-to-cement ratios were selected based on effective hydraulic reactions, aligning with recommendations from the American Concrete Institute, ranging between 0,4 to 0,6. (Zhang et al., 2019).

According to the investigation, stabilized quarry fine specimens, achieving a 96 % degree of compaction, satisfy pavement base and subbase requirements when appropriately designed

and constructed. In the case of cement-stabilized quarry fines, a minimum compaction level of 93 % is recommended for base layer applications. Ecolan 80 or fly ash with cement as stabilizers demonstrate improved performance with higher compaction. Increased cement content and reduced water-to-cement ratio result in stiffer materials. A similar situation was also observed on quarry fine specimens stabilized with the fly ash and activator, while strength of the Ecolan 80 correlates positively with higher stabilizer content and water-to-stabilizer ratio. Unconfined compression commonly exhibits combined extension and shear failures. Freeze-thaw cycles impact bearing capacity and deformation, with limited effects on cement-stabilized quarry fines. Ecolan 80 or fly ash-stabilized quarry fines display heightened frost susceptibility. Adjustments in gradation or an increase in compaction degree can fulfill high-strength requirements for base layers employing stabilized quarry fines. (Zhang et al., 2019).

3 Precast interlocking concrete blocks

This chapter elucidates an alternative approach to wall construction, namely, the utilization of precast interlocking concrete blocks (PICB). PICBs are modular, pre-manufactured building components that are designed to fit together seamlessly without the need for mortar or adhesive. These blocks are typically made from reinforced concrete but in this thesis the term is also used when utilizing recycled materials instead of traditional concrete. PICBs are known for their ease of assembly, durability and versatility and they are commonly used in various construction applications such as retaining walls, flood protection, erosion control. The goal was to research how well recycled materials would work in precast structure. In construction phase of the wall precasting-method would provide advantages over rammed earth method such as ease of construction, less material for molds and in general faster constructing.

PICBs were selected for possible wall construction method based on several key considerations. First, their interlocking design incorporates features that enable a secure fit, fostering the creation of a stable structure. This interlocking feature not only facilitates convenient assembly but also allows for efficient disassembly and reassembly. Second, the blocks exhibit a modular and precast nature. The term “precast” denotes their manufacture in a controlled environment, ensuring consistent quality and strength. The modularity of these blocks enables production in diverse sizes and shapes, rendering them easily transportable and conducive to on-site assembly. Furthermore, the characteristics of this project align well with the suitability of PICBs, given that the ultimate structure is a relatively low wall that does not have to bear additional loads beyond its own weight.

3.1 History

The historical origins of precast concrete can be traced back to ancient civilizations, notably the Romans, who employed a precursor to precast concrete in the construction of aqueducts, arches, and various structures. This early form of precast concrete involved the use of wooden molds to shape concrete elements at centralized locations, subsequently transporting them to construction sites. The Romans demonstrated pioneering ingenuity by introducing pozzolanic material, derived from volcanic ash in the town of Pozzuoli, into their concrete mixture. This innovative blend, incorporating lime and aggregate, marked a significant technological advancement. Employing a technique reminiscent of modern precasting methods, the Romans created intricate and durable structures, exemplified by the Pantheon temple and its precast concrete dome, constructed between 118 and 125 AD (in figure 3.1). Remarkably, the Pantheon’s dome remains the world’s largest unreinforced concrete dome to this day. (Delatte, 2001).

The utilization of these precast-like techniques in ancient Rome showcased the Romans’ engineering prowess and efficiency. The practice of casting elements offsite and transporting them for on-site assembly contributed to the durability of their structures. While the technological methodologies of ancient Rome differed from contemporary precasting methods, the underlying principles of creating standardized components in controlled environments

for subsequent assembly bear a resemblance to contemporary precast concrete practices. (Delatte, 2001).



Figure 3.1. The Pantheon dome – World's largest unreinforced concrete dome (Sean O'Neill, 2014).

For extended period, there was a lack of significant progress in concrete construction. However, in the 19th century, a pivotal advancement occurred with the development of Portland cement by Joseph Aspdin in 1824, marking a transformative milestone in concrete technology. Aspdin, a British bricklayer and stonemason, obtained a patent for Portland cement, which was named after its resemblance when set – a limestone variant found on the Isle of Portland in England. The patented process involved heating a mixture of limestone and clay to high temperatures, followed by grinding it into a fine powder, resulting in the creation of hydraulic cement. This invention represented a substantial improvement over preceding cementitious materials, rendering it more suitable for construction projects and swiftly gaining widespread adoption. Portland cement emerged as a cornerstone of the Industrial Revolution, supporting the growth of the construction industry. (Courland, 2011).

In the early 20th century, there was a notable upswing in experimentation with precast concrete. The refinement of the process highlighted its advantages, notably cost-effectiveness and efficiency. The historical roots of precast concrete extend to 1905 when John Brodie, an engineer from Liverpool, pioneered the development of precast panel buildings. This innovative concept introduced the principles of industrialization and standardization in construction. From 1948 until the late 1980s, state-organized construction initiatives produced numerous large-scale, prefabricated free-standing apartment blocks, relying on the

standardized precast concrete panels to facilitate fast-track construction methods. During that era, various other precast concrete elements, including blocks and pipes commenced production for diverse construction applications. (Hogan-O'Neill, 2021).

The introduction of concrete blocks to the public market traces back to the 1860s, marked by the development of several proprietary systems for precast concrete block manufacturing on the East Coast of the United States. However, the significant evolution occurred in the mid-20th century with the emergence of precast interlocking concrete blocks, exemplified by the ANSI modular standard block, commonly referred to as a concrete masonry unit. Initially utilized in infrastructure and civil engineering projects to address challenges associated with erosion control, flood protection, and retaining walls, these blocks gained popularity due to their innovative interlocking mechanisms, providing enhanced stability and simplified assembly without the necessity of mortar. The ensuing years witnessed continual refinement in both design and manufacturing processes. Engineers and manufacturers diversified interlocking systems, incorporating variations such as tongue-and-groove, pin-and-socket, or key-and-lock mechanisms to augment the stability and load-bearing capacity of the blocks. With ongoing enhancements in design and manufacturing, the applications of these blocks expanded beyond civil engineering and infrastructure to encompass landscaping, environmental protection, and diverse sectors, including military and security applications. (Fitz et al., 2016).

3.2 Constructing method of precast interlocking concrete blocks

In this study, emphasis is placed on formulating a working recipe that maximizes the utilization of recycled or by-product materials in using PICBs. However, PICBs are fabricated using a manufacturing process akin to other precast concrete structures, delineated into several key steps that are presented in the figure 3.1. The initial stage involves the preparation of a concrete mixture, encompassing cement, aggregates, water, and often additives or admixtures to optimize concrete properties, particularly strength and workability. The subsequent critical step involves the design of molds tailored to produce specific interlocking features, typically crafted from materials such as steel or rubber to achieve desired shapes and textures. Following mold preparation, a meticulously oiled mold receives the concrete mixture, with automated or semi-automated methods employed depending on block design and size. Vibrational or compaction processes eliminate air bubbles and ensure dense and homogeneous mixture. Upon mold filling, the blocks undergo a curing phase crucial for enhancing concrete strength and durability. Curing methods encompass controlled environments like curing chambers, wet curing, or steam curing, with on-site alternatives involving plastic coverings to retain moisture. Post-curing, demolding takes place, facilitated by well-designated interlocking features and pre-casting material oiling to prevent damage. Subsequent quality control inspections assess dimensional accuracy, strength, and surface finish, with non-conforming blocks subject to rejection. Depending on the intended use and aesthetic considerations, additional finishing processes, including texture addition, coloring, or surface treatments, may be applied to achieve the desired appearance. (Fibo Intercon, 2023).

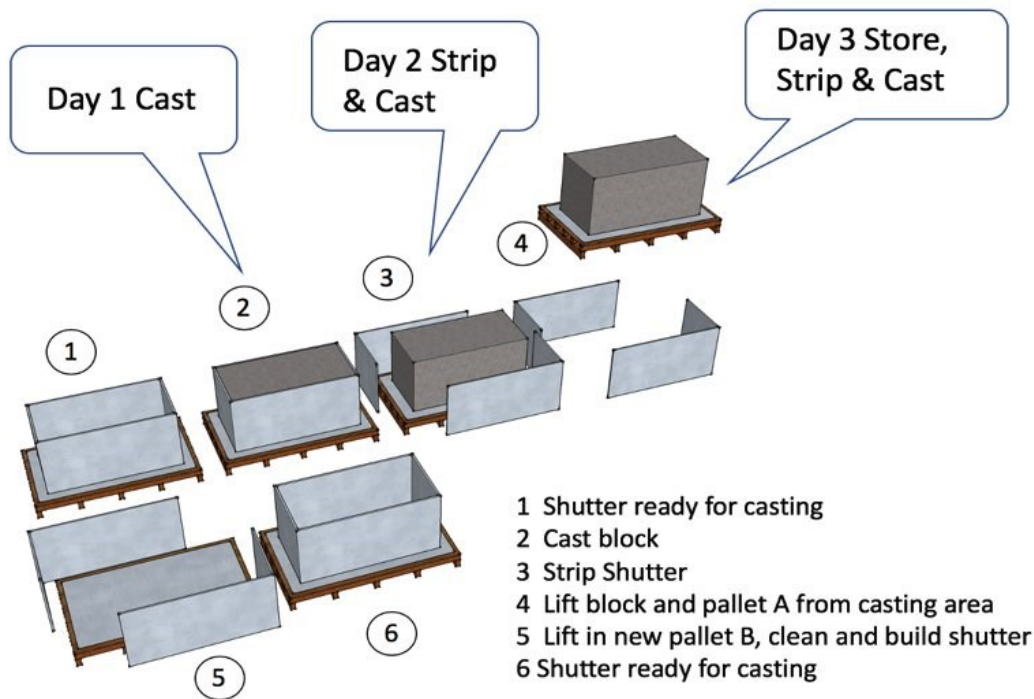


Figure 3.1. Principal stages in the manufacturing process of Precast Interlocking Concrete Blocks (PICB). (Fibo Intercon, 2023).

The primary emphasis and endeavor in the utilization of PICBs can be deemed to lie within the block manufacturing process. Depending on the specific design and structure erected using PICBs, the design phase may entail considerable effort. Nonetheless, the construction procedures involving PICBs are generally characterized by simplicity, although necessitating the use of heavy machinery (refer to figure 3.2) due to the substantial weight of individual blocks, typically ranging from 1 to 2,5 tons.



Figure 3.2. Installation of PICBs with reacher stacker. (Poundfield Precast, 2023).

The ensuing delineation outlines the fundamental steps for construction employing PICBs:

1. **Site preparation:** Ensure the construction site is properly prepared. The ground should be leveled, compacted, and free from debris. Proper drainage considerations are essential. Depending on the structure, site investigations, such as soundings, are usually needed.
2. **Foundation preparation:** Depending on the project, a concrete foundation may be required. Ensure that the foundation is structurally sound and provides a stable base for the interlocking blocks.
3. **Layout and design:** Plan the layout and design of the structure, considering the dimensions and specifications of the PICBs. Account for openings, corners, and other design elements. Make sure to ensure structures safety, by performing stability checks for failure by toppling, sliding, bearing and overall stability.
4. **Installation of base course:** Begin by laying the first course of interlocking blocks on the prepared foundation. Ensure that the blocks are leveled and aligned properly by using laser or string line.
5. **Interlocking mechanism:** Utilize the interlocking features of the blocks to secure them together, when installing upper layers. Use machinery such as light cranes, excavators or reach stackers to install heavy blocks on top of each other. Depending on the specific design, interlocking mechanisms may include tongue-and-groove, pin-and-socket, or key-and-lock systems.
6. **Alignment and leveling:** As you progress with the installation, regularly check for alignment and levelness. Adjust as necessary to maintain the structural integrity of the wall or structure. The joints of the blocks must be installed so that they overlap with each other.
7. **Capping and finishing:** Complete the structure by adding cap blocks or finishing elements to the top course. Ensure a secure and level capping to provide a finished appearance.
8. **Quality control:** Regularly inspect the installation for quality control. Check for alignment, levelness, and overall stability.
(Poundfield Precast, 2023; Tellus Design, 2017).

3.3 Properties of precast interlocking concrete blocks

One of the primary characteristics distinguishing PICBs lies in the compressive strength inherent in its structural composition. This compressive strength is significantly influenced by used materials, design, and manufacturing process of the PICB which is confirmed by the existing literature and empirical investigations about the PICBs. Concrete is distinguished by its elevated compressive strength but exhibits relatively low tensile strength, posing a specific challenge in applications involving unreinforced concrete. While PICBs can be reinforced, the prevailing practice involves the construction of unreinforced PICB structures. In such instances, the tensile strength of PICB is commonly approximated to be around 10% of its compressive strength. Therefore, PICBs are most appropriate for structures that primarily experience compressive forces and minimal tensile forces. (Aswad et al., 2022; Iskhakov et al., 2021).

The mechanical resistance properties of PICBs are assessed using methodologies employed in concrete engineering. Material properties can be evaluated through either direct or indirect approaches. Direct methods, exemplified by the unconfined compression test (UCT) test conforming to SFS-EN 12390-3:2019, offer the advantage of furnishing a precise and realistic assessment of the compressive strength of the specific specimen. However, a drawback is inherent, as the specimen undergoes irreversible damage during the test, limiting its applicability to a single examination. Consequently, this testing methodology necessitates the production of a substantial number of specimens to ensure a statistically significant sample size, and to mitigate potential distortions arising from manufacturing discrepancies. This approach presents challenges in assessing properties at distinct stages of the curing process, as each curing period necessitates the preparation of a distinct set of samples. (SFS-EN 12390-3, 2019).

An alternative testing approach involves the indirect method as per SFS-EN 13791, utilizing devices like the rebound hammer or ultrasonic pulse velocity. These instruments furnish measured values that, based on empirical findings, offer an approximation of the specimen's properties, notably its compressive strength. The merit of these methodologies lies in their non-destructive nature, enabling the examination of the same specimen at various intervals and facilitating the comparison of its property evolution over time. However, a drawback is evident as the indirect test does not yield an absolute value but provides solely an estimate of the tested specimen's properties. (Wallenius et al., 2023).

Another notable attribute of PICB is their capacity to assess the overall durability of a structure. Given that joints are typically not mortared, it becomes crucial to verify the ability of the structure to withstand applied shear forces when necessary. Alwathaf et al. (2005) delved into this aspect, conducting laboratory tests to determine the shear strength, and sliding resistance of PICB joints. The failure of mortarless masonry joints under shear, especially under moderate pre-compression levels, can be elucidated by the Coulomb friction law (Equation 3.1). This law establishes a linear correlation between the shear strength and the normal stress on the joint area.

$$\tau_u = \tau_0 + \mu \times \sigma_n \quad (3.1)$$

where

σ_n = normal stress from pre – compression load

τ_0 = shear strength at zero pre – compression stress or cohesion strength

μ = actual friction coefficient in joint interface

The linear Coulomb's law is applicable for normal stresses on less than 2 MPa. Under higher axial stresses, masonry walls may experience failure, even when the friction resistance in joints is not fully mobilized. This failure is attributed to the principal tensile stress reaching the diagonal tensile strength of the units, leading to unit cracking. In the context of mortarless interlocking masonry, it is imperative to establish failure criteria for joints under a combined normal shear envelop to comprehend the behavior of the interlocking system. Moreover, these criteria are essential for predicting joint failures and analyzing interlocking walls using finite element methods. (Alwathaf et al., 2005).

The findings of the study include successful utilization of the modified triplet test for small panels to assess the shear behavior of the mortarless interlocking masonry. Experimental tests revealed that the observed friction behavior for interlocking mortarless joints under different axial compressions aligns with the linear Coulomb-type failure criterion. The unevenness of the joints significantly impacts the shear strength of the system, as the area for friction resistance is not fully utilized. Tolerances provided in the interlocking keys for the ease of block assembly affect the transfer of shear stress between adjacent block units. In the pre-peak range of loads, the average shear-slip response of the interlocking masonry joint is characterized by insignificant slip at shear loads lower than 80% of the peak value. Conversely, in the post-peak range of loads, the joint exhibits a relatively constant shear load, representing a notable difference from conventional masonry systems. (Alwathaf et al., 2005).

3.4 Environmental impact

One of the key advantages of the precast interlocking blocks are its environmentally friendly properties. Using the precast interlocking concrete blocks, it is possible to use less material for the structure itself and for formwork. Traditional casted concrete structures often require extensive formwork and reinforcement to achieve necessary structural integrity. These materials are resource-intensive and often end up as construction waste. Interlocking concrete blocks on the other hand requires only minimal and reusable formwork as shown in the figure 3.3, and their design can reduce or eliminate the need for reinforcing steel. Interlocking concrete blocks can be designed for easy disassembly and reuse, making them more sustainable in long term. Traditional casted concrete structures are typically less adaptable to future changes or demolition and may result in significant waste. (Poundfield precast, 2023).



Figure 3.3. Reusable formwork for PICB in HSY Ämmässuo.

The construction sector demonstrates a notable capacity for assimilating substantial quantities of waste, repurposing it into valuable products. This exemplifies a broader trend within industrial ecology, aligning with the pursuit of a sustainable global future, wherein industrial by-products can serve as raw materials for diverse industries. The utilization of waste materials in concrete offers manifold advantages, encompassing the conservation of a country's mineral resources, including aggregates and sand obtained from natural sources. This approach contributes to environmental impact and positively effects the economy of the nation by mitigating the high costs associated with waste storage. Recognizing that natural

resources are not inexhaustible, the construction commitment of the construction industry to maintainability and sustainable enhancement primarily revolves around environmental protection through the adoption of alternative materials, innovative methodologies, and recycling practices. (Uygunoglu et al., 2012).

In concrete production, the substantial environmental advantages associated with PICB production stem from the utilization of environmentally friendly materials. Within concrete production it is estimated that approximately 70% of the carbon footprint is attributed to cement production. Therefore, the most significant environmental gains are realized through the incorporation of more environmentally sustainable binders capable of partially replacing cement. Furthermore, opting for recyclable aggregates, such as crushed concrete instead of natural aggregates, contributes to overall resource savings. (Winnefeld et al., 2022).

In contrast to larger precast concrete structures, the relatively compact dimensions of PICB enable on-site manufacturing, leading to a substantial reduction in emissions associated with material transportation and precast component delivery. Consequently, the primary objective of this thesis is to assess the feasibility of incorporating crushed concrete waste, quarry fines, as well as locally available ashes and slags in the production of PICBs. The study aims to elucidate the impact of these materials on the physical and mechanical properties of the resultant blocks.

3.5 Suitable materials for precast interlocking concrete blocks

PICBs have predominantly found application in construction using conventional concrete as the primary material. However, the contemporary emphasis on environmental considerations and material emissions in construction projects has underscored the increasing significance of utilizing environmentally friendly materials. Investigations into PICBs have primarily focused on their use in road or pavement construction when incorporating by-products from various industries or recycled materials. Nevertheless, it is posited that the construction methods and materials employed in the production of these paver blocks share similarities with techniques applicable to the manufacturing of PICBs for structural wall constructions.

3.5.1 Case study (Attri et al., 2022)

This chapter refers to case study conducted by Attri et al. (2022). Attri et al. (2022) investigated the applicability of recycled concrete aggregates in combination with stone crusher dust and silica dust in making zero-slump concrete for producing paver blocks. The investigation assesses the impact of integrating varying percentages (0 %, 15 %, 30 %, 45 %, 60 %, 75 %) of coarse recycled concrete aggregate. Subsequently, the viability of introducing different proportions (0 %, 20 %, 40 %, 60 %, 80 %, 100 %) of stone crusher dust and silica dust in conjunction with the optimal coarse recycled concrete aggregate content was examined. Ordinary Portland cement was used as a binding agent in this investigation.

Paver blocks samples were made by utilizing concrete mixer, vibrating table, and PVC molds. First materials were mixed to establish homogenous mixture. Within the wet mix, superplasticizer was incorporated. The zero-slump concrete mixture was then introduced into PVC molds in three layers and compacted using a vibrating table. The compacted molds were subsequently stacked for a 24-hour period at room temperature (27° C) to facilitate initial setting. After this curing period, the paver blocks were demolded and immersed in a curing tank for a duration of 28 days.

Attri et al. (2022) propose several recommendations for consideration in future research endeavors. Firstly, they advocate for the utilization of soaked coarse recycled concrete aggregates to enhance workability through the contribution to the hydration process via internal curing. However, caution is advised when removing dust and fines, as this may diminish the mixture's surface area, potentially resulting in gap-graded concrete despite reductions in water and cement demand. Furthermore, the authors suggest the application of specialized chemical admixtures to diminish water demand and improve workability in zero-slump concrete, targeting micro pores inherent in recycled concrete mixes. The mechanized or chemically facilitated removal of adhered mortar is recommended to enhance hardened properties, although at an increased cost. Exploring the incorporation of mineral admixtures, such as silica fumes, fly ash, or rice husk ash, is suggested to further augment the workability and microstructure of zero-slump concrete. Finally, the installation of specialized construction and demolition waste recycling plants within a 20 km radius of demolition sites is recommended to mitigate environmental impacts and alleviate the ecological and economic influences associated with transportation and crushing, accounting for 80 % of the overall impact.

The empirical observation of the investigation indicates that these industrial by-products have the capacity to substitute a substantial proportion of natural aggregates in the resulting concrete blocks without significantly altering their properties. While the incorporation of these wastes may not lead to a notable reduction in CO₂ emissions and primary energy consumption relative to cement alternatives, it holds promise in conserving a substantial quantity of natural resources. This approach also contributes to a potential reduction in the burden on land resources by redirecting waste streams away from landfills towards productive utilization.

3.5.2 Case study (Uygunoglu et al., 2012)

This chapter refers to an investigation conducted by Uygunoglu et al. (2012), where the impact of fly ash content and the replacement of sandstone aggregate with concrete and marble wastes on PICBs was explored. The study involved assessing properties of PICBs with varying fly ash replacement ratios for aggregate. Parameters such as compressive strength, tensile splitting strength, density, apparent porosity, water absorption by weight, abrasion resistance, alkali-silica- reaction, and freeze-thaw resistance were evaluated. Comparisons with PICBs using crushed sandstone revealed that the replacement of sandstone with concrete and marble waste led to diminished physical and mechanical properties. Conversely, the substitution of cement with fly ash (ranging from 10% to 20%) exhibited a notable enhancement in crucial properties of PICBs.

The binders utilized in their research comprised Ordinary Portland Cement (OPC), specifically the CEM I 42,5 R type, and fly ash sourced from Tunçbilek, Kütahya/Turkey Thermal Power. The aggregates were categorized into two primary groups: fine and coarse. The coarse aggregate constituted crushed limestone with a particle size of 6-12 mm and a specific gravity of 2,71. Fine aggregates included marble waste, concrete waste, and crushed sandstone, all with a particle size of 0-4 mm.

The study was structured into two segments. The first part aimed to ascertain the impact of fly ash content on the properties of blocks manufactured with different types of aggregates. The second part focused on evaluating the influence of aggregate type on the properties of PICBs. In total, 15 series of PICBs were produced, with fly ash content ranging from 0% to 40% through the replacement of OPC by weight. Three distinct types of fine aggregates, namely crushed sandstone, marble waste, and concrete waste, were employed. The PICB mix constituents were proportioned to achieve optimal particle packing and, consequently, minimal voids. A constant water-to-binder ratio of 0,45 was maintained across all series, with a binder content of 300 kg/m³. The aggregate composition of the specimens consisted of 40% coarse and 60% fine aggregate.

The influence of cement replacement with fly ash and the impact of various types of fine aggregates on the compressive strength of PICBs are illustrated in figure 3.4. A noticeable decline in compressive strength is observed with an increase in the fly ash replacement ratio in each series, particularly evident beyond 10%. Furthermore, the substitution of crushed sandstone (CSS) with concrete waste (CW) and marble waste (MW) leads to a reduction in the compressive strength of PICBs.

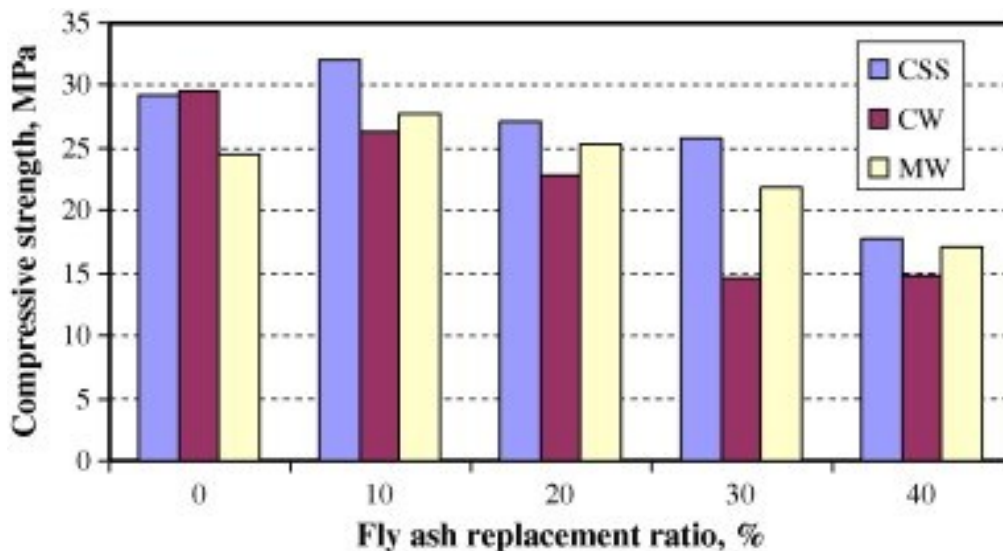


Figure 3.4. Comparison of compressive strength of PICB vs. fly ash content. CSS=Crushed sandstone, CW=Concrete waste, MW=Marble waste. (Uygunoglu et al.,2012).

The findings of the study elucidate various aspects concerning the properties of PICBs incorporating fly ash, waste marble, and waste concrete. A decline in compressive strength is observed with an escalating fly ash replacement ratio, and the substitution of CSS with CW and MW further contributes to this reduction in compressive strength. Despite this

decrease, the splitting tensile strength of PICBs with CSS, CW and MW remains satisfactory, meeting the strength standards within 28 days, except for a 40% fly ash replacement ratio. The presence of marble aggregate has a negligible impact on splitting tensile strength. Density experiences a decrease with higher fly ash replacement ratios, particularly in paving blocks with CW. Porosity and water absorption exhibit an upward trend with increasing fly ash replacement, with CW blocks displaying the highest values. Freeze-thaw durability witnesses a decrease with the rise in fly ash ratio, although blocks with CSS and MW fulfill strength requirements post the freeze-thaw cycle. In summary, the study concludes that the incorporation of waste marble and concrete results in PICBs of satisfactory quality, considering the observed variations in strength, density, porosity, water absorption, and freeze-thaw durability.

4 Researched materials and methods

Laboratory methodologies employed in the evaluation of materials utilized within this research are presented in this chapter. The aggregate materials subjected to testing encompassed crushed concrete, quarry fines of various grain sizes, and combination of crushed concrete and quarry fines. These aggregates were specifically sourced from the Saramäki division of Kiertomaa Oy, primarily owing to their abundant availability and compact geographical proximity. The binders studied in this thesis were fly- and bottom ashes from bio-based waste incineration and blast furnace slag from steel industry production, selected primarily from the Turku region.

4.1 Aggregate materials

Aggregate materials play a pivotal role in the context of sustainable construction practices. In both rammed earth and casting -methods, the aggregate component constitutes the predominant proportion of the construction material, typically encompassing approximately 75-85 dry mass percentage (m-%) with casting method and 70-80 m-% for rammed earth method (Mehta et al. 2014). Within the purview of this research, the aggregate content for various materials exhibited a range of 75-85 m-% concerning the dry material content. It is imperative to underscore the significance of this factor, particularly during the material selection process, as greatest transportation distances for aggregates result in escalated emissions attributable to the transportation phase.

To address this concern, a conscientious approach was adopted in the selection of aggregate materials for scrutiny in this study. Specifically, an emphasis was placed on sourcing materials that are readily available on-site, thereby minimizing the environmental footprint associated with material transportation. Furthermore, the materials of interest predominantly comprise quarry-derived by-product such as quarry fines and crushed concrete, obtained from construction waste, aligning with sustainable practices, and reducing the reliance on distant sources for construction aggregates (refer to figures 4.1 and 4.2).



Figure 4.1 Quarry fines (0-5 mm) at Kiertomaa Oy Saramäki site.



Figure 4.2. Crushed concrete (0-63 mm) at Kiertomaa Oy Saramäki site.

4.1.1 Crushed concrete

The crushed concrete, later referred to as CC, researched within this study originates from diverse demolished infrastructure projects within Turku region. Subsequently, this concrete material was transported from the demolition sites to Kiertomaa Oy, where it underwent fragmentation, resulting in particle sizes ranging from 0 to 63 mm. To ascertain its suitability for various applications, the CC was subjected to laboratory tests conducted in accordance with the standard SFS 5884:2022. These tests encompassed assessments of grain size distribution, specific gravity, impact resistance, constituent classification, and compressive strength.

The compressive strength of the CC samples made with ICT were on average 0,81 MPa after 7 days and 0,98 MPa after 28 days. Based on the outcomes of these examinations, the crushed concrete material scrutinized in this study was classified as class II. Summarized table of the unfloating material content of the CC is presented in table 4.1 and in figure 4.3 is depicted the material. The amount of floating materials measured from the material was 7,2 cm³/kg. For comprehensive details of the CC and the precise parameters of the laboratory tests, reference can be made to attachment 1, which elucidates the laboratory tests performed on the CC commissioned by Kiertomaa Oy in alignment with national established quality control system. Deviating from the results in attachment 1, the specific gravity was determined again at the Aalto University laboratory, resulting in 2,62 g/cm³.

Table 4.1. Material content of the crushed concrete in particle size 4-63 mm. (Kiertomaa Oy, 2023).

Unfloating materials	[m-%]
Concrete (including mortar)	89,0
Aggregates	8,9
Bricks, tiles	2,2
Bituminous materials	0,0
Glass	0,0
Other	0,2



Figure 4.3. Crushed concrete 0–63 mm.

4.1.2 Quarry fines

Quarry fines, later referred to as QF, investigated in this study originates from the Saramäki site of Kiertomaa Oy. Kiertomaa Oy is engaged in the production of crushed rock of various grain sizes, primarily obtained from their on-site quarrying operations. An incidental outcome of the quarrying process is the production of finer aggregate known as QF, characterized by a higher fines content. This attribute often renders it more intricate to identify a commercial application for QF, in contrast to coarser crushed rock, for example. Kiertomaa Oy has conducted laboratory assessments on the crushed rock according to standard SFS-EN 13242+A1, with detailed results elucidated in attachment 2. Specific gravity was determined also at the Aalto University laboratory, and the result was confirmed to be 2,71 g/cm³. Based on the findings presented in the attachment 2, the geological composition of the quarried rock is identified as quartz syenite. The QF examined in this study exhibit grain sizes ranging from 0-3 mm, 0-5 mm, and 0-8 mm. Summarized properties of the mineral composition of the QF is presented in the table 4.2 and in figure 4.4 is depicted the material with gradings of 0-8 mm and 0-3 mm.

Table 4.2. Mineral composition of the quarry fines. Vol-%=Volume percentage. (Kiertomaa Oy, 2023).

Mineral	Vol-%	Grain size (mm)
Potassium feldspar	61	0,5-12,0
Quartz	16	<0,1-6,0
Biotite	10	<0,1-3,0
Plagioclase	8	0,3-5,0
Other minerals	4	<0,1-4,0



Figure 4.4. Quarry fines. 0-8 mm on the left and 0-3 mm on the right.

4.1.3 Mixture of quarry fines and crushed concrete

In addition to utilizing exclusively crushed concrete and quarry fines, a mixture of these materials was also incorporated into the study. The selection of this combination was methodically undertaken to align the aggregate gradation with the optimal gradation curve conventionally employed within the rammed earth construction technique. Specifically, the mixture

was composed of 0-3 mm quarry fines and crushed concrete, with each constituent contributing equally at a 50 % ratio. Elucidation of the optimal gradation curve is provided within chapter 2.4.

4.2 Binder materials

In both casting and reinforced rammed earth construction technique, the necessity of a binding agent in conjunction with the aggregate, becomes apparent. Within the framework of this study, the selection of binding agents has been underpinned by a commitment to environmental conscientiousness. Furthermore, this investigation has diligently considered the ecological footprint arising from the conveyance of these binding agents, thereby initially focusing on materials procured from the south-western region of Finland for analysis. As the research evolved, and supported by the initial findings, a deliberate expansion of the study's scope transpired. This expansion encompassed the inclusion of binding agents from geographically more distant sources, with an emphasis on the incorporation of environmentally sustainable blast furnace slag cement produced within the commercial steel industry, CEM III/B. In accordance with the delineated criteria, the materials designated for scrutiny encompassed blast furnace slag sourced from the former Koverhar steelworks in Hanko, bio-based fly ash and bottom ash originating from the Naantali power plant. Subsequently, the study's purview was augmented to encompass bio-based fly ash derived from Stora Enso's Varkaus power plant, along with the inclusion of CEM III/B obtained from Finnsementti, which broadened the spectrum of materials under investigation.

Ashes and slags originating from the steel industry typically necessitate the incorporation of an activator to serve as binding agents, primarily due to the inherently sluggish hydration reactions involved (Alarache et al., 2016; Solismaa et al., 2021). The activator deployed in this study was FinnSementti's class I cement, CEM I, characterized by a clinker content ranging from 95-100 %. The fundamental objective underlying this selection was to employ the purest attainable form of cement as the activator, thus facilitating the precise determination of substance concentrations. Drawing from a comprehensive investigation conducted by Kasper Holopainen (2022), the proportions of binding agents were delineated allocating 20 % of the binder composition to CEM I, while the remaining 80 % was allocated to various ashes or slags. The sole exception to this framework was encountered in the case of CEM III/B, where the binder composition exclusively comprised CEM III/B.

The binder's cement content was deliberately minimized to mitigate the environmental impact associated with its production. On a global scale, it has been estimated that cement production contributes to approximately 7 % of the annual anthropogenic greenhouse gas emissions (Miller et al., 2021). Nonetheless, prior investigations have indicated that recycled materials may encounter challenges in attaining the requisite strength when employed in conjunction with reduced cement quantities (Kasper Holopainen, 2022).

4.2.1 CEM I

Finnsementti's "Ykkössementti" is a portlandcement, denoted as CEM I. It is served as the activator for the ashes and blast furnace slag. CEM I adheres to the specifications outlined

in SFS-EN 197-1, boasting a purity range of 95-100 % cement content. In accordance with environmental considerations, a concerted effort was made to limit the CEM I content in the research, while ensuring that the final product's characteristics were not compromised using excessively reduced cement. The cement proportion in the binder was set at 20 %, and it varied between 3,33-5,00 % of the total dry mass of the material, contingent upon the binder type and its inherent properties. More detailed properties of CEM I are shown in the technical data sheet from FinnSementti in the attachment 3.

4.2.2 Blast furnace slag

The blast furnace slag, later referred to as Hanko BFS, investigated in this thesis, was procured from the site of the former Koverhar steelworks in Hanko (refer to figure 4.5). The Koverhar facility ceased operations in 2012, and since then, the slag has been stored in expansive heaps within the premises of the former plant, exposed to the vagaries of the elements. In preparation for testing as a binder, samples of the slag underwent a controlled oven-drying process lasting 24 hours, followed by subsequent sieving through a 0,25 mm mesh.

It is worth noting that blast furnace slag is recognized for its sluggish hydration process, wherein a higher proportion of slag within the binder is correlated with decelerated hydration process (Schuldyakov et al., 2016).



Figure 4.5. Sieved blast furnace slag from Koverhar steel factory, Hanko.

4.2.3 CEM III/B

The sole commercial binder subject to investigation in this thesis is “Kolmosbertta” by FinnSementti, specified as CEM III/B (refer to figure 4.6). In conformity with the standards established by SFS-EN 197-1, CEM III/B is expected to comprise a range of 66-80 % of steel industry blast furnace slag and 20-34 % of pure cement clinker. In this instance, the composition of CEM III/B comprised 30% cement clinker and 70% blast furnace slag, which renders CEM III/B an exceptionally eco-friendly alternative among binders, particularly regarding carbon emissions. The elevated proportion of steel industry slag within the product's composition attributes it with a protracted hydration process, while currently mitigating

heat generation, ultimately culminating in the attainment of robust final strength characteristics. More detailed properties of CEM III/B are shown in the technical data sheet from FinnSementti in the attachment 4.



Figure 4.6. CEM III/B from FinnSementti.

4.2.4 Naantali bio-based fly ash and bottom ash

Due to its proximate location, viability of fly ash and bottom ash produced by the Naantali power plant was assessed as binding agents. Naantali power plant is operated by Turun Seudun Energiantuotanto (TSET) Oy. The ashes from Naantali power plant are later referred to as Naantali FA (fly ash) and Naantali BA (bottom ash) and they are depicted in the figure 4.7. Naantali power plant is primarily engaged in the generation of electricity, district heating, and process steam, with a notable transition to biofuel as its principal energy source since 2017. Consequently, the ashes subjected to examination in this research originate as by-products of this biofuel utilization. A substantial proportion of the biofuel feedstock, such as wood chips and bark, is sourced from the immediate vicinity of the plant. The ashes utilized in this study were supplied by TSET and emanate from the multi-fuel unit (NA4) at the Naantali power plant. Attachment 5 presents the outcomes of the laboratory assessments pertaining to their suitability for both earth construction and landfill disposal. (Turun Seudun Energiantuotanto Oy, 2023).



Figure 4.7. Naantali bio-based bottom ash (left) and Naantali bio-based fly ash (right).

4.2.5 Stora Enso Varkaus bio-based fly ash

The selection of bio-based fly ash from Stora Enso's Varkaus facility as an additional binder material stemmed from preliminary findings indicating the unsuitability of Naantali FA for the intended purpose. This bio-based fly ash is later referred to as Stora Enso FA (refer to figure 4.8). Furthermore, on-going research conducted by Wayu (2023) at Aalto University, had reported highly promising outcomes from preliminary laboratory assessments of Stora Enso FA. Stora Enso FA source originates from boiler K6 at the Varkaus plant, characterized as a circulation boiler with a heat output of 150 MW and an efficiency rate of 88 %. Its primary fuel source encompasses bark derived from the factory and external sawmills, as well as various wood-based fuels, including sawdust, forest chips, and wood waste categories A and B. Additionally, the boiler has the capacity to combust peat, sewage sludge, and coal as auxiliary fuels. During its operation as a parallel incineration plant, it also disposes of waste and recycled fuels subject to waste incineration regulations, including aluminum-free plastic from the fiberization process, separately collected plastic and fiber fractions, and recycled wood categorized under AB. Heavy fuel oil is employed as both starting and auxiliary fuel in this context. Attachment 6 presents the outcomes of the laboratory assessments pertaining to their suitability for both earth construction and landfill disposal. (Stora Enso, 2023).

Although the use of this material may transcend the bounds of immediate regional sourcing, it is nevertheless prudent to contemplate broadening the geographical scope, especially in the context of binder research. Favorable material attributes often enable reductions in binder quantities, thereby diminishing the impact of material transportation emission on the overall project. Furthermore, it is important to note that the transportation of binder materials is associated with a relatively modest level of CO₂-emissions when compared to the emissions stemming from the actual manufacturing process of the binders. Although not an optimal scenario, this could be considered a reasonable trade-off, especially if the binder demonstrates commendable performance characteristics. (Autiola, 2023).

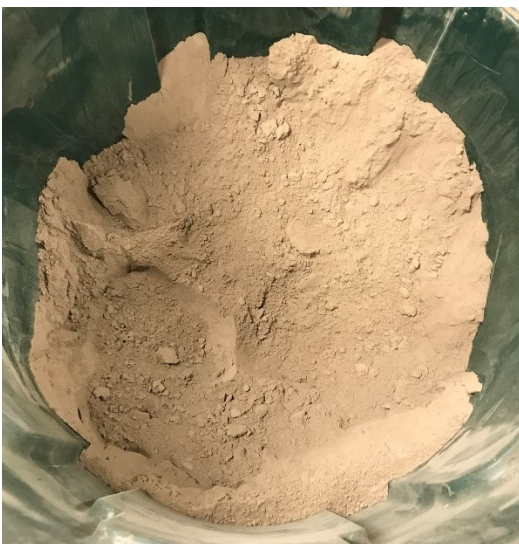


Figure 4.8. Stora Enso bio-based fly ash from Varkaus.

5 Laboratory tests

This chapter serves to provide an overview of the laboratory research methods applied for the materials under examination. The laboratory investigations encompassed a comprehensive analysis of seven distinct recycled materials, comprising two aggregate materials, quarry fines and crushed concrete, with a specific division of quarry fines into three varying grain sizes, and five diverse binders. A more comprehensive elucidation of these recycled materials is provided in the preceding chapter.

The initial phase of the experimentation involved the execution of what are referred to as “index tests”. These index tests were instrumental in elucidating the fundamental characteristics of the materials under scrutiny, encompassing aspects such as grain size distribution, moisture content, and density. Testing matrix for index tests is presented in the table 5.1.

Table 5.1. Testing matrix for index tests of the materials.

Material	Tests performed
Aggregates:	
QF 0-3 mm	Water content, sieving, specific gravity, modified Proctor
QF 0-5 mm	Water content, sieving, specific gravity, modified Proctor
QF 0-8 mm	Water content, sieving, specific gravity, modified Proctor
CC	Water content, sieving, specific gravity, modified Proctor, pH
Binders:	
Naantali FA	Water content, specific gravity, pH
Naantali BA	Water content, specific gravity, pH
Hanko BFS	Water content, specific gravity, pH
Stora Enso FA	Water content, specific gravity, pH

5.1 Water content

The laboratory experiments commenced with the determination of the water content for all materials. This initial step holds particular significance as the laboratory tests necessitated an examination of completely dried materials. This approach was adopted to ensure precise control over the water quantity employed in each experimental recipe. In practical field applications, materials tend to absorb moisture, especially when subjected to storage. It is imperative to consistently consider this moisture absorption, as it directly impacts the accurate addition of water to the materials, crucial for achieving the optimal recipe.

5.2 Sieving

The determination of the grain size curve for the aggregate materials holds considerable significance. The grain size curve serves as a key tool for categorizing the material and, to a significant degree, predicting its mechanical characteristics. To establish the grain size curves, the dried samples underwent sieving following the guidelines of standard SFS-EN

933-1. This process employed a sieve set encompassing a range from 0,063 mm to 30 mm sieve sizes.

5.3 Specific gravity

Specific gravity for each aggregate and binder was conducted with pycnometer test. The test adhered to the guidelines outlined in standard SFS-EN ISO 17892-3. Initially, the samples were dried in the oven for 24 hours and then subjected to sieving using a 2 mm mesh sieve to achieve a finely powdered consistency. Following this, the pycnometers used in the experiment were weighed to establish the dry mass of the entire material under investigation. Approximately 15 to 30 mm uniform layers of each sample was used in each pycnometer. Two samples were extracted from each material, and the resulting average was employed to ascertain the specific gravity of the material.

After the dry mass determination, the pycnometers were filled with distilled water and introduced into a vacuum desiccator, refer to figure 5.1, wherein the removal of excess air was accomplished over a duration of approximately 30-45 minutes. Subsequently, the pycnometers were immersed to the level of upper surface of the capillary tube in a temperature-controlled water bath for one hour, ensuring precise temperature control of the samples. Temperature of the water bath was kept around 20-23 °C. Finally, the caps of the pycnometers were securely sealed, the outer surfaces of the pycnometers were meticulously dried, and the samples were weighed. With this data the solid densities of each material were calculated based on the acquired masses. Temperature corrections were made in case necessary.



Figure 5.1. Pycnometers in vacuum desiccator.

5.4 Modified Proctor test

Modified Proctor tests were conducted in accordance with the SFS-EN 13286-2:en standard. A test mold with dimension of 100 mm in diameter and 120 mm in height was employed. Notably, the modified Proctor test was utilized in this instance, characterized by the application of a heavier rammer. Prior to conducting the modified Proctor tests, the samples underwent sieving to exclude materials retained by a 16 mm sieve or larger, and necessary adjustments were made to account for these larger particles according to standard.

Modified Proctor tests were exclusively executed for the aggregates in this study. For a more precise determination of the optimum water content, it would be advantageous to perform Proctor tests on the specific mixtures intended for use. However, this would entail conducting modified Proctor tests for a diverse array of compositions, necessitating a substantial quantity of materials. In this context, logistical challenges, particularly pertaining to the accessibility of the binder materials, were a determining factor in the decision not to pursue extensive Proctor testing for various compositions including binders.

5.5 pH-values

The determination of pH values constituted an integral component of the laboratory examinations. pH measurements were executed utilizing the HI99121 portable soil pH meter manufactured by Hanna Instruments. Assessments of pH values encompassed all binder materials and crushed concrete aggregate.

Conforming to the guidelines provided by the meter, measurements were systematically conducted. Initial procedures involved the proper configuration of the meter and calibration of the pH electrode. Prior to sample preparation, it was imperative to confirm that the materials had undergone drying and sieving using a 2 mm sieve. The sample preparation entailed blending approximately 10-20 g of material with water, so that the samples were approximately at their natural water content. Following this, the pH electrode was immersed into the prepared sample and swirled gently. Upon stabilization of the measurement, the observed value was recorded. In case the sample was not wet enough, water content was added so that the measurement would be stable. Prior to the analysis of the subsequent sample, the electrode was rinsed with tap water, and any surplus material was delicately removed from the electrode.

5.6 Preparing of test samples

The experimental approach encompassed the preparation of samples via a variety of methods, commencing with the least labor-intensive technique. This systemic process was undertaken with the objective of determining an optimal binder-to-aggregate ratio for the materials. Additionally, it facilitated the exclusion of weaker materials or those incompatible with the chosen methods. Consequently, as the testing advanced, construction samples were exclusively derived from the most promising materials, allowing for a more focused investigation.

Samples formulated from the most promising recipes were prepared using two distinct methods: casting and rammed earth techniques. This deliberate selection enabled an examination of how differing construction approaches influenced the mechanical properties of the resulting samples.

5.6.1 Casting of the binder samples

To obtain data pertaining solely to the binders, samples were casted into molds in accordance with SFS-EN 196-1:2016:en standard. Preceding this step, the appropriate water-to-binder ratio was ascertained. In this process, water was meticulously incorporated into the oven-dried binder during mixing in a planetary mixer. Each binder consisted of CEM I (20%) and various ashes or slag (80%). Upon attaining the optimal composition of the material, the water-binder ratio was determined by dividing the mass of water by the mass of the binder. Subsequently, this established water-to-binder ratio was employed in the preparation of binder samples and subsequently in the casting of samples incorporating aggregates. Testing matrix for casted binder samples and the established water contents are presented in the table 5.2.

Table 5.2. Testing matrix of the binder samples. (UPV=Ultrasonic pulse velocity; UCT=Unconfined compression test)

Material	CEM (%)	Water-binder ratio	Tests performed
Naantali FA+CEM I	20	0,6	UPV, UCT, 3-point bending
Naantali BA+CEM I	20	0,35	UPV, UCT, 3-point bending
Hanko BFS+CEM I	20	0,5	UPV, UCT, 3-point bending
Stora Enso FA+CEM I	20	0,6	UPV, UCT, 3-point bending
CEM III/B	30	0,5	UPV, UCT, 3-point bending

The binder samples were prepared by adding water and then subjected to a mixing cycle comprising 90 seconds of low-speed mixing. Subsequently, the mixer was halted for a duration of 30 seconds, allowing for scraping of the mixture from the container's walls. Following this, high-speed mixing was carried out for 60 seconds. Mixer used in this process was Hobart's planetary mixer. Subsequently, the mixed material was transferred into oiled molds in two separate batches. Following the addition of each material batch, the material was compacted using a jolting apparatus employing 60 compaction strokes. After the second compaction cycle, any excess material was removed, and the molds were placed in a room at ambient temperature, covered, for a duration ranging from 20 to 24 hours.

The molds employed for casting were of dimensions 40x40x160 mm, and each specimen necessitated the creation of three samples (refer to figure 5.2). Following the casting process, demolding was executed within a timeframe ranging from 20 to 24 hours. Subsequently, the samples were transferred to a humidity-controlled curing chamber and covered with plastic sheet to prevent direct water accumulation on the samples. Samples were cured in the curing room for 28 days.



Figure 5.2. Casted samples.

5.6.2 Intensive compaction tester

The initial samples in this investigation were produced using gyratory compactor called intensive compaction tester (ICT). These tests were conducted on material mixtures in accordance with the predefined testing matrix presented in table 5.3. The ICT trials adhered to the standards outlined in SFS-EN 12697-31, as well as the former guidelines provided by the Road Administration in 2001 pertaining to ICT.

The ICT trials were executed in accordance with a test matrix, incorporating five aggregate materials and five binder materials. Aggregate materials used were QF 0-3 mm, QF 0-5 mm, QF 0-8 mm, CC (classified as class II) and mixture of QF 0-3 mm and CC. Binder materials used were Naantali FA, Naantali BA, Hanko BFS, with the addition of cement. CEM III/B and Stora Enso's FA were included in the research at a later stage. All binding agents were assessed with cement concentrations of 20 %. The initial weight ratio between the binder and the aggregate materials was set at 1:5 and 1:6. In cases where the results indicated insufficient strength, ratio was subsequently increased to 1:3. In preparation for the experiments, the materials were subjected to a drying process within an oven, set at a temperature of 105 °C, for a duration of 24 hours.

The dry components of the test materials were meticulously weighed in accordance with the predetermined testing matrix. These dry constituents were thoroughly blended with Hobart's planetary mixer before the introduction of water, ensuring the material achieved a visibly homogeneous state. After addition of water, the material was mixed with low speed for 90 seconds. Subsequently, the mixer was halted for a duration of 30 seconds, allowing for scraping of the mixture from the container's walls. Following this, high-speed mixing was carried out for 60 seconds. Notably, the minimal water concentrations employed in the experiments resulted in a notably dry mass. Despite the exceedingly low water content utilized in the experiments, the resulting mass could be compacted into a cohesive, ball-shaped structure when compressed within a closed hand.

Base plates were positioned at the base of the ICT test cylinder, followed by the precise dosing of the prepared mass into the cylinder. The entire assembly, inclusive of the mass, was subsequently weighed prior to the commencement of the experiment. The experiment

involved a predetermined number of compaction cycles, set at 160 repetition per individual specimen. Pressure of the machine was set to 600 kPa and gyratory angle was 1,16 degrees. It is noteworthy that the ICT experiments in this study employed parameters consistent with those employed by Kasper Holopainen (2022). Consequently, the results obtained in this study can be considered directly comparable to the findings presented in his work. The ICT machine computed the measured density of the material by considering both the weight and height measurements obtained during the experiment. The cross-sectional area of the specimen adhered to the dimensions of a standard cylinder mold with 100 mm diameter. Following preparation with the ICT apparatus, the samples were compressed out from the mold (refer to figure 5.3) and placed in a humidity room for a period of 7 days for curing. Plastic bags were utilized to cover the samples, serving as a precautionary measure to prevent excessive water accumulation.



Figure 5.3. ICT sample compressed out of the cylinder mold.

Table 5.3. Testing matrix for samples made with ICT-machine.

Identifier No.	Aggregate	Binder	Aggregate-Binder	Cement (%)	Water content (%)	Curing Age (days)	Tests performed
1	QF 0-3 mm	Naantali FA	1:5	3,33 %	12	7	UPV, UCT
2	QF 0-3 mm	Naantali FA	1:6	2,86 %	12	7	UPV, UCT
3	QF 0-3 mm	Naantali BA	1:5	3,33 %	12	7	UPV, UCT
4	QF 0-3 mm	Naantali BA	1:6	2,86 %	12	7	UPV, UCT
5	QF 0-3 mm	Hanko BFS	1:5	3,33 %	12	7	UPV, UCT
6	QF 0-3 mm	Hanko BFS	1:6	2,86 %	12	7	UPV, UCT
7	QF 0-5 mm	Naantali FA	1:5	3,33 %	11	7	UPV, UCT
8	QF 0-5 mm	Naantali FA	1:6	2,86 %	11	7	UPV, UCT
9	QF 0-5 mm	Naantali BA	1:5	3,33 %	11	7	UPV, UCT
10	QF 0-5 mm	Naantali BA	1:6	2,86 %	11	7	UPV, UCT
11	QF 0-5 mm	Hanko BFS	1:5	3,33 %	11	7	UPV, UCT
12	QF 0-5 mm	Hanko BFS	1:6	2,86 %	11	7	UPV, UCT
13	QF 0-8 mm	Naantali FA	1:5	3,33 %	10	7	UPV, UCT
14	QF 0-8 mm	Naantali FA	1:6	2,86 %	10	7	UPV, UCT
15	QF 0-8 mm	Naantali BA	1:5	3,33 %	10	7	UPV, UCT
16	QF 0-8 mm	Naantali BA	1:6	2,86 %	10	7	UPV, UCT
17	QF 0-8 mm	Hanko BFS	1:5	3,33 %	10	7	UPV, UCT
18	QF 0-8 mm	Hanko BFS	1:6	2,86 %	10	7	UPV, UCT
19	CC	Naantali FA	1:5	3,33 %	10	7	UPV, UCT
20	CC	Naantali FA	1:6	2,86 %	10	7	UPV, UCT
21	CC	Naantali BA	1:5	3,33 %	10	7	UPV, UCT
22	CC	Naantali BA	1:6	2,86 %	10	7	UPV, UCT
23	CC	Hanko BFS	1:5	3,33 %	10	7	UPV, UCT
24	CC	Hanko BFS	1:6	2,86 %	10	7	UPV, UCT
25	CC+QF 0-3 mm	Naantali FA	1:5	3,33 %	11	7	UPV, UCT
26	CC+QF 0-3 mm	Naantali FA	1:6	2,86 %	11	7	UPV, UCT
27	CC+QF 0-3 mm	Naantali BA	1:5	3,33 %	11	7	UPV, UCT
28	CC+QF 0-3 mm	Naantali BA	1:6	2,86 %	11	7	UPV, UCT
29	CC+QF 0-3 mm	Hanko BFS	1:5	3,33 %	11	7	UPV, UCT
30	CC+QF 0-3 mm	Hanko BFS	1:6	2,86 %	11	7	UPV, UCT
31	QF 0-8 mm	Naantali BA	1:3	5,00 %	10	7	UPV, UCT
32	QF 0-8 mm	Hanko BFS	1:3	5,00 %	10	7	UPV, UCT
33	CC+QF 0-3 mm	Naantali BA	1:3	5,00 %	11	7	UPV, UCT
34	CC+QF 0-3 mm	Hanko BFS	1:3	5,00 %	11	7	UPV, UCT
35	CC+QF 0-3 mm	CEM III/B	1:5	5,00 %	11	7	UPV, UCT
36	CC+QF 0-3 mm	CEM III/B	1:6	4,29 %	11	7	UPV, UCT
37	CC+QF 0-3 mm	CEM III/B	1:3	7,50 %	11	7	UPV, UCT

5.6.3 VTT compaction hammer

Following the completion of testing on the samples created using the ICT device, the most promising material mixtures were chosen for the VTT compaction hammer stage. The VTT compaction hammer (figure 5.4) is a mechanical hammer that offers a valuable insight into the properties of structures constructed using rammed earth technique. In the compaction process, compaction guidelines outlined in Aromaa's (2021) and Holopainen's (2022) Master's theses were followed, maintaining consistent compaction energy to ensure the comparability of results. Unlike previous studies, the samples were prepared in cylindrical ICT molds, as cube-shaped molds had previously encountered issues during the demolding process.



Figure 5.4. The VTT compaction hammer and 100 mm cylindrical ICT-mold.

The experimentation commenced with the screening of crushed concrete with a maximum grain size of 16 mm, the largest feasible size for the 100 mm diameter ICT mold utilized in the experiments. The materials employed in the experiments were subjected to 24 hours of drying in an oven for 105 °C to ensure precise water content measurements. The aggregate and binder materials were subsequently mixed using a Hobart's planetary mixer to achieve homogeneity. Water was then introduced to the mixture and mixing for 90 seconds at a low-speed setting, followed by a 30-second interval to manually scrape any material adhering to the sides of the mixer bowl back into the center. Finally, the material was mixed for an additional 60 seconds at a high-speed setting. Each sample was mixed separately. The prepared mass was dosed into an oiled ICT mold in four distinct layers, with each layer

subjected to 20 drops of the compaction hammer, yielding a compaction energy of 353 Joules per compaction layer and 1412 Joules per sample. Post-compaction, the samples were immediately released from the mold, as only one ICT mold was available. This technique ensured the preservation of all samples and prevented material adhesion to the mold. Regardless of the materials used, the samples formed a cohesive mass immediately following the compaction process, remaining intact without complications even prior to the material's actual consolidation.

With the VTT compaction hammer device, samples were prepared for a total of 8 material mixtures to be used in the 28- and 90-day tests. The specific compositions and mixture ratios of the material mixtures employed in the tests can be found in the testing matrix in the table 5.4. For the 28-day tests, six samples were created for each materials mixture. All 28-day samples were stored under conditions of 20 °C and 100 % room humidity. After 28 days, half of the samples were subjected to unconfined compression testing in accordance with the standard SFS-EN 13286-41, while the other half of the underwent a freeze-thaw test, followed by subsequent unconfined compression testing. As for the 90-day tests, three samples were prepared for each material mixture, although these tests will be carried out at a later stage, post-publication of this thesis. The intention behind these tests is to explore the final strength of materials, as ashes and slags continue to hydrate beyond the 28-day mark.

Table 5.4. Testing matrix for samples made with VTT compaction hammer. (F-T=Freeze-thaw test)

Aggregate	Binder	Amount of samples	Aggregate-Binder	Cement (%)	Water content (%)	Curing Age (days)	Tests performed
QF 0-8 mm	Stora Enso FA	3	1:5	3,33 %	10	28	F-T, UPV, UCT
QF 0-8 mm	Stora Enso FA	3	1:5	3,33 %	10	28	UPV, UCT
QF 0-8 mm	Naantali BA	3	1:3	5,00 %	10	28	F-T, UPV, UCT
QF 0-8 mm	Naantali BA	3	1:3	5,00 %	10	28	UPV, UCT
QF 0-8 mm	Hanko BFS	3	1:3	5,00 %	10	28	F-T, UPV, UCT
QF 0-8 mm	Hanko BFS	3	1:3	5,00 %	10	28	UPV, UCT
QF 0-8 mm	CEM III/B	3	1:6	4,29 %	10	28	F-T, UPV, UCT
QF 0-8 mm	CEM III/B	3	1:6	4,29 %	10	28	UPV, UCT
CC+QF 0-3 mm	Stora Enso FA	3	1:5	3,33 %	11	28	F-T, UPV, UCT
CC+QF 0-3 mm	Stora Enso FA	3	1:5	3,33 %	11	28	UPV, UCT
CC+QF 0-3 mm	Naantali BA	3	1:3	5,00 %	11	28	F-T, UPV, UCT
CC+QF 0-3 mm	Naantali BA	3	1:3	5,00 %	11	28	UPV, UCT
CC+QF 0-3 mm	Hanko BFS	3	1:3	5,00 %	11	28	F-T, UPV, UCT
CC+QF 0-3 mm	Hanko BFS	3	1:3	5,00 %	11	28	UPV, UCT
CC+QF 0-3 mm	CEM III/B	3	1:6	4,29 %	11	28	F-T, UPV, UCT
CC+QF 0-3 mm	CEM III/B	3	1:6	4,29 %	11	28	UPV, UCT

5.6.4 Casting

In the case of samples created through the casting method, the procedures adhered to SFS-EN 196-1;2016:en standard. The materials and recipes employed for casted samples remained fundamentally consistent with those used in VTT compaction hammer tests, however with a higher water content to facilitate the casting process and to ensure the workability of the mixture. The specific compositions and mixture ratios of the material mixtures employed in the tests can be found in the testing matrix in the table 5.5. The casted samples were subjected to a 28-day curing period before testing.

The initial work phase involved drying the materials for 24 hours in a 105 °C oven to ensure the precise control of water content. Given that these mixtures contained coarse aggregates, the subsequent step entailed sieving the aggregates to a maximum grain size of 8 mm, thereby rendering them suitable for casting into 40x40x160 mm molds. Subsequently, the dried constituents were diligently homogenized with a Hobart planetary mixer before the introduction of water, with meticulous attention to achieving a visibly consistent mixture. After water addition, the material was subjected to low-speed mixing for 90 seconds, followed by a 30-second pause during which the mixture adhering to the container's walls was manually scraped back into the center. This was followed by high-speed mixing for 60 seconds. The mixed material was then dispensed into oiled molds in two separate portions. After each addition of material, compaction was performed using a jolting apparatus, involving 60 compaction strokes. Following the second compaction cycle, any excess material was removed, and the molds were stored in a room at ambient temperature, covered, for a duration ranging from 20 to 24 hours. After this the samples were demolded and subsequently, they were placed in the curing room with 20 °C temperature and 100 % room moisture. Samples were covered with a plastic sheet to prevent direct water accumulation on the samples.

In preparation for the 28-day tests, a total of 6 samples were casted for each material mixture. Upon completion of the 28-day curing period, the samples were subjected to evaluation of their strength properties. Half of the samples underwent testing in accordance with the established SFS-EN 13286-41 standard, while the remaining half were assigned to the freeze-thaw test. After the freeze-thaw cycles were completed, also the other half of the samples underwent the same strength tests according to SFS-EN 13286-41.

Table 5.5. Testing matrix for casted samples. (3-PB=3-point bending test)

Aggregate	Binder	Amount of samples	Aggregate-Binder	CEM (%)	Water content (%)	Curing Age (days)	Tests performed
QF 0-8 mm	Stora Enso FA	3	1:5	3,33 %	17,57 %	28	F-T, UPV, UCT, 3-PB
QF 0-8 mm	Stora Enso FA	3	1:5	3,33 %	17,57 %	28	UPV, UCT, 3-PB
QF 0-8 mm	Naantali BA	3	1:3	5,00 %	13,40 %	28	F-T, UPV, UCT, 3-PB
QF 0-8 mm	Naantali BA	3	1:3	5,00 %	13,40 %	28	UPV, UCT, 3-PB
QF 0-8 mm	Hanko BFS	3	1:3	5,00 %	16,40 %	28	F-T, UPV, UCT, 3-PB
QF 0-8 mm	Hanko BFS	3	1:3	5,00 %	16,40 %	28	UPV, UCT, 3-PB
QF 0-8 mm	CEM III/B	3	1:6	4,29 %	15,44 %	28	F-T, UPV, UCT, 3-PB
QF 0-8 mm	CEM III/B	3	1:6	4,29 %	15,44 %	28	UPV, UCT, 3-PB
CC+QF 0-3 mm	Stora Enso FA	3	1:5	3,33 %	18,00 %	28	F-T, UPV, UCT, 3-PB
CC+QF 0-3 mm	Stora Enso FA	3	1:5	3,33 %	18,00 %	28	UPV, UCT, 3-PB
CC+QF 0-3 mm	Naantali BA	3	1:3	5,00 %	15,80 %	28	F-T, UPV, UCT, 3-PB
CC+QF 0-3 mm	Naantali BA	3	1:3	5,00 %	15,80 %	28	UPV, UCT, 3-PB
CC+QF 0-3 mm	Hanko BFS	3	1:3	5,00 %	18,80 %	28	F-T, UPV, UCT, 3-PB
CC+QF 0-3 mm	Hanko BFS	3	1:3	5,00 %	18,80 %	28	UPV, UCT, 3-PB
CC+QF 0-3 mm	CEM III/B	3	1:6	4,29 %	15,88 %	28	F-T, UPV, UCT, 3-PB
CC+QF 0-3 mm	CEM III/B	3	1:6	4,29 %	15,88 %	28	UPV, UCT, 3-PB

5.7 Ultrasonic pulse velocity

The Ultrasonic Pulse Velocity (UPV) test represents a non-destructive testing method that indirectly provides insights into the strength properties of the samples. It has been chosen for inclusion in this thesis for several reasons. It is a straightforward test to administer, offering reliable estimates of the strength properties of the samples. Furthermore, the results obtained through this thesis serve as a valuable comparative database for the wall construction project. It is important to note that UPV testing is typically associated with concrete structures; thus, while it may not yield direct strength property values in this unique materials context, it remains a pertinent and useful assessment method.

UPV testing was conducted in conjunction with the UCT testing, according to the standard SFS-EN 12504-4:2021:en using A1410 Pulsar tester made by ACS. Initially, the sampled specimens were removed from the curing room and allowed to air-dry at room temperature for 2 hours to eliminate any excess surface moisture. Before testing, each sample's weight and height were measured meticulously, following the UPV measuring procedure outlined in figure 5.5. Measurements were taken from the central point of each sample. The equipment provided the precise time taken for the pulse to travel from the transmitter to receiver, from which the pulse velocity within the material was calculated. A higher pulse velocity is indicative of increased material strength properties. Each sample underwent three measurements, and the resulting averages were computed for analyses.



Figure 5.5. Measuring with UPV device.

5.8 Unconfined compression test

The Unconfined Compression Test (UCT) was employed to determine the uniaxial compressive strength (UCS) of the specimens. As this study is primarily concerned with identifying suitable materials for wall structure, the UCT serves as a pivotal means of acquiring mechanical properties data. The UCT adhered to the guidelines outlined in SFS-EN 13286-41, using Aalto University's construction technology laboratory's Zwick & Roell apparatus (refer to figure 5.6). Prior to the compression test, the samples were weighed and measured to calculate their densities. The UCT involved a 200 N pre-load and a loading rate of 1,5 mm/min. In addition to measuring the load, the elastic modulus E_{50} was determined from the load displacement curve.



Figure 5.6. UCT apparatus.

5.9 Freeze-thaw test

In Finland, where winters bring extreme cold, considerations for freezing and thawing effects are paramount in structural design. In this study, freeze-thaw tests were conducted in accordance with the CEN/TS 13286-54:en standard. A total of 10 freeze-thaw cycles were selected for examination, as the primary focus of this research did not revolve around the freeze-thaw phenomenon. The potential building site lies within an industrial area, where road salts and de-icing chemicals are not utilized, and thus, their influence was not factored into this study.

Freeze-thaw tests were performed on samples prepared using both the VTT hammer and casting methods. Each material type underwent testing with three samples, and their compositions can be found in tables 5.4 and 5.5. For the freeze-thaw test, the samples were removed from the curing room, surface moisture was wiped off, and then the samples were securely wrapped in plastic cling film. Subsequently, the wrapped samples were placed into a freeze-thaw device, as illustrated in figure 5.7. The freeze-thaw device was programmed following the guidelines set forth by CEN/TS 13286-54:en. The temperature of the samples was monitored using a thermocouple meter positioned inside a metal container filled with aggregates and water, while the ambient temperature within the freeze-thaw device was also tracked.

Upon the completion of the 10 freeze-thaw cycles, the samples were transferred back to the curing room for 24 hours to ensure complete thawing. After this period, the samples underwent testing using UPV and UCT procedures.



Figure 5.7. Free-thaw device.

6 Results of laboratory tests

Results of the laboratory tests are elucidated in this chapter. The results served as a basis for the selection of materials and optimum mixing ratios for the wall structure. The properties of both ramming and casting methods are also analysed in this chapter. Additionally, the chapter scrutinizes the impact of freeze-thaw cycles on compressive strength.

6.1 Index-tests

6.1.1 Water content

The water content values of the materials are presented in the table 6.1. To ascertain accurate water content of each material, samples were initially weighed in their wet stage, with the weight of the container excluded. Subsequently, the samples underwent drying in an oven at 105° C for 16 hours. After drying, the material was reweighed, and the water content was computed using equation 6.1.

$$w = \frac{(w_w - w_d)}{w_d} \times 100\% \quad (6.1)$$

where

w = water content

w_w = wet mass of the soil sample [kg]

w_d = dry mass of the soil sample [kg]

Table 6.1. Water content values of the materials.

Material	Water content [%]
Aggregates:	
QF 0-3 mm	3,96
QF 0-5 mm	2,44
QF 0-8 mm	2,66
CC 0-63 mm	10,93
Binders:	
Naantali FA	0,82
Naantali BA	0,13
Hanko BFS	12,72
Stora Enso FA	0,50

6.1.2 Sieving

The grain size curves in figure 6.1 show that, of all the samples that were analyzed, crushed concrete has the highest percentage of material classified as gravel. Sieving was also carried out to confirm the proportions of fines in the different materials (presented in the table 6.2). The mixture of the CC and QF 0-3 mm resulted to the gradation curve depicted as the light blue curve. The goal of this mixture was to produce a gradation curve that is in line with the ideal gradation range shown in the figure 2.4. This theoretical determination was employed

to identify the optimal aggregate from the available materials. Curves in the figure 6.1 also indicate that the materials are not frost-susceptible. This is evidenced by the curves being situated in the areas 3 and 4 and the curves do not cross the area lines. Area 1 would indicate that the material is frost-susceptible and area 1L indicates that the material is moderately frost-susceptible.

Table 6.2. Amount of fines in each aggregate.

Material	<0,063 mm [%]
QF 0-3 mm	7,09
QF 0-5 mm	6,03
QF 0-8 mm	6,15
CC 0-63 mm	2,63

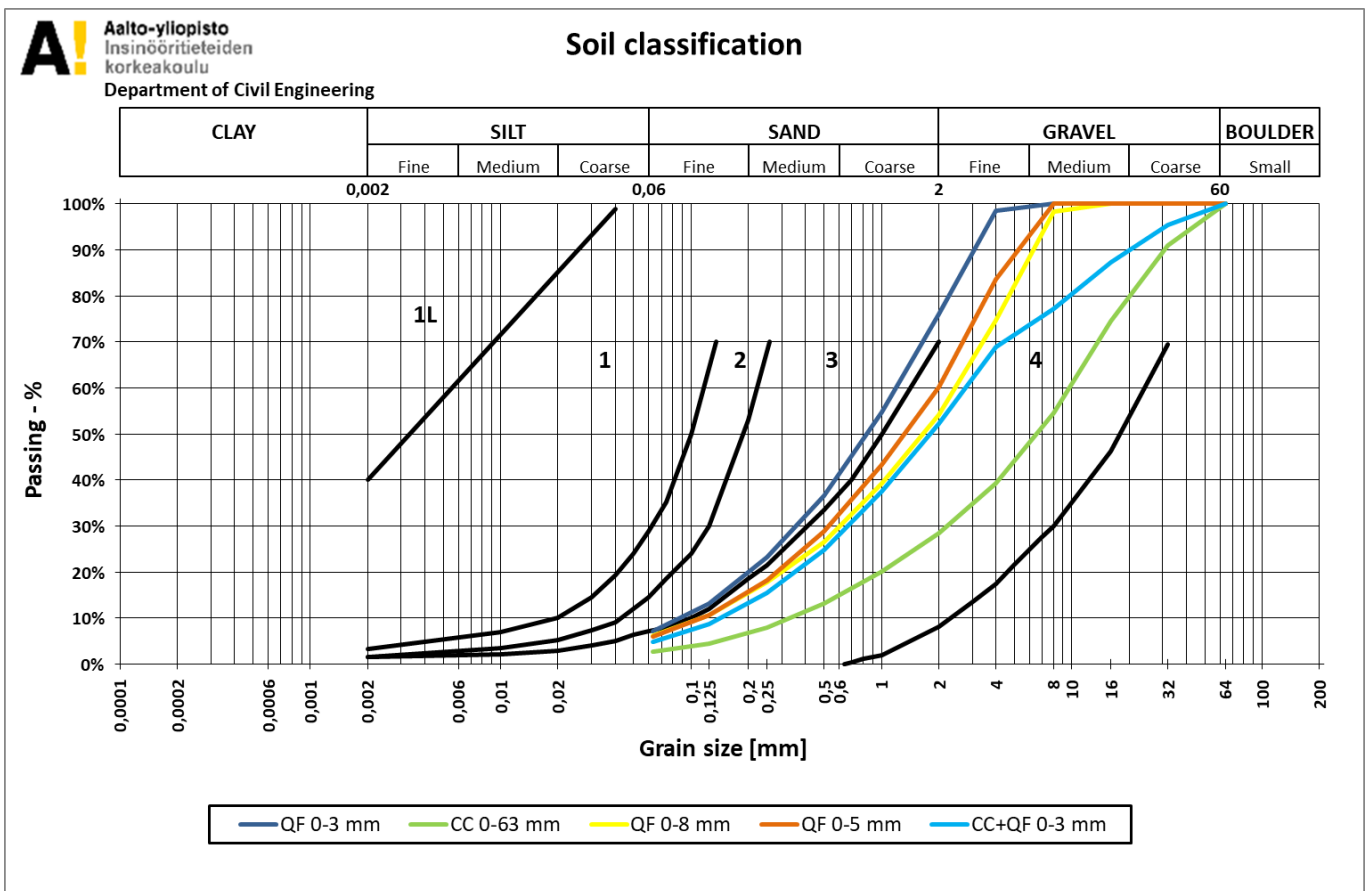


Figure 6.1. Gradation curves of the aggregates defined with dry sieving. Materials are not frost-susceptible since the curves are in the areas 3 and 4.

6.1.3 Specific gravity

Specific gravity of the soil can be computed with the equation 6.2.

$$\rho_s = \frac{w_0}{w_0 - (w_b - w_a)} \quad (6.2)$$

where

w_0 = mass of the dry sample [kg]

w_a = mass of the pycnometer filled with water at constant temperature [kg]

w_d = mass of the pycnometer filled with water and soil at constant temperature [kg]

The specific gravity for each material was determined by calculating the average of two samples. The specific gravity values are detailed in table 6.3.

Table 6.3. Specific gravities of the materials defined by pycnometer tests.

Cont. N:o	Point/ pile N:o	Depth m	Pycnometer		Pycn. + dry sample g	Dry sample m_k g	Tempe- rature T °C	Pycn. + sample + water m_b g	Pycn. + water m_a g	$m_k +$ $m_a -$ m_b g	ρ_w g/cm ³	ρ_s g/cm ³	Avera ge g/cm ³
			N:o	g									
QF 0-3		-	1461	29,53	74,77	45,24	21,30	163,54	135,13	16,83	0,998	2,682	2,679
QF 0-3		-	101	26,80	66	39,20	21,30	168,59	144,01	14,62	0,998	2,676	
QF 0-5			178	18,18	36,96	18,78	21,30	84,93	73,05	6,90	0,998	2,717	2,720
QF 0-5			1106	17,66	40,12	22,46	21,30	87,44	73,21	8,23	0,998	2,722	
QF 0-8			107	18,00	36,4	18,40	21,30	83,94	72,28	6,74	0,998	2,724	2,719
QF 0-8			1148	19,24	46,31	27,07	21,30	93,28	76,16	9,95	0,998	2,714	
CC 0-63			50	19,55	36,66	17,11	21,30	86,16	75,52	6,47	0,998	2,638	2,620
CC 0-63			1307	18,05	36,67	18,62	21,30	85,98	74,50	7,14	0,998	2,603	
Hanko BFS		-	178	18,17	29,37	11,20	22,30	80,46	73,04	3,78	0,998	2,958	3,023
Hanko BFS		-	1307	18,05	34,24	16,19	22,30	85,45	74,49	5,23	0,998	3,089	
Naantali FA		-	178	18,18	24,15	5,97	23,00	76,8	73,03	2,20	0,998	2,705	2,701
Naantali FA		-	1180	17,55	24,28	6,73	23,00	78,06	73,82	2,49	0,998	2,696	
Naantali BA			107	18,00	38,97	20,97	23,00	85,51	72,26	7,72	0,998	2,710	2,705
Naantali BA			1069	18,67	40,45	21,78	23,00	88,29	74,56	8,05	0,998	2,700	
Stora Enso FA		-	1022	19,45	24,69	5,24	23,00	78,61	75,21	1,84	0,998	2,837	2,786
Stora Enso FA		-	57	19,55	25,71	6,16	23,00	78,58	74,67	2,25	0,998	2,734	

As indicated in the table 6.3, Hanko BFS exhibits the highest specific gravity among the scrutinized materials, while QF 0-3 mm displays the lowest. According to Finnsementti (2023), the CEM I and CEM III/B utilized possess specific gravities ranging from 3,0-3,2 g/cm³. The theoretical specific gravities of the prepares mixtures can be obtained by computing from the established specific gravities of the component materials and their corresponding ratios in the mixture. Table 6.4 presents a summary of the created mixture compositions together with the corresponding theoretical specific gravities.

Table 6.4. Theoretical specific gravities [g/cm³] of the prepared mixtures.

Aggregate	Binder	1:6	1:5	1:3
QF 0-8 mm	Naantali FA	2,73	2,73	-
	Naantali BA	2,73	2,73	2,74
	Hanko BFS	2,76	2,77	2,80
	Stora Enso FA	2,74	2,74	-
	CEM III/B	2,77	2,78	-
	CC+QF 0-3 mm	Naantali FA	2,67	2,67
Naantali BA		2,67	2,67	2,68
Hanko BFS		2,71	2,71	2,75
Stora Enso FA		2,68	2,68	-
CEM III/B		2,71	2,72	-

6.1.4 Modified Proctor test

Modified Proctor tests were carried out on the aggregates, and the results are elucidated in table 6.5. Through these modified Proctor tests, the optimum water content for each aggregate was determined. Curves of the modified Proctor tests are presented in the attachment 7. At this optimal water content, the material attains maximum dry density. For the mixture of CC and QF 0-3 mm the optimal water content is computed according to the weighted fractions from the values in table 6.5.

Table 6.5. Optimal water contents of the aggregates.

Aggregate	Optimal water %	Dry density (g/cm ³)
QF 0-3 mm	12	2,00
QF 0-5 mm	11	2,08
QF 0-8 mm	10,5	2,15
CC 0-63 mm	10	1,83
CC+QF 0-3 mm	11	1,92

6.1.5 pH-values

Measured pH values for the materials employed in this study is presented in the table 6.6. The pH value for CEM I and CEM III/B has been sourced from the product data of FinnSementti Oy (2023). As demonstrated in table 6.6, all the binders, excluding Hanko BFS, are highly alkaline. The highly alkaline materials are expected to enhance the compressive strength of the material, because higher alkalinity increases reactivity in the mass. In contrast, the Hanko BFS is characterized by lower alkalinity, implying an expected slower reaction, and an extended duration for the development of compressive strength in the material. CC aggregate has a high alkalinity, presumably attributed to the presence of reacted cement which is highly alkaline.

Table 6.6. pH values of the materials.

Material	pH
CC	11,3
Naantali FA	12,5
Naantali BA	13,3
Hanko BFS	9,6
Stora Enso FA	12,8
CEM I	11-13,5 (Finnsementti Oy, 2023)
CEM III/B	11-13,5 (Finnsementti Oy, 2023)

6.2 Ultrasonic pulse velocity

UPV measurements have been conducted for all the samples that were tested. Initially, the length of the samples must be measured. This defines the distance between the measuring sensors of the UPV device. When measuring, the device indicates the time it takes for the pulse to move from one sensor to another. Subsequently, the velocities can be defined with equation 6.3. The UPV values of the materials are shown in the tables 6.7 and 6.8.

$$V = \frac{L}{T} \quad (6.3)$$

where

$V = \text{pulse velocity} \left[\frac{m}{s} \right]$

$L = \text{length of the sample [m]}$

$T = \text{transit time [s]}$

The results presented in the tables below depict the standard deviation within the test series, representing the average deviation from the expected value. Subsequently, the coefficient of variation is computed by dividing the standard deviation by the mean. A lower coefficient of variation indicates a lower standard deviation within an individual test set, thereby characterizing the homogeneity of the test pieces.

Table 6.7. UPV values for the casted samples. Values have been measured after 28 days of curing. For F-T samples values have been measured after additional 10 freeze-thaw cycles.

	Aggregate	Binder	Aggregate-Binder ratio	No. of Sample [m/s]			Average [m/s]	Standard deviation [m/s]	Variation coefficient
				1	2	3			
No Freeze-Thaw	QF 0-8 mm	Naantali BA	1:3	1987	1743	2036	1922,0	156,9	8,2 %
	QF 0-8 mm	Stora Enso FA	1:5	2818	2590	2532	2646,7	151,2	5,7 %
	QF 0-8 mm	Hanko BFS	1:3	2143	2168	2337	2216,0	105,5	4,8 %
	QF 0-8 mm	CEM III/B	1:6	3415	3466	3365	3415,3	50,5	1,5 %
	CC+QF 0-3 mm	Naantali BA	1:3	2402	2446	2466	2438,0	32,7	1,3 %
	CC+QF 0-3 mm	Stora Enso FA	1:5	2243	2238	2296	2259,0	32,1	1,4 %
	CC+QF 0-3 mm	Hanko BFS	1:3	2265	2097	2109	2157,0	93,7	4,3 %
	CC+QF 0-3 mm	CEM III/B	1:6	3096	3067	3152	3105,0	43,2	1,4 %
Freeze-Thaw	QF 0-8 mm	Naantali BA	1:3	918	937	792	882,3	78,8	8,9 %
	QF 0-8 mm	Stora Enso FA	1:5	1860	1937	1540	1779,0	210,5	11,8 %
	QF 0-8 mm	Hanko BFS	1:3	981	1081	865	975,7	108,1	11,1 %
	QF 0-8 mm	CEM III/B	1:6	1406	1540	1579	1508,3	90,7	6,0 %
	CC+QF 0-3 mm	Naantali BA	1:3	1191	1150	1252	1197,7	51,3	4,3 %
	CC+QF 0-3 mm	Stora Enso FA	1:5	1697	1616	1748	1687,0	66,6	3,9 %
	CC+QF 0-3 mm	Hanko BFS	1:3	1134	1231	1161	1175,3	50,1	4,3 %
	CC+QF 0-3 mm	CEM III/B	1:6	2125	2363	2067	2185,0	156,9	7,2 %

UPV is used to measure indirectly the strength properties of the material. Higher velocity value indicates higher strength properties. When samples were made by casting technique, the highest velocities have been measured with CEM III/B as a binder, as illustrated in the table 6.7. Conversely, the lowest values were measured with Naantali BA as binder and QF 0-8 mm as an aggregate and when the samples have been subjected to freeze-thaw cycles. Notably, the influence of freeze-thaw cycles is significant in the samples prepared with casting technique. Examining the coefficient of variation, it is observed that in samples subjected to freeze-thaw cycles, there is an increase in deviations within the test sets.

Table 6.8. UPV values for the samples made with VTT hammer. Values have been measured after 28 days of curing. For F-T samples values have been measured after additional 10 freeze-thaw cycles.

	Aggregate	Binder	Aggregate-Binder ratio	No. of Sample [m/s]			Average [m/s]	Standard deviation [m/s]	Variation coefficient
				1	2	3			
No Freeze-Thaw	QF 0-8 mm	Naantali BA	1:3	2844	2951	2867	2887,3	56,3	2,0 %
	QF 0-8 mm	Stora Enso FA	1:5	3195	3372	3057	3208,0	157,9	4,9 %
	QF 0-8 mm	Hanko BFS	1:3	3002	2780	3072	2951,3	152,5	5,2 %
	QF 0-8 mm	CEM III/B	1:6	3620	3867	3985	3824,0	186,3	4,9 %
	CC+QF 0-3 mm	Naantali BA	1:3	3027	3076	3298	3133,7	144,4	4,6 %
	CC+QF 0-3 mm	Stora Enso FA	1:5	3126	2914	2812	2950,7	160,2	5,4 %
	CC+QF 0-3 mm	Hanko BFS	1:3	2771	2662	2706	2713,0	54,8	2,0 %
	CC+QF 0-3 mm	CEM III/B	1:6	3703	3726	3831	3753,3	68,2	1,8 %
Freeze-Thaw	QF 0-8 mm	Naantali BA	1:3	1835	1590	1324	1583,0	255,6	16,1 %
	QF 0-8 mm	Stora Enso FA	1:5	3036	3130	3183	3116,3	74,4	2,4 %
	QF 0-8 mm	Hanko BFS	1:3	2939	2756	2765	2820,0	103,2	3,7 %
	QF 0-8 mm	CEM III/B	1:6	3574	3546	3554	3558,0	14,4	0,4 %
	CC+QF 0-3 mm	Naantali BA	1:3	2957	2141	2878	2658,7	450,0	16,9 %
	CC+QF 0-3 mm	Stora Enso FA	1:5	2928	2754	1876	2519,3	563,9	22,4 %
	CC+QF 0-3 mm	Hanko BFS	1:3	2457	2709	2272	2479,3	219,4	8,8 %
	CC+QF 0-3 mm	CEM III/B	1:6	3437	3445	3568	3483,3	73,4	2,1 %

Upon examination of the samples made with VTT hammer, it is evident that the obtained values are significantly higher compared to the samples made with casting method. Likewise, samples prepared with VTT hammer and CEM III/B as a binder exhibit the highest UPV values. Conversely, the lowest values are recorded with this preparation method

utilizing Naantali BA as a binder and QF 0-8 mm as an aggregate and when samples were exposed to freeze-thaw cycles. Analogous to the samples made with casting method, velocities experience a decline following freeze-thaw cycles. Freeze-thaw cycles are also increasing the coefficient of variation. These findings suggest that VTT hammered samples exhibit greater strength than samples made with casting method, while the strength properties of both are decreased after exposure to freeze-thaw cycles.

6.3 Unconfined compression test

The strength properties of the test specimen prepared in this thesis was tested using an unconfined compression test according to SFS-EN 13286-41. The UCT machine is presenting results in graphical representation in the XY chart illustrating the relationship between displacement and force. The compressive strengths presented in the results correspond to peak values, indicating the points at which the samples attain their maximum compressive strength. The compressive strength determined in this test can be calculated using equation 6.4.

$$R_c = \frac{F}{A_c} \quad (6.4)$$

where

R_c = Compressive strength of the sample [MPa]

F = Force applied to the sample [N]

A_c = Area of the sample [mm^2]

In addition to maximum compressive strengths, the Young's modulus E_{50} have been defined for final samples made with casting and VTT hammer methods. E_{50} represents the slope of the linear segment in the stress-strain curve of the test specimen. It is computed by dividing the stress corresponding to 50% of the maximum breaking stress by the relative deformation observed at the point of that stress. In geotechnical investigations, E_{50} is often used to characterize the mechanical behavior of soils and other materials. High E_{50} values indicates that the material is relatively stiff and less compressible, so it resists higher compression within the elastic range and tend to experience smaller deformations under load. Low E_{50} values indicates that the material is soft, and more compressible, so it has lower resistance within elastic range, and it may experience larger deformations under load.

6.3.1 Binder samples

Initially, UCTs were exclusively conducted for the binders, aiming to assess the properties of the binders. In the case of recycled binder materials, 20% of the binder composition included CEM I, serving as an activator. For binders composed of CEM III/B, additional CEM I was not included, as CEM III/B comprises 30% CEM I and 70% blast furnace slag. Binder samples were made with casting method, and they underwent a curing period of 28 days. After the curing they were subjected to testing using a 3-point bending machine to obtain flexural strength and UCT machine for compressive strength. The results of the tests are presented in table 6.9.

Table 6.9. Strength properties of the binders. Curing time 28 days.

	Binder	No. of Sample [MPa]			Average [MPa]	Standard deviation [MPa]	Variation coefficient
		1	2	3			
Compressive strength [Mpa]	Naantali FA	-	-	-	-	-	-
	Naantali BA	19,1	18,4	19,2	18,8	0,4	2,3 %
	Hanko BFS	3,8	3,7	3,2	3,5	0,3	9,0 %
	CEM III/B	41,9	36,7	38,3	39,0	2,7	6,8 %
	Stora Enso FA	7,3	7,7	7,6	7,5	0,2	3,1 %
Flexural strength [MPa]	Naantali FA	-	-	-	-	-	-
	Naantali BA	5,1	4,2	4,7	4,7	0,4	9,2 %
	Hanko BFS	1,7	1,7	1,7	1,7	0,0	0,9 %
	CEM III/B	5,0	5,6	6,1	5,5	0,5	9,5 %
	Stora Enso FA	2,4	2,5	2,6	2,5	0,1	2,2 %

Analyzing these results, it is evident that CEM III/B exhibits the highest values for both compressive and flexural strengths, as expected from a commercially standardized product. Naantali BA demonstrates commendable performance, achieving an average compressive strength of 18,8 MPa and a flexural strength of 4,7 MPa and Stora Enso FA yields also respectable values. Despite Hanko BFS not attaining high strength properties, it has been chosen for further investigation, considering the known slower hydration reaction of blast furnace slag. In contrast, Naantali FA encountered an issue when reacting with water, resulting in the formation of a swollen and soft mixture. This mixture did not stay intact while demolding of the samples, rendering it unsuitable for testing. As a result, Naantali FA was excluded from further testing. Figure 6.2 illustrates Naantali FA samples captured after the demolding phase. Nevertheless, four binders were considered appropriate for additional research, indicating that the findings at this point were satisfactory.



Figure 6.2. Naantali FA samples after demolding.

6.3.2 ICT compacted samples

Upon obtaining binder properties, UCTs were conducted on samples produced using the ICT machine. The samples prepared with the ICT machine underwent a curing period of 7 days. The objective was to determine the optimal ratio between aggregates and binders for each material based on these results. If a particular mixture failed to attain acceptable strength

properties, the aggregate-binder ratio was increased, or it was excluded from subsequent testing. The outcomes from the UCT tests conducted on ICT samples are presented in table 6.10. Figure 6.2 provides a visual comparison of various sample ratios depicting also the UPV values that were measured for each sample.

Table 6.10. Compressive strengths of the samples made with ICT machine. Curing time 7 days.

Aggregate	Binder	Aggregate-Binder ratio	Peak compressive strength [MPa]
QF 0-5 mm	Naantali FA	1:6	0,1
QF 0-5 mm	Naantali FA	1:5	0,1
QF 0-5 mm	Naantali BA	1:6	1,2
QF 0-5 mm	Naantali BA	1:5	1,4
QF 0-5 mm	Hanko BFS	1:6	1,2
QF 0-5 mm	Hanko BFS	1:5	1,3
QF 0-8 mm	Naantali FA	1:6	0,1
QF 0-8 mm	Naantali FA	1:5	0,1
QF 0-8 mm	Naantali BA	1:6	1,5
QF 0-8 mm	Naantali BA	1:5	1,7
QF 0-8 mm	Naantali BA	1:3	2,4
QF 0-8 mm	Hanko BFS	1:6	1,4
QF 0-8 mm	Hanko BFS	1:5	1,5
QF 0-8 mm	Hanko BFS	1:3	2,4
CC	Naantali FA	1:6	0,2
CC	Naantali FA	1:5	0,1
CC	Naantali BA	1:6	1,2
CC	Naantali BA	1:5	0,7
CC	Hanko BFS	1:6	0,8
CC	Hanko BFS	1:5	0,7
CC+QF 0-3 mm	Naantali FA	1:6	0,3
CC+QF 0-3 mm	Naantali FA	1:5	0,2
CC+QF 0-3 mm	Naantali BA	1:6	1,5
CC+QF 0-3 mm	Naantali BA	1:5	1,8
CC+QF 0-3 mm	Naantali BA	1:3	3,0
CC+QF 0-3 mm	Hanko BFS	1:6	1,0
CC+QF 0-3 mm	Hanko BFS	1:5	1,2
CC+QF 0-3 mm	Hanko BFS	1:3	2,6
CC+QF 0-3 mm	CEM III/B	1:6	8,8
CC+QF 0-3 mm	CEM III/B	1:5	10,5
CC+QF 0-3 mm	CEM III/B	1:3	13,5

Both table 6.10 and figure 6.3 collectively demonstrate that, except for CEM III/B the compressive strengths of the samples generated using the ICT machine exhibit relatively low values. Figure 6.2 further illustrates that an increase in the proportion of binder relative to the aggregates correlates with higher compressive strength values for the samples. This outcome aligns with the expectations, as a higher proportion of binder augments the reactivity

of the mixture and, consequently, the compressive strength. Predicated on these preliminary findings, Naantali BA with 1:3 aggregate-binder ratio, Hanko BFS with a 1:3 aggregate-binder ratio and CEM III/B with a 1:6 aggregate-binder ratio was chosen to preparation of the test samples using the casting and ramming methods. The inclusion of Stora Enso FA in the study is based on the results of tests conducted by Wayu (2023), indicating that a 1:5 aggregate-binder ratio is recommended for Stora Enso FA.

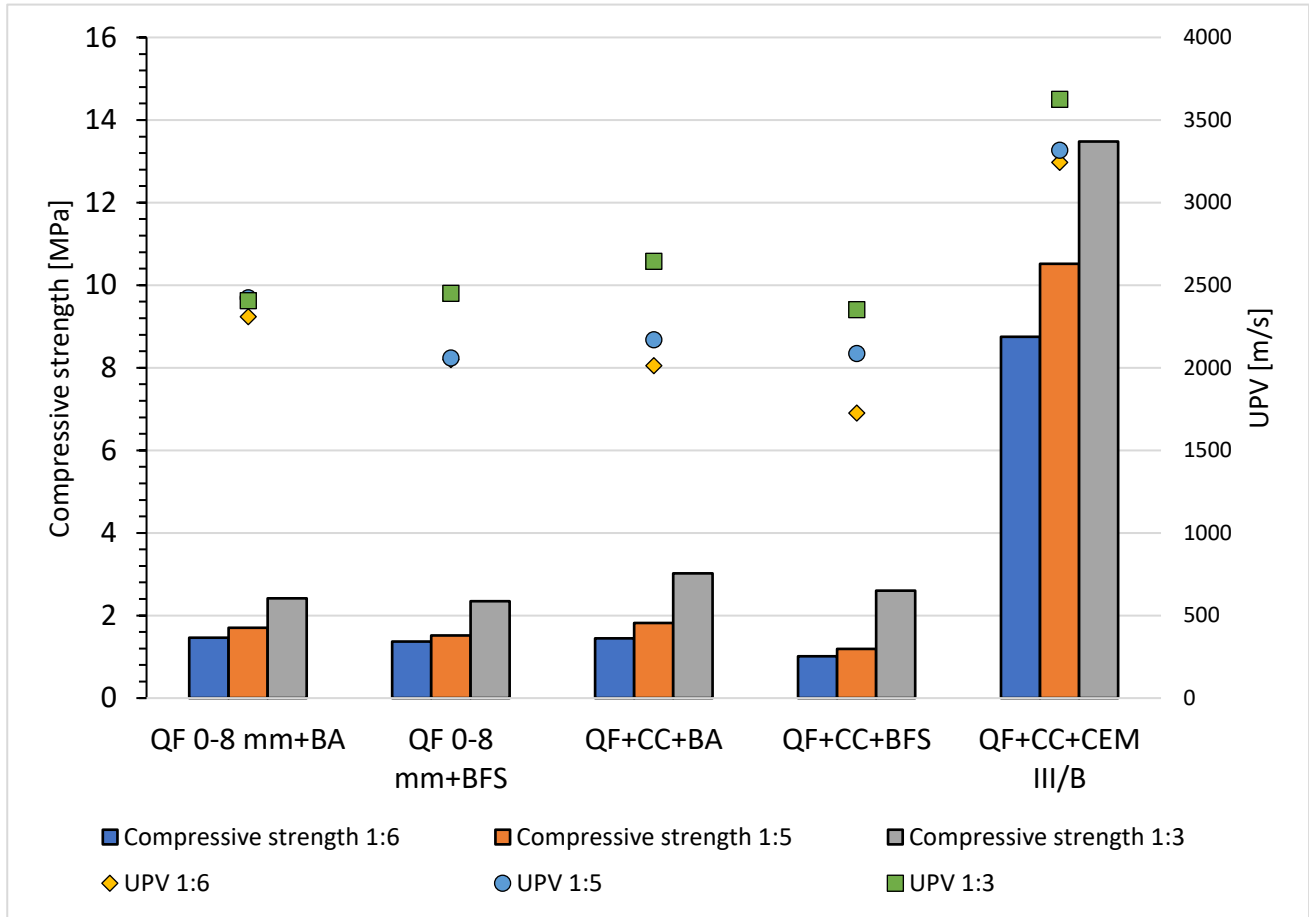


Figure 6.3. Compressive strengths and UPV values of the samples made with ICT. Samples were made with 1:6; 1:5 and 1:3 aggregate-binder ratio. Curing time 7 days.

6.3.3 Samples made with VTT hammer (ramming)

The most auspicious mixtures were prepared by both casting and ramming with VTT hammer. The results of the UCTs conducted on samples prepared with the VTT hammer are delineated in table 6.11. Examination of the table reveals that numerous mixtures UCS values achieved decent values, ranging from 5 MPa up to 18,1 MPa. However, even with higher aggregate-binder ratio, the combination of Naantali BA with QF 0-8 mm and the combination of Hanko BFS with both aggregates, resulted in UCS values of less than 5 MPa. This was unfortunate since both binders were from Turku region. Consequently, while there was room for slight improvement in the results, the overall satisfaction stems from high strength properties of CEM III/B and Stora Enso FA. Notably, CEM III/B manifested compressive strengths ranging from 16-18 MPa. These results suggested the potential to further diminish the binder content, even though it was initially employed with a 1:6 aggregate-binder ratio.

Arguably the most intriguing observation obtained from the results of the table 6.11 pertains to the impact of freeze-thaw cycles on the samples. Notably, there is no significant alteration in the compressive strengths when comparing samples subjected to freeze-thaw cycles with those that have not undergone such conditions. Additionally, a subtle distinction in the aggregates emerges upon comparison, wherein samples prepared with CC+QF 0-3 mm exhibit slightly higher results than those made with QF 0-8 mm.

Table 6.11. Compressive strengths of the samples made with VTT hammer. Values have been measured after 28 days of curing. For F-T samples values have been measured after additional 10 freeze-thaw cycles.

	Aggregate	Binder	Aggregate-Binder ratio	No. of Sample [MPa]			Average [MPa]	Standard deviation [MPa]	Variation coefficient
				1	2	3			
No Freeze-Thaw	QF 0-8 mm	Naantali BA	1:3	3,4	2,8	3,4	3,2	0,3	10,7 %
	QF 0-8 mm	Stora Enso FA	1:5	test fail	8,9	5,6	7,2	2,4	33,1 %
	QF 0-8 mm	Hanko BFS	1:3	5,1	4,4	4,9	4,8	0,4	7,5 %
	QF 0-8 mm	CEM III/B	1:6	15,1	17,8	16,3	16,4	1,4	8,3 %
	CC+QF 0-3 mm	Naantali BA	1:3	5,8	5,9	5,5	5,8	0,2	3,3 %
	CC+QF 0-3 mm	Stora Enso FA	1:5	8,9	8,1	7,5	8,2	0,7	8,6 %
	CC+QF 0-3 mm	Hanko BFS	1:3	5,4	4,9	4,3	4,9	0,5	10,9 %
	CC+QF 0-3 mm	CEM III/B	1:6	17,1	18,9	18,4	18,1	0,9	5,2 %
Freeze-Thaw	QF 0-8 mm	Naantali BA	1:3	3,5	3,0	2,7	3,1	0,4	14,6 %
	QF 0-8 mm	Stora Enso FA	1:5	12,2	11,7	10,3	11,4	1,0	8,5 %
	QF 0-8 mm	Hanko BFS	1:3	5,5	4,4	4,9	4,9	0,5	10,6 %
	QF 0-8 mm	CEM III/B	1:6	15,2	15,9	13,0	14,7	1,5	10,2 %
	CC+QF 0-3 mm	Naantali BA	1:3	5,8	4,5	5,2	5,1	0,6	12,5 %
	CC+QF 0-3 mm	Stora Enso FA	1:5	9,0	8,8	7,6	8,5	0,8	8,9 %
	CC+QF 0-3 mm	Hanko BFS	1:3	4,7	4,7	4,1	4,5	0,4	8,3 %
	CC+QF 0-3 mm	CEM III/B	1:6	18,9	18,3	15,9	17,7	1,6	8,8 %

Ramming constitutes a construction technique demanding a considerable degree of expertise. Consequently, variations in sample quality may arise, even when utilizing identical materials. In this instance, each sample was prepared one by one, entailing the separate mixing of materials for each individual sample. This approach contributes to a divergence among the samples, despite the uniformity in material composition. The substantiated high coefficient of variation in table 6.11 attests to the notable variability in strength properties observed among samples prepared with the VTT hammer.

Table 6.12 illustrates the Young's modulus E_{50} of samples prepared with the VTT hammer. Notably, the E_{50} values align with the high compressive strengths exhibited by corresponding samples. The sole conspicuous anomaly in the E_{50} values pertains to the sample generated with QF 0-8 mm and Stora Enso FA. The sample presented in the first column of the table displays an E_{50} value nearly twice that of the subsequent samples. Generally, the E_{50} values indicate a correlation between high compressive strength and increased rigidity and elasticity, and vice versa. Furthermore, it appears that ramming with the VTT hammer does not adversely impact the E_{50} values of the samples.

Table 6.12. Young's modulus (E_{50}) values of the samples made with VTT hammer. Values have been measured after 28 days of curing. For F-T samples values have been measured after additional 10 freeze-thaw cycles.

	Aggregate	Binder	Aggregate-Binder ratio	Secant modulus, E_{50} [MPa]			Average [MPa]
				1	2	3	
No Freeze-Thaw	QF 0-8 mm	Naantali BA	1:3	148,7	121,8	155,1	141,8
	QF 0-8 mm	Stora Enso FA	1:5	test fail	477,0	441,5	459,3
	QF 0-8 mm	Hanko BFS	1:3	322,4	230,2	309,0	287,2
	QF 0-8 mm	CEM III/B	1:6	1276,9	1967,5	1407,1	1550,5
	CC+QF 0-3 mm	Naantali BA	1:3	358,4	303,5	331,2	331,0
	CC+QF 0-3 mm	Stora Enso FA	1:5	857,3	459,6	579,4	632,1
	CC+QF 0-3 mm	Hanko BFS	1:3	371,4	245,7	227,6	281,6
	CC+QF 0-3 mm	CEM III/B	1:6	1367,6	1427,3	1695,6	1496,9
Freeze-Thaw	QF 0-8 mm	Naantali BA	1:3	161,0	225,7	181,6	189,4
	QF 0-8 mm	Stora Enso FA	1:5	1403,5	681,1	719,2	934,6
	QF 0-8 mm	Hanko BFS	1:3	315,0	218,7	236,7	256,8
	QF 0-8 mm	CEM III/B	1:6	933,6	1214,6	970,3	1039,5
	CC+QF 0-3 mm	Naantali BA	1:3	296,5	269,4	262,5	276,1
	CC+QF 0-3 mm	Stora Enso FA	1:5	602,7	501,4	601,0	568,4
	CC+QF 0-3 mm	Hanko BFS	1:3	254,1	330,9	224,7	269,9
	CC+QF 0-3 mm	CEM III/B	1:6	1211,0	1256,8	974,2	1147,3

6.3.4 Samples made by casting

The results of the UCTs conducted on casted samples are detailed in table 6.13. Analysis of the table reveals the underwhelming strength properties of the casted samples. Only CEM III/B is reaching decent values yielding 9-11 MPa depending on the aggregate used. Conversely, the remaining binders exhibit diminished values, particularly when subjected to freeze-thaw cycles, with the lowest recorded value being 0,8 MPa for Naantali BA and QF 0-8 mm.

The E_{50} values for casted samples, as presented in table 6.14, are also notably lower compared to samples prepared through ramming. This discrepancy suggests a propensity for plastic deformations in the casted samples. CEM III/B registers the highest E_{50} values, albeit this time reaching only 329 MPa, compared to 1695 MPa, which was highest recorded value for sample made with VTT hammer.

Table 6.13. Compressive strengths of the samples made by casting. Values have been measured after 28 days of curing. For F-T samples values have been measured after additional 10 freeze-thaw cycles.

	Aggregate	Binder	Aggregate-Binder ratio	No. of Sample [MPa]			Average [MPa]	Standard deviation [MPa]	Variation coefficient
				1	2	3			
No Freeze-Thaw	QF 0-8 mm	Naantali BA	1:3	1,8	1,6	1,7	1,7	0,1	4,3 %
	QF 0-8 mm	Stora Enso FA	1:5	3,8	3,5	3,4	3,4	0,2	6,1 %
	QF 0-8 mm	Hanko BFS	1:3	2,2	2,1	2,2	2,1	0,1	3,4 %
	QF 0-8 mm	CEM III/B	1:6	9,9	10,0	10,3	10,0	0,2	1,8 %
	CC+QF 0-3 mm	Naantali BA	1:3	1,9	2,3	1,7	2,0	0,3	17,2 %
	CC+QF 0-3 mm	Stora Enso FA	1:5	3,0	2,1	2,4	2,5	0,5	19,5 %
	CC+QF 0-3 mm	Hanko BFS	1:3	2,1	2,3	1,6	2,0	0,3	16,8 %
	CC+QF 0-3 mm	CEM III/B	1:6	10,8	11,4	11,4	11,2	0,3	2,8 %
Freeze-Thaw	QF 0-8 mm	Naantali BA	1:3	0,7	1,0	0,8	0,8	0,2	18,4 %
	QF 0-8 mm	Stora Enso FA	1:5	2,8	2,0	2,0	2,3	0,4	19,7 %
	QF 0-8 mm	Hanko BFS	1:3	0,8	0,9	0,8	0,9	0,0	5,1 %
	QF 0-8 mm	CEM III/B	1:6	6,9	6,8	6,4	6,7	0,3	4,3 %
	CC+QF 0-3 mm	Naantali BA	1:3	1,2	1,4	1,5	1,4	0,2	12,6 %
	CC+QF 0-3 mm	Stora Enso FA	1:5	1,8	1,7	1,9	1,8	0,1	5,6 %
	CC+QF 0-3 mm	Hanko BFS	1:3	1,0	1,1	1,0	1,0	0,1	6,7 %
	CC+QF 0-3 mm	CEM III/B	1:6	9,8	8,7	8,9	9,1	0,6	6,3 %

Table 6.14. Young's modulus (E_{50}) values of the samples made by casting. Values have been measured after 28 days of curing. For F-T samples values have been measured after additional 10 freeze-thaw cycles.

	Aggregate	Binder	Aggregate-Binder ratio	E_{50} [MPa]			Average [MPa]	Standard deviation [MPa]	Variation coefficient
				1	2	3			
No Freeze-Thaw	QF 0-8 mm	Naantali BA	1:3	11,1	12,1	12,1	11,8	0,6	4,8 %
	QF 0-8 mm	Stora Enso FA	1:5	71,1	57,4	35,2	46,3	18,1	39,1 %
	QF 0-8 mm	Hanko BFS	1:3	15,5	31,6	20,9	22,7	8,2	36,2 %
	QF 0-8 mm	CEM III/B	1:6	325,4	318,2	329,4	324,3	5,7	1,8 %
	CC+QF 0-3 mm	Naantali BA	1:3	20,3	29,4	14,1	21,2	7,7	36,2 %
	CC+QF 0-3 mm	Stora Enso FA	1:5	19,5	25,3	39,1	28,0	10,1	36,0 %
	CC+QF 0-3 mm	Hanko BFS	1:3	15,6	24,0	15,9	18,5	4,8	25,7 %
	CC+QF 0-3 mm	CEM III/B	1:6	139,7	150,3	185,2	158,4	23,8	15,0 %
Freeze-Thaw	QF 0-8 mm	Naantali BA	1:3	3,9	6,9	18,3	9,7	7,6	78,2 %
	QF 0-8 mm	Stora Enso FA	1:5	22,1	12,4	11,2	15,2	6,0	39,5 %
	QF 0-8 mm	Hanko BFS	1:3	3,3	5,1	4,7	4,3	0,9	21,8 %
	QF 0-8 mm	CEM III/B	1:6	77,1	59,9	63,5	66,8	9,1	13,6 %
	CC+QF 0-3 mm	Naantali BA	1:3	7,5	13,5	10,5	10,5	3,0	28,6 %
	CC+QF 0-3 mm	Stora Enso FA	1:5	14,6	17,2	14,4	15,4	1,6	10,1 %
	CC+QF 0-3 mm	Hanko BFS	1:3	5,2	6,5	5,3	5,6	0,7	13,2 %
	CC+QF 0-3 mm	CEM III/B	1:6	228,1	145,4	164,2	179,2	43,4	24,2 %

7 Analysis of the research results

The results of the laboratory tests are analysed in this chapter. The primary focus of the analysis is the evaluation of the interplay between materials and preparation techniques in terms of compressive strength and ultrasonic pulse velocities. Moreover, a comparative analysis is carried out by juxtaposing the current findings with those documented in existing studies. The presentation and comparison of results are executed through a diverse array of graphs and tables, thereby facilitating an understanding of the influences exerted by various variables on the strength properties of distinct samples.

7.1 Relationship of UPV and UCS

The initial analysis pertains to the correlation between UPV and UCS. Figures 7.1; 7.2; 7.3 and 7.4 present the UCS of samples with diverse mixtures in relation to their UPV values. The relationship between UCS and UPV in the material serves as a basis for estimating the mechanical properties of the samples. The observed trend indicates that a higher UPV value corresponds to elevated strength properties in the sample. This assumption is substantiated through the analysis of the figures, wherein an exponential trendline is fitted to values from all samples depicted in each figure. The ascending trendline affirms that as the UPV value increases, the UCS value also ascends. It is noteworthy that the increased steepness of the trendline angle adds complexity to the analysis of UCS via UPV. This aspect is evident when comparing figures 7.1 and 7.2 when the certain UPV values may correspond to multiple UCS values.

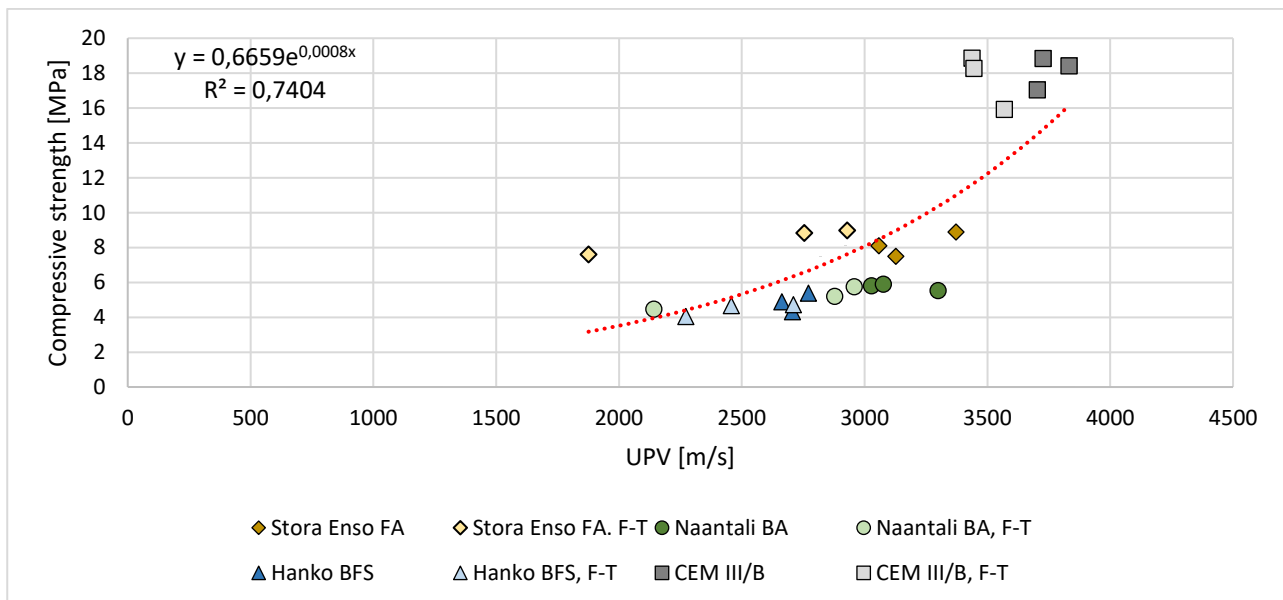


Figure 7.1. The correlation between UPV values and the UCS values of the samples made by ramming. Aggregate: CC+QF 0-3 mm. Values have been measured after 28 days of curing. For F-T samples values have been measured after additional 10 freeze-thaw cycles.

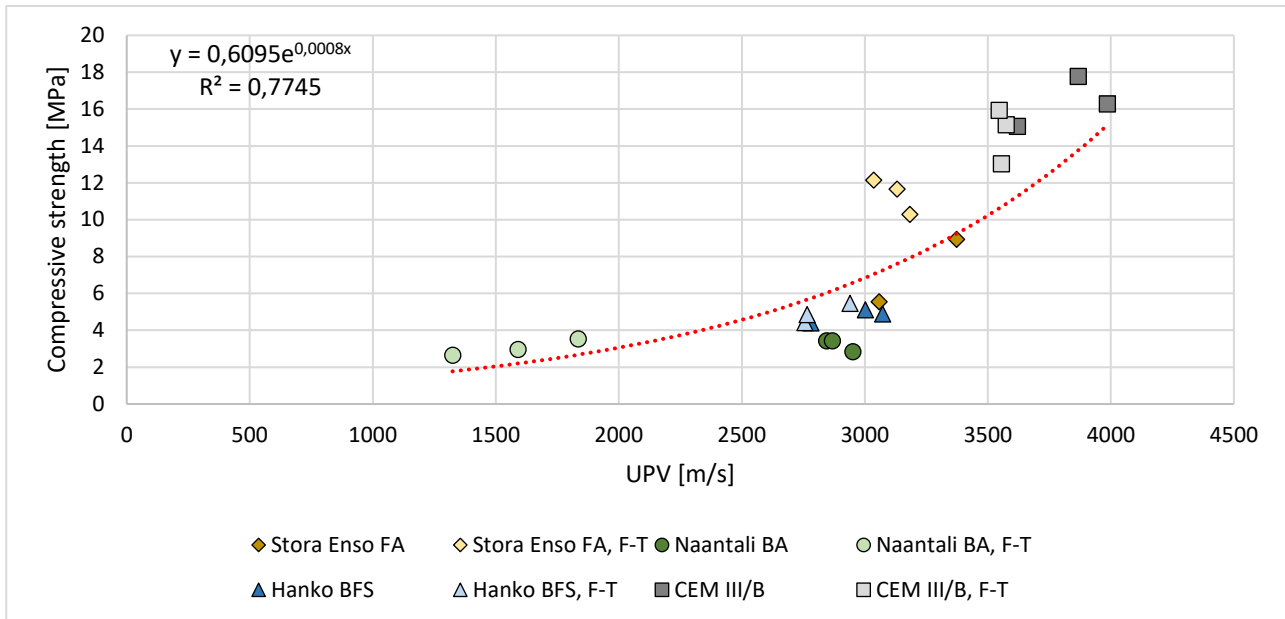


Figure 7.2. The correlation between UPV values and the UCS values of the samples made by ramming. Aggregate: QF 0-8 mm. Values have been measured after 28 days of curing. For F-T samples values have been measured after additional 10 freeze-thaw cycles.

Beyond minor inconsistencies attributable to sample variability, notable anomalies were observed in samples produced through the casting method. Figures 7.3 and 7.4 reveal that, for instance, samples prepared with CEM III/B and subjected to freeze-thaw cycles exhibit significantly higher UCS values compared to those prepared with Hanko BFS, Naantali BA or Stora Enso FA. Intriguingly, the UPV value for the CEM III/B sample remains roughly the same or even lower than that of samples produced with other binder materials.

Upon scrutinizing the interplay between UPV and UCS in specific materials, it is evident that freeze-thaw cycles induce a decrease in UPV values. However, in samples prepared by ramming with the VTT hammer, the UCS values exhibit relative stability even as UPV values decline. In contrast, when samples are prepared by the casting method, it is observed that a decrease in UPV values correlates with a decrease in UCS values.

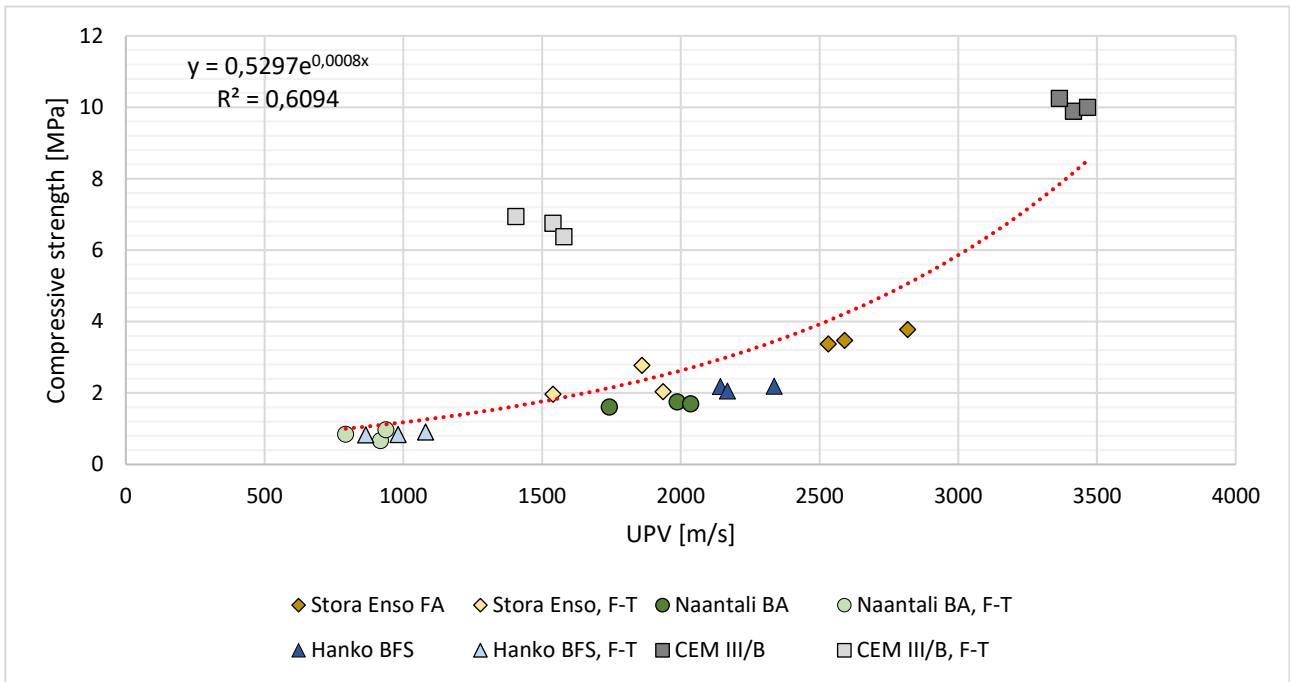


Figure 7.3. The correlation between UPV values and the UCS values of the samples made by casting. Aggregate: QF 0-8 mm. Values have been measured after 28 days of curing. For F-T samples values have been measured after additional 10 freeze-thaw cycles.

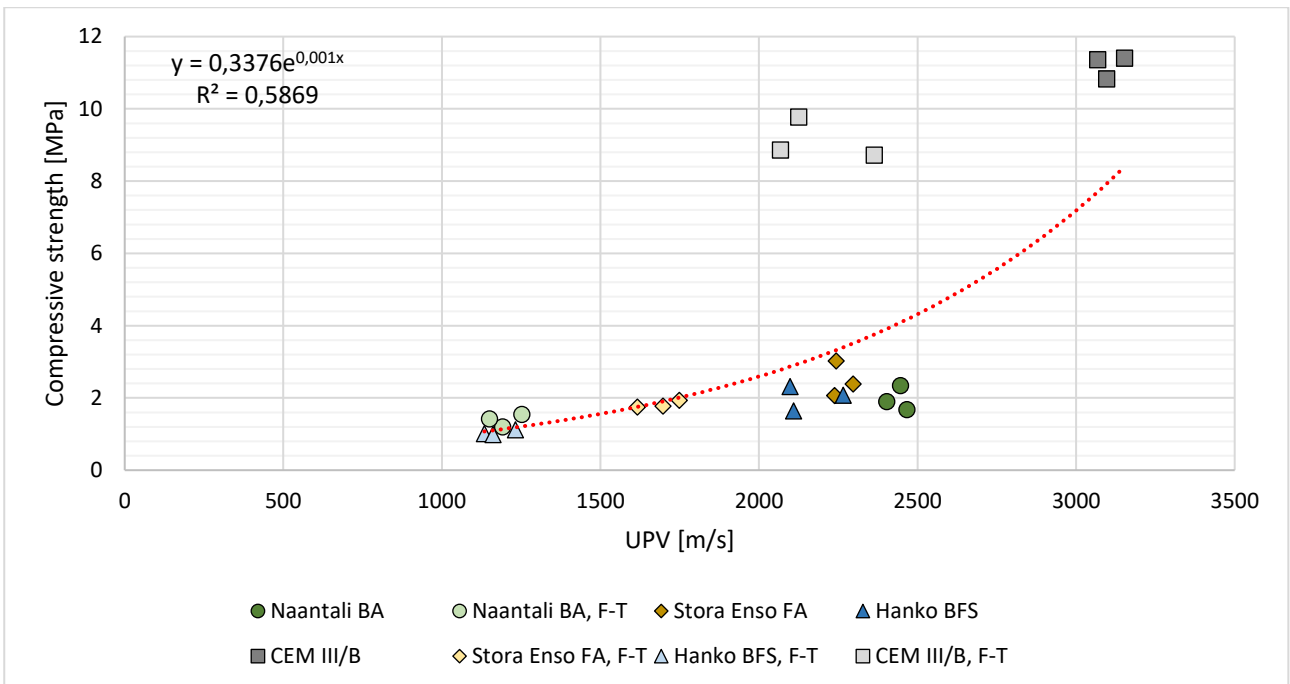


Figure 7.4. The correlation between UPV values and the UCS values of the samples made by casting. Aggregate: CC+QF 0-3 mm. Values have been measured after 28 days of curing. For F-T samples values have been measured after additional 10 freeze-thaw cycles.

In summary, the UPV may not be an inherently precise method for directly comparing the strength properties of distinct materials. The correlation between UPV and UCS is often empirical and subject to variation based on the unique characteristics of different materials.

However, the comparison of UPV values can offer valuable information when observing the strength increase over time within the same material. Therefore, it is recommended that regular monitoring of UPV values for the structure is implemented when a full-size structure is being constructed.

7.2 Ramming vs. casting

Figure 7.5 depicts the maximum compressive strengths of each sample, clearly indicating the higher strength properties of the ramming preparation method in this study. Samples prepared with the VTT hammer using CEM III/B achieved UCS values of 14,7-18,1. With Stora Enso FA the samples achieved UCS values of 7,3-11,4. When Naantali Ba serves as a binder, the UCS values reached 5,1-5,8 when combined with CC+QF 0-3 mm as an aggregate. With other combinations of binders and aggregates resulted more moderate levels of UCS values ranging from 4,8 MPa and below. Conversely, for samples prepared by casting, only those with CEM III/B as a binder attained decent strength levels ranging between 6,7 and 11,2 MPa. With other binders, the obtained values were notably lower, ranging from 0,8 to 3,4 MPa.

When scrutinizing the impact of freeze-thaw cycles, a general decline in UCS values is observed for samples exposed to these conditions. While the difference is not substantial, it remains perceptible, as evident in both figure 7.5 and table 7.1. Noteworthy exceptions are observed in samples created with the VTT hammer and utilizing Stora Enso FA as a binder, as these specimens exhibit increased UCS values after exposure to freeze-thaw cycles.

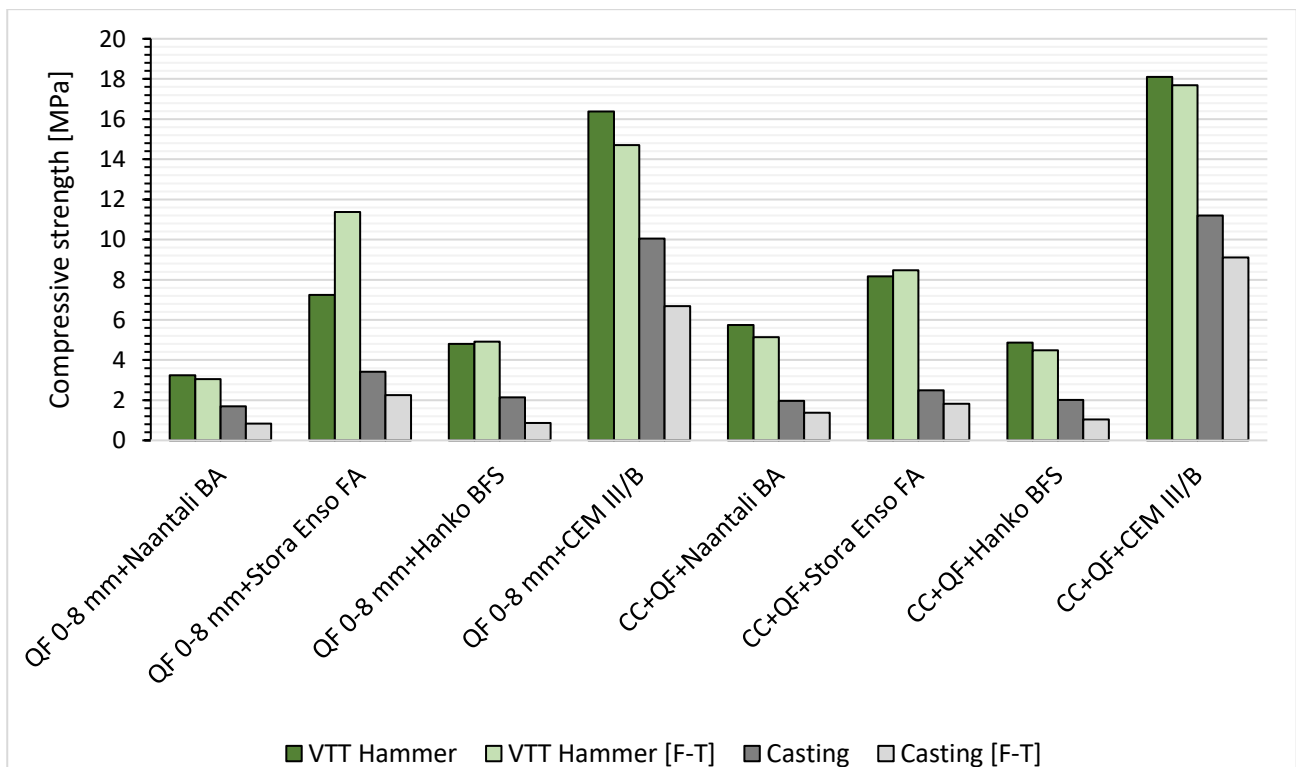


Figure 7.5. Maximum UCS values of samples. Ramming vs. casting. Values have been measured after 28 days of curing. For F-T samples values have been measured after additional 10 freeze-thaw cycles.

Table 7.1 displays the numerical values for UCS and E_{50} . The table also features the respective ratios for each value, with values above 1 indicating higher values attained with samples produced by ramming. In certain instances, the disparities in UCS values between ramming and casting reach up to ratio of 5,7, while even the smallest differences exceed ratio of 1,6.

Table 7.1. Difference of compressive strength and Young's modulus E_{50} between ramming and casting methods. Values have been measured after 28 days of curing. For F-T samples values have been measured after additional 10 freeze-thaw cycles.

	Aggregate	Binder	Aggregate-Binder ratio	Compressive strength [MPa]			Young's modulus, E_{50} [MPa]		
				Ramming	Casting	Ratio	Ramming	Casting	Ratio
No Freeze-Thaw	QF 0-8 mm	Naantali BA	1:3	3,2	1,7	1,9	142	12	12,1
	QF 0-8 mm	Stora Enso FA	1:5	7,2	3,4	2,1	459	46	9,9
	QF 0-8 mm	Hanko BFS	1:3	4,8	2,1	2,2	287	23	12,7
	QF 0-8 mm	CEM III/B	1:6	16,4	10,0	1,6	1551	324	4,8
	CC+QF 0-3 mm	Naantali BA	1:3	5,8	2,0	2,9	331	21	15,6
	CC+QF 0-3 mm	Stora Enso FA	1:5	8,2	2,5	3,3	632	28	22,6
	CC+QF 0-3 mm	Hanko BFS	1:3	4,9	2,0	2,4	282	19	15,2
	CC+QF 0-3 mm	CEM III/B	1:6	18,1	11,2	1,6	1497	158	9,5
Freeze-Thaw	QF 0-8 mm	Naantali BA	1:3	3,1	0,8	3,7	189	10	19,5
	QF 0-8 mm	Stora Enso FA	1:5	11,4	2,3	5,0	935	15	61,3
	QF 0-8 mm	Hanko BFS	1:3	4,9	0,9	5,7	257	4	59,1
	QF 0-8 mm	CEM III/B	1:6	14,7	6,7	2,2	1040	67	15,6
	CC+QF 0-3 mm	Naantali BA	1:3	5,1	1,4	3,7	276	11	26,3
	CC+QF 0-3 mm	Stora Enso FA	1:5	8,5	1,8	4,7	568	15	36,9
	CC+QF 0-3 mm	Hanko BFS	1:3	4,5	1,0	4,3	270	6	47,9
	CC+QF 0-3 mm	CEM III/B	1:6	17,7	9,1	1,9	1147	179	6,4

Table 7.2 displays the difference of density between rammed and casted samples. The table also features the respective ratios for each value, with values above 1 indicating higher values attained with samples produced by ramming. It is evident that the densities of rammed samples are generally higher, except when considering the combination of CC+QF 0-3 mm and Hanko BFS. Despite this, the densities between ramming and casting methods are consistently close to each other in all cases. Therefore, the disparity in compressive strength properties can not be solely attributed to differences in sample densities.

Table 7.2. Difference of density between ramming and casting methods. Values have been measured after 28 days of curing. For F-T samples values have been measured after additional 10 freeze-thaw cycles.

	Aggregate	Binder	Aggregate-Binder ratio	Density [kg/m ³]		
				Ramming	Casting	Ratio
No Freeze-Thaw	QF 0-8 mm	Naantali BA	1:3	2242,6	2145,6	1,05
	QF 0-8 mm	Stora Enso FA	1:5	2300,1	2256,2	1,02
	QF 0-8 mm	Hanko BFS	1:3	2141,0	2163,2	0,99
	QF 0-8 mm	CEM III/B	1:6	2404,0	2216,7	1,08
	CC+QF 0-3 mm	Naantali BA	1:3	2081,0	2034,6	1,02
	CC+QF 0-3 mm	Stora Enso FA	1:5	2044,5	1888,6	1,08
	CC+QF 0-3 mm	Hanko BFS	1:3	1978,9	2010,1	0,98
	CC+QF 0-3 mm	CEM III/B	1:6	2191,8	2031,4	1,08
Freeze-Thaw	QF 0-8 mm	Naantali BA	1:3	2251,7	2144,8	1,05
	QF 0-8 mm	Stora Enso FA	1:5	2296,7	2222,5	1,03
	QF 0-8 mm	Hanko BFS	1:3	2155,9	2155,8	1,00
	QF 0-8 mm	CEM III/B	1:6	2400,9	2163,7	1,11
	CC+QF 0-3 mm	Naantali BA	1:3	2050,8	2000,9	1,02
	CC+QF 0-3 mm	Stora Enso FA	1:5	2036,7	1799,2	1,13
	CC+QF 0-3 mm	Hanko BFS	1:3	1959,8	1935,5	1,01
	CC+QF 0-3 mm	CEM III/B	1:6	2128,2	2116,6	1,01

Figures 7.6 and 7.7 depict the stress-strain curves of samples prepared through ramming and casting, utilizing CC+QF 0-3 mm aggregate along with Stora Enso FA or CEM III/B as a binder. These figures reveal substantial distinctions among the stress-strain curves. These differences provide a more comprehensive understanding of disparities resulting from the various preparation methods applied to these samples. Notably, the figures illustrate that when samples were prepared using the VTT hammer, the effects of freeze-thaw cycles were negligible. Conversely, for samples produced through casting, freeze-thaw cycles markedly diminished both peak compressive strengths and E_{50} values. The figures also indicate that there is a notably small amount of strain for both the rammed earth and the casting technique with these materials. However, a distinct contrast between the methods is evident, with the UCS peak value achieved at approximately 0,005% strain with rammed earth method. In contrast, the strain measured at the peak values with the casting technique varies, ranging from about 2 to 15 times higher than with the rammed earth samples.

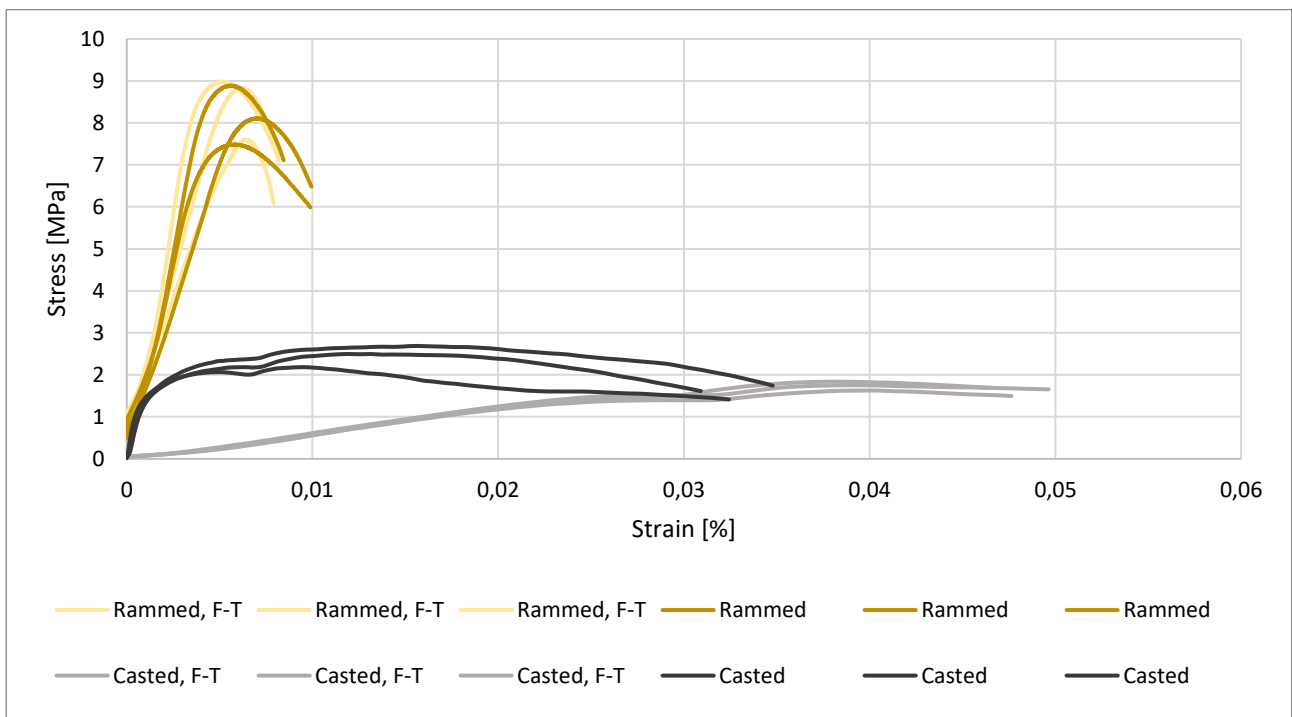


Figure 7.6. Difference of stress-strain curves between rammed and casted samples. Material: CC+QF 0-3 mm+Stora Enso FA. Values have been measured after 28 days of curing. For F-T samples values have been measured after additional 10 freeze-thaw cycles.

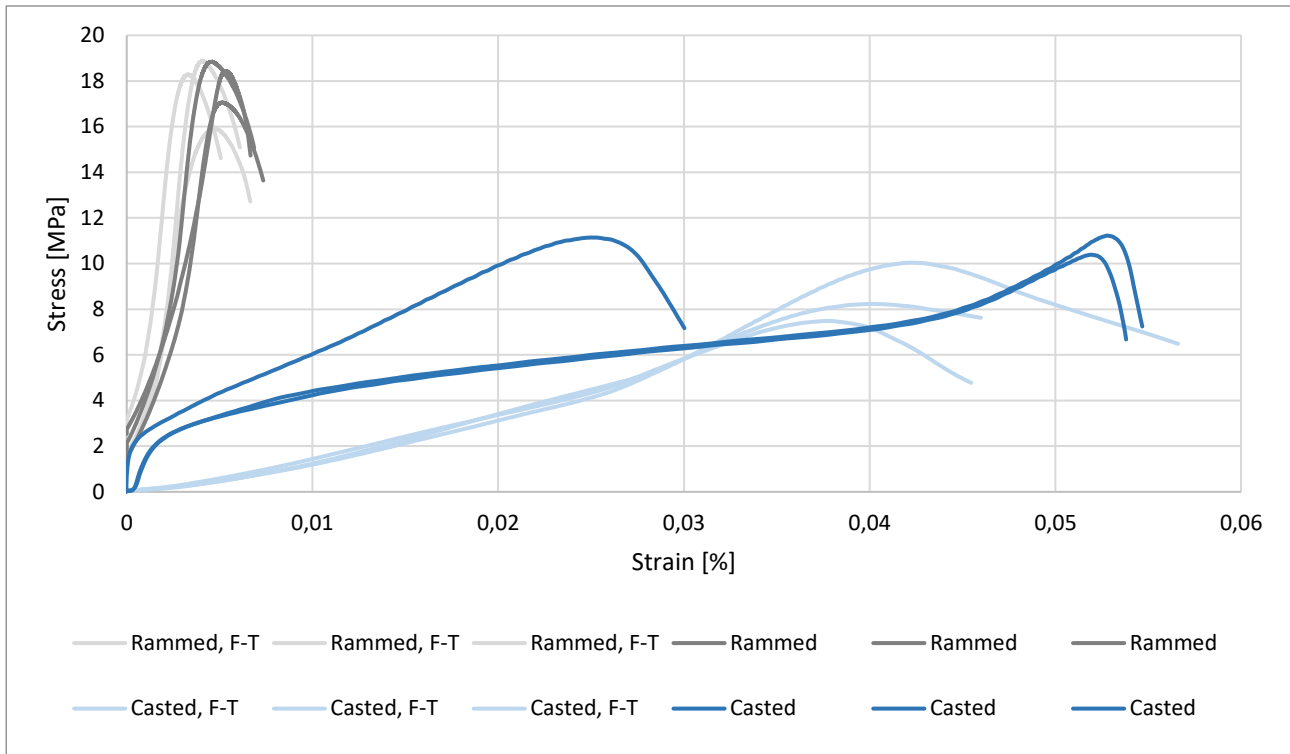


Figure 7.7. Difference of stress-strain curves between rammed and casted samples. Material: CC+QF 0-3 mm Values have been measured after 28 days of curing. For F-T samples values have been measured after additional 10 freeze-thaw cycles.

The contrast in results between ramming and casting in this study is evident. However, the reasons for the markedly higher values observed in rammed samples compared to casted samples could be attributed to several factors. Firstly, a notable enhancement in the research would involve conducting tests with samples of identical dimensions. In this study, the rammed samples were cylindrical, with a diameter of 100 mm and a height ranging from approximately 140 to 170 mm. In contrast, the casted samples took the form in prisms measuring 40x40x160 mm. The discrepancy in mould sizes inherently positioned the samples unevenly, given that the maximum grain size for the rammed samples was 16 mm, whereas for the casted samples, it was 8 mm. For future research, it is recommended that, larger casting moulds are used to achieve a more comparable maximum grain size.

Moreover, the compaction inherent in the ramming method results in slightly higher material density, which is subsequently correlated with increased compressive strength. However, since the difference between the densities were not significant, it is possible that the combination of the smaller particles and decreased density are causing the differences in compressive strength. One possible factor could also be the increased water content, which will lead into lowered cohesion between the particles. When using cement, the hydration process will create bonds that substitutes the decreased cohesive forces, but it can be concluded from the binder testing done in this thesis, that the hydration process is not as strong with recycled materials than it is with cement.

The primary vulnerability of casted samples is likely attributed to void formation. The casting process makes the samples more prone to void formation, especially when the vibration

is made with the jolting machine that was used in this study, instead of vibrating table. With ramming method, the compaction of the VTT hammer likely prevents the formation of excess voids. The porosity of the material could also account for the recorded lower UPV values in casted samples and their lowered freeze-thaw durability.

As always, testing variability and the heterogeneity of the materials used may influence the results. This influence could be mitigated by expanding the size of the test sets. However, given the relatively low coefficient of variation between samples within the same test set in this research, it can be inferred that the impact of testing variability is also minimal.

7.3 Effects of freeze-thaw cycles

The impact of the freeze-thaw cycles has been tested and analyzed throughout the thesis. Table 7.3 presents the UCS values, while table 7.4 displays the UPV values for both rammed and casted samples. Additionally, the tables also feature the corresponding ratios for each value, where ratios exceeding 1 signify higher values observed in samples tested without exposure to freeze-thaw cycles.

When scrutinizing the impact of freeze-thaw cycles from table 7.3, a general decline in UCS values is observed for samples exposed to these conditions. For rammed samples the difference is not substantial, but it remains perceptible, since the ratio values are mostly slightly above 1. Noteworthy exceptions are observed in rammed samples utilizing Stora Enso FA as a binder, as these specimens exhibit increased UCS values after exposure to freeze-thaw cycles. This could be due to the on-going curing process, that has increased the UCS values for the sample during the 10 days of freezing and thawing cycles. To research this, it is necessary to conduct UCT tests after 90 days of curing, to ensure that the samples have reached their final strengths and then compare the values before and after freeze-thaw cycles.

For the casted samples, there is a substantial difference observed before and after freeze-thaw cycles, as indicated by the ratios ranging from 1,23 to 2,03 in table 7.3. This discrepancy may be attributed to the increased porosity of casted samples, rendering them more susceptible to the freeze-thaw effect. Additionally, casted samples typically have higher water content, and any presence of unreacted water could lead to the expansion of freezing water, further weakening the samples in comparison to rammed samples. Moreover, the weakness of casted samples from the outset makes them more susceptible to the effects of freeze-thaw cycles when compared with rammed samples.

Table 7.3. Difference of compressive strength for ramming and casting methods before and after freeze-thaw cycles. Values have been measured after 28 days of curing. For F-T samples values have been measured after additional 10 freeze-thaw cycles.

Aggregate	Binder	Aggregate-Binder ratio	Compressive strength Ramming [MPa]			Compressive strength Casting [MPa]		
			No Freeze-thaw	Freeze-thaw	Ratio	No Freeze-thaw	Freeze-thaw	Ratio
QF 0-8 mm	Naantali BA	1:3	3,2	3,1	1,06	1,7	0,8	2,03
QF 0-8 mm	Stora Enso FA	1:5	7,2	11,4	0,64	3,4	2,3	1,51
QF 0-8 mm	Hanko BFS	1:3	4,8	4,9	0,98	2,1	0,9	2,49
QF 0-8 mm	CEM III/B	1:6	16,4	14,7	1,11	10,0	6,7	1,50
CC+QF 0-3 mm	Naantali BA	1:3	5,8	5,1	1,12	2,0	1,4	1,42
CC+QF 0-3 mm	Stora Enso FA	1:5	8,2	8,5	0,96	2,5	1,8	1,37
CC+QF 0-3 mm	Hanko BFS	1:3	4,9	4,5	1,09	2,0	1,0	1,94
CC+QF 0-3 mm	CEM III/B	1:6	18,1	17,7	1,02	11,2	9,1	1,23

Table 7.4 shows that both rammed and casted samples are experiencing a decline following freeze-thaw cycles. For rammed samples the decrease of the values is more subtle, since the ratios are varying from 1,03 to 1,82. Notably, the change in the UPV values does not completely correlate with the change of UCS values before and after freeze-thaw exposure. Some of the UCS values increased, despite the decrease in UPV values after freeze-thaw cycles. Conversely, for casted samples, the decrease of UPV values is significant, varying from 1,23 to 2,49. These values correlate well with the substantial decrease in UCS values after freeze-thaw cycles.

Table 7.4. Difference of UPV values for ramming and casting methods before and after freeze-thaw cycles. Values have been measured after 28 days of curing. For F-T samples values have been measured after additional 10 freeze-thaw cycles.

Aggregate	Binder	Aggregate-Binder ratio	UPV - Ramming [m/s]			UPV - Casting [m/s]		
			No Freeze-thaw	Freeze-thaw	Ratio	No Freeze-thaw	Freeze-thaw	Ratio
QF 0-8 mm	Naantali BA	1:3	2887,3	1583,0	1,82	1922,0	882,3	2,18
QF 0-8 mm	Stora Enso FA	1:5	3208,0	3116,3	1,03	2646,7	1779,0	1,49
QF 0-8 mm	Hanko BFS	1:3	2951,3	2820,0	1,05	2216,0	975,7	2,27
QF 0-8 mm	CEM III/B	1:6	3824,0	3558,0	1,07	3415,3	1508,3	2,26
CC+QF 0-3 mm	Naantali BA	1:3	3133,7	2658,7	1,18	2438,0	1197,7	2,04
CC+QF 0-3 mm	Stora Enso FA	1:5	2950,7	2519,3	1,17	2259,0	1687,0	1,34
CC+QF 0-3 mm	Hanko BFS	1:3	2713,0	2479,3	1,09	2157,0	1175,3	1,84
CC+QF 0-3 mm	CEM III/B	1:6	3753,3	3483,3	1,08	3105,0	2185,0	1,42

In general, the rammed samples appear to withstand the effects of freezing and thawing quite effectively. Conversely, the UCS values of the casted samples experienced a notable decrease, posing a concern in Finland where multiple freeze-thaw cycles occur annually. The primary limitation of the freeze-thaw testing in this instance was the relatively short duration, consisting only 10 cycles. To obtain more pertinent data regarding the freeze-thaw durability of the material, it would be advantageous to conduct tests for a minimum of 28 days in the future. Additionally, a more realistic scenario could involve exposing the samples to additional water during the freeze-thaw cycles.

7.4 Comparison with previous research

Comparison of the maximum UCS values is depicted in the figure 7.8. All samples included in the comparison that were made with ramming method, have been made using the VTT hammer. The assessment of inter-work strength properties of materials primarily focuses on samples not subjected to freeze-thaw cycles, as not all research investigated the effects of such tests. Various studies encompassed a range of aggregate and binder materials, resulting in a substantial number of samples. However, the emphasis here is on comparing the best outcomes and materials.

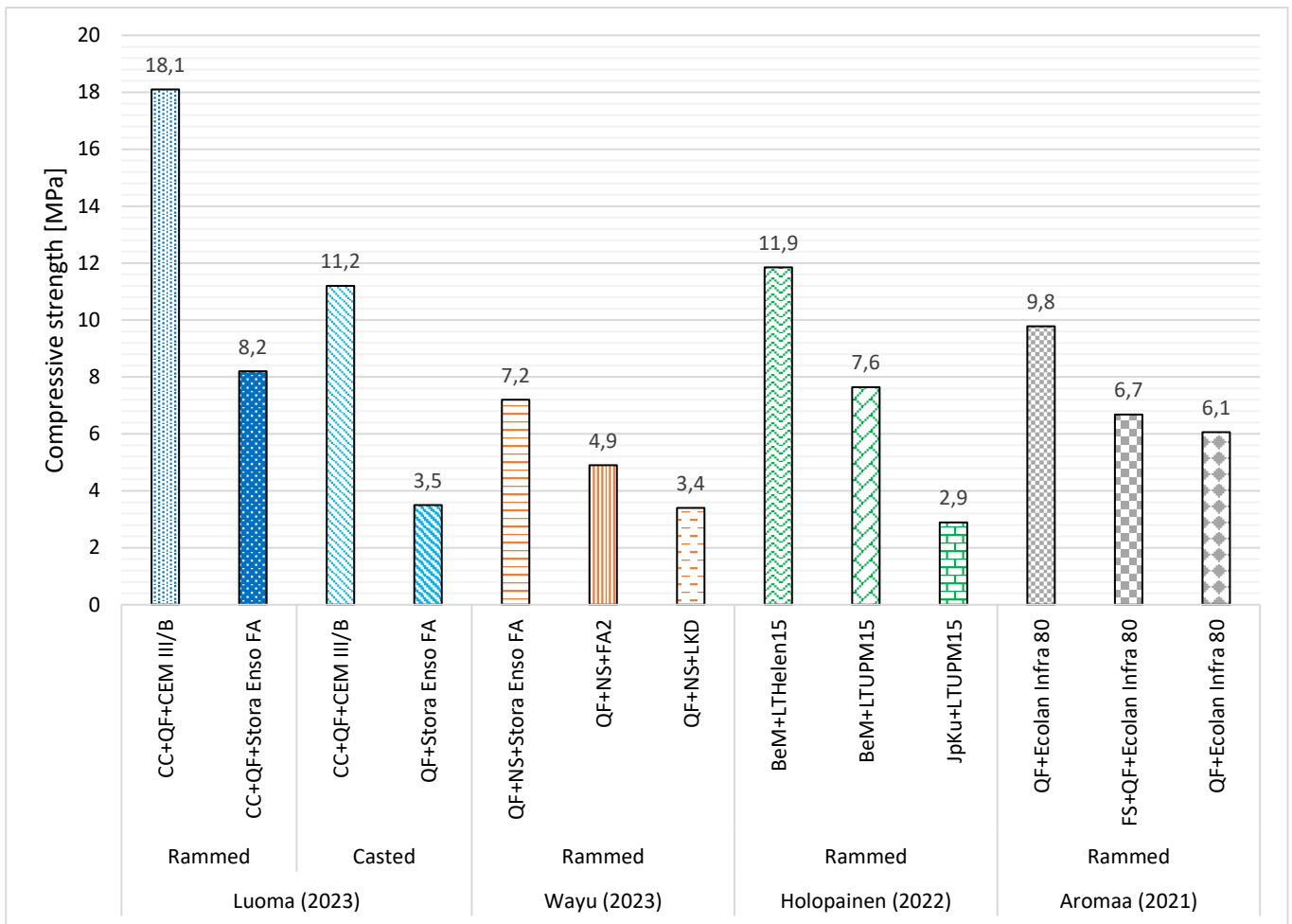


Figure 7.8. Comparison of the compressive strengths between previous researches. Values have been measured after 28 days of curing. (NS=Nilsia Sand; BeM=crushed concrete; LT=Fly ash; FS=Foundry sand; JpKu=Waste incineration slag)

In Wayu's (2023) study, the first aggregate used was quartz-silica sand from the Nilsia quarry (NS). The second aggregate employed in his study was quarry fines from Kiertomaa Oy's Saramaki site, also featured in this work. The quarry fines utilized had a particle size 0-8 mm. While exploring various binder options, the majority exhibited unsatisfactory performance. Wayu's investigation included an examination of Stora Enso FA, which was chosen for this study due to its preliminary results. The reported strength properties in Wayu's study were generally moderate. Stora Enso FA proved to be the most effective binder, demonstrating improved strengths when combined with a QF 0-8 mm+NS mixture in equal proportions (50 % each). This combination resulted in compressive strength around 7 MPa.

Holopainen (2022) examined waste incineration slag, crushed concrete, and a combination of excavated fly ash and desulphurization by-product as aggregates in his thesis. Binders he investigated included fly ash from coal combustion at Helsingin Energia (Helen) and fly ash from UPM bio-based fly ash. Both Helen's and UPM's fly ashes demonstrated effective binding properties. With the aggregates, the only satisfactory results were obtained with crushed concrete as an aggregate. However, when utilizing crushed concrete and Helen fly ash or UPM fly ash the results were good. The material that composed of crushed concrete and Helen fly ash exhibited a compressive strength of 11,85 MPa, and the combination of UPM

fly ash and crushed concrete resulted in a compressive strength of 7,64 MPa. In contrast the combination of waste incineration slag (JpKu) and UPM fly ash yielded only 2,9 MPa. This is a noteworthy illustration of how varying aggregates can influence the compressive strength of the material.

In Aromaa's study (2021), quarry fines and a combination of quarry fines and foundry sand, with equal proportions of 50% for each aggregate were employed. The binder under investigation was a commercial product called Ecolan Infra 80, comprising 80% coal combustion fly ash and 20% cement and additional materials. It is noteworthy that the current production of Ecolan Infra 80 may no longer align with the formulation used in Aromaa's study. At its peak, the material formed by quarry fines and Ecolan Infra 80 attained an average strength of 9,78 MPa. Meanwhile, the aggregate comprised of foundry sand and quarry fines reached a maximum compressive strength of 6,68 MPa. A notable aspect of Aromaa's work is the exceptionally low amount of binder utilized, as the strengths achieved demonstrated an aggregate-binder ratio of 1:9. Additionally, test samples with a ratio of up to 1:15,5 were examined, and the highest compressive strength obtained was 6,72 MPa. This illustrates that the aggregate-binder ratio of functional commercial product can be adjusted quite low if desired while still achieving high strengths.

7.5 Aggregates

The optimal results from the ICT experiments were obtained with QF 0-8 mm and CC+QF 0-3 mm as aggregates. Consequently, these aggregates were chosen for both the rammed earth technique and the casting technique. In both cases, the grain size distribution was favorable, encompassing both fine and slightly coarser grain sizes.

Upon considering the preparation method and the binder, both materials proved highly suitable as aggregates. However, CC+QF 0-3 mm exhibited the highest compressive strengths. It is anticipated that for larger structures, the difference in favor of CC+QF 0-3 mm may become more pronounced. This is attributed to the fact that the crushed concrete used in the aggregate had a grain size distribution of 0-63 mm, allowing for the potential to obtain an aggregate with an even broader grain size if the construction specifications permit.

The aggregate comprising crushed concrete and 0-3 mm quarry fines offers the added advantage of limited market appeal for alternative commercial applications. Given its coarser grain size, QF 0-8 mm is well-suited for various applications in construction industry. Hence, it has a higher commercial value in comparison to crushed concrete or QF 0-3 mm. Therefore, it is recommended to give preference to materials with reduced commercial value.

7.6 Binders

The investigated binders included bio-based bottom and fly ash from the Naantali power plant, blast furnace slag from the former Koverhar steelworks in Hanko, bio-based fly ash from Stora Enso Varkaus, and CEM III/B as a commercial environmentally friendly alternative.

The fly ash from the Naantali power plant was promptly deemed unsuitable for the intended purpose, as the resulting pieces exhibited softness and failed to strengthen during curing process. Conversely, the bottom ash from the Naantali power plant demonstrated considerable strength of 18,8 MPa when 20% of CEM I was utilized as an activator in the mixture. However, when subjected to ICT testing, Naantali BA proved weaker than anticipated, necessitating an increase in its aggregate-binder ratio to 1:3.

Despite the modest performance in ICT tests, the material formed by CC+QG 0-3 mm and Naantali BA reached a compressive strength of 3,02 MPa. Nevertheless, it was decided to include Naantali BA in the rammed earth and casting test samples, with the anticipation that an extended curing time might enhance its strength properties. After 28 days, it was observed that Naantali BA performed decently in the rammed earth method, when combined with crushed concrete and quarry fines. With CC+QF 0-3 mm as an aggregate, the sample achieved a compressive strength of 5,8 MPa. However, with casting method the Naantali BA exhibited the lowest performance among all the binders, yielding a compressive strength of only 2 MPa.

Hanko BFS exhibited low strength characteristics based on preliminary binder tests. Nevertheless, it was decided to further investigate the material through ICT tests and by creating test samples using rammed earth and casting techniques. Following the ICT tests, it was determined to employ a 1:3 aggregate-binder ratio for Hanko BFS. With ramming method, Hanko BFS achieved nearly 5 MPa with both aggregates, attaining a compressive strength of 4,9 MPa when combined with the CC+QF 0-3 mm. Unfortunately, the casting technique resulted in average compressive strengths remaining in the range of 1-2 MPa. Additionally, Hanko BFS exhibited significant moisture content and a coarse-grained texture. Using it as a binder would likely necessitate drying and, at the very least, sieving. Therefore, the utilization of Hanko BFS would entail considerable additional effort, coupled with the fact that its strength properties were at the lower end of the test set.

Stora Enso FA was introduced to the study at a later stage, prompted by the rejection of Naantali FA in initial tests, and the unsatisfactory performance of Naantali BA and Hanko BFS in terms of their strength properties. Despite its geographical distance from Turku, Stora Enso FA was included in the investigation with the anticipation that similar ashes might be available closer to the site in the future, providing a foundation for subsequent studies. In the binder test, Stora Enso FA achieved a compressive strength of 7,5 MPa and a flexural strength of 2,5 MPa after 28 days of curing. The aggregate-binder ratio was determined based on tests conducted by Wayu (2023), resulting in a ratio of 1:5.

In the rammed earth method, Stora Enso FA attained a maximum compressive strength of 11,4 MPa. Notably, samples made with Stora Enso FA exhibited an increase in compressive strength during freeze-thaw cycles when utilizing the rammed earth technique. Like other recycled materials, Stora Enso FA exhibited moderate performance in samples created with the casting technique, reaching a maximum compressive strength of 3,4 MPa for the QF 0-8 mm as an aggregate. However, considering the considerable logistical distance of Stora Enso FA from the Turku region, it may present challenges for practical use in wall structure. Nevertheless, due to its favorable characteristics, its usage could be comparatively less than,

for instance, Naantali BA or Hanko BFS. This would mitigate potential concerns related to transportation costs and emissions, even over considerable distances.

CEM III/B was included in laboratory testing at a later stage, following a similar reasoning as Stora Enso FA. Given that CEM III/B is a commercial product, the attained strengths are expected to be relatively consistent, aligning with the values specified in the product documentation. Binder tests were conducted, revealing that CEM III/B samples achieved an average compressive strength of 39 MPa and a flexural strength of 5,5 MPa. The ICT tests indicated that the lowest aggregate-binder ratio examined, 1:6, could be chosen. This ratio could potentially be further reduced based on the final results of the study.

Employing the rammed earth technique, CEM III/B demonstrated an exceptional compressive strength of 18,1 MPa when using CC+QF 0-3 mm, marking the highest result in the entire test. Even the lowest value of 14,7 MPa obtained with the rammed earth technique surpassed the second-best binder in the tests, Stora Enso FA. CEM III/B was the sole binder in the tests to achieve high strengths in the casted samples, ranging from a high of 11,2 MPa to a low of 6,7 MPa. Despite containing 30 % cement, the significantly higher strength properties allow the use of smaller quantities of binder compared to the aggregate. Consequently, the proportion of cement in the total weight of the material remains within the same range as other binders tested in the study, while achieving the highest strength properties.

8 Conclusions and recommendations for further research

The objective of this study was to identify the optimal composition for a non-load bearing wall structure using recycled materials. Additionally, alternative construction methods, specifically rammed earth, and casting techniques, were investigated for their influence on material properties. While the primary focus was on compressive strength, the study also explored the freeze-thaw durability. The utility of UPV values in structures constructed from recycled materials was also examined.

Laboratory investigations revealed that rammed samples exhibited significantly higher strengths compared to those prepared through the casting method. Furthermore, it was observed that UPV values could offer indicative information but were not a reliable method for comparing different materials. However, they proved useful for monitoring the evolution of strength properties over time without destructing the structure. When assessing the impact of freeze-thaw cycles, it was noted that freezing and thawing alone, without exposure to water or salt, had minimal effect on samples prepared using the rammed earth technique with these materials. Conversely, for casted samples, the compressive strength was approximately 30% lower on average after undergoing freeze-thaw cycles.

The investigation delved into the manufacturing processes of both rammed earth and casting techniques and analyzed the implications of various choices made during these processes. The compressive strength of the samples was contingent on factors such as the type of aggregate employed, the quantity and quality of the binder, and the water content. Quarry fines and combination of quarry fines and crushed concrete were the aggregates utilized in the research. These aggregates were systematically employed to ascertain the optimal water content for sample preparation. The samples were prepared with the dual objective of achieving an optimal aggregate-binder ratio for each material combination to ensure sufficient strength while minimizing the use of cement. The study allowed the samples to set for 7 days to ascertain the optimum aggregate-binder ratio and 28 days to identify the optimal material combination and its corresponding compressive strengths. Unfortunately, the investigation could not incorporate the results from a subsequent 90 days of cured samples.

For further research is proposed comprehensive study of these materials on a larger scale. This could entail establishing an experimental structure where the properties of the materials are examined at a real scale and under various environmental conditions. Exploring opportunities for optimizing different construction methods would be beneficial in this context. The construction phase in the case of rammed earth can be labor-intensive without optimization. The construction of structures using casting technology and precast interlocking concrete blocks becomes more streamlined if structures made from recycled materials can be rendered more durable. Another valuable aspect of research would be to assess the cost-efficiency of structures that were constructed with recycled materials and ramming method or using PICBs. To further advance in this field, a life-cycle analysis is recommended to evaluate the environmental impact of a rammed earth or PICB structure constructed from recycled materials. While recycled materials were primarily studied in this work as an ecologically friendly alternatives to a high carbon footprint virgin materials, conducting an analysis of the actual environmental impact would be insightful for further development.

Regarding binders, future research could concentrate on investigating various activators and the composition of the binders. Ashes and slag inherently exhibit slow hydration process, posing a potential challenge if these materials are to be utilized in the construction industry in the future. In this study, only CEM I was employed as an activator; however, the introduction of alkali solutions, such as lye, may enhance the reactivity of the materials, consequently reducing their curing time. Further examination of the binder compositions could provide insights into the elements influencing the binders and the reasons behind variations in their performance.

To integrate recycled materials alongside conventional materials and methods, a productization process is essential. This process involves through study and testing of the materials, resulting in a new, competitive product for the market. Legislative support plays a role in productization, and the willingness of customers, producers, and designers to embrace innovation is crucial. The primary challenge for recycled materials lies in their variable quality. To enhance their incorporation into building technology, extensive research on potential binder materials should be conducted using consistent methodologies. This approach aims to identify effective products and reasons for their success, leading to the creation of standardized products with as predictable properties as possible.

References

- Alahrache, S. Winnefeld, F. Champenois, J-B. Hesselbarth, F. Lothenbach, B. 2016. Chemical activation of hybrid binders based on siliceous fly ash and Portland cement. *Cement and Concrete Composites*. Vol. 66. pp. 10-23. ISSN 0958-9465.
- Alwathaf, A.H. Thanoon, W.A. Jaafar, M.S. Noorzaei, J. Kadir, M.R.A. 2005. Shear Characteristic of Interlocking Mortarless Block Masonry Joints. *Masonry International*. Vol. 18. pp. 139-146.
- Aromaa, R. 2021. Uusiomateriaaleista valmistetun hydraulisesti sitoutuvan meluseinän pakkaskestävyys. Master's thesis. Master's programme in Geoengineering. Aalto University. Espoo, Finland. 70 p.
- Arrigoni, A. Beckett, C.T.S. Ciancio, D. Pelosato, R. Dotelli, G. Grillet, A-C. 2018. Rammed Earth incorporating Recycled Concrete Aggregate: a sustainable, resistant and breathable construction solution. *Resources, Conservation and Recycling*. Vol. 137. pp. 11-20. ISSN 0921-3449. <https://doi.org/10.1016/j.rescon-rec.2018.05.025>.
- Aswad, A. Yilmaz, M.C. Ismail, S.H. 2022. A Systematic review study on different kinds of interlocking concrete blocks designs and properties. *Turkish Journal of Engineering*. 6(4). pp. 327-337. ISSN 2587-1366. <https://doi.org/10.31127/tuje.931076>
- Attri, G.K. Gupta, R.C. Shrivastava, S. 2022. Sustainable precast concrete blocks incorporating recycled concrete aggregate, stone crusher, and silica dust. *Journal of Cleaner Production*. Vol. 362. 132354. ISSN 0959-6526. <https://doi.org/10.1016/j.jclepro.2022.132354>.
- Autiola, M. 2023. Uusiosideaineet koheesiomaiden stabiloinnissa-käyttökokemukset ja ympäristövaikutukset. Pohjanvahvistuspäivä 2023. Aalto Yliopisto. 28.8.2023. [Cited 2 Nov 2023] Available at: <https://sgy.fi/content/uploads/2023/05/uusiosideaineet-koheesiomaiden-stabiloinnissa-kayttokokemukset-ja-ymparistovaikutukset-opas-merja-autiola.pdf>
- Ávila, F. Puertas, E. Gallego, R. 2021. Characterization of the mechanical and physical properties of unstabilized rammed earth: A review. *Construction and Building materials*. Vol. 270. ISSN 0950-0618. <https://doi.org/10.1016/j.conbuildmat.2020.121435>.
- Beckett, C. Ciancio, D. 2014. Effect of compaction water content on the strength of cement-stabilized rammed earth materials. *Canadian Geotechnical Journal*. Vol. 51. Issue 5. pp. 583-590. <https://doi.org/10.1139/cgj-2013-0339>.
- Bui, Q.B. Morel, J.C. Venkatarama Reddy, B.V. Ghayad, W. 2009. Durability of rammed earth walls exposed for 20 years to natural weathering. *Building and Environment*. Vol. 44. Issue 5. pp. 912-919. ISSN 0360-1323. <https://doi.org/10.1016/j.buildenv.2008.07.001>.
- CEN/TS 13286-54:en. 2014. Unbound and hydraulically bound mixtures. Part 54: test method for the determination of frost susceptibility. Resistance to freezing and thawing of hydraulically bound mixtures. Helsinki: Finnish standards association. 17 p.
- Courland, R. 2011. *Concrete Planet: The Strange and Fascinating Story of the World's Most Common Man-made Material*. Prometheus Books. 396 p. ISBN 978-1616144814.

- Cristelo, N. Glendinning, S. Miranda, T. Oliveira, D. Silva, R. 2012. Soil stabilization using alkaline activation of fly ash for self compacting rammed earth construction. *Construction and Building materials*. Vol. 36. pp. 727-735. ISSN 0950-0618. <https://doi.org/10.1016/j.conbuildmat.2012.06.037>.
- Dahmen, A.J. 2015. 'Who's afraid of raw earth? Experimental wall in New England and the environmental cost of stabilization', in D. Ciancio, C. Beckett (eds). *Rammed Earth Construction – Cutting-Edge Research on Traditional and Modern Rammed Earth*. CRC Press. pp. 85-88. ISBN 978-1-138-02770-1.
- Delatte, N.J. 2001. Lessons from Roman Cement and Concrete. *Journal of Professional Issues in Engineering Education and Practice*. Vol. 127. Issue 3. American Society of Civil Engineers. pp. 109-115. ISSN 1052-3928. [https://doi.org/10.1061/\(ASCE\)1052-3928\(2001\)127:3\(109\)](https://doi.org/10.1061/(ASCE)1052-3928(2001)127:3(109)).
- Fibo Intercon. [Cited 25 Nov 2023]. Available at: [How To Make Concrete Blocks - Fibo Intercon Batching Plant](#)
- Finnsementti Oy. 2023. Käyttöturvallisuustiedote CEM I 42,5 R Parainen. [Cited 6 Dec 2023]. Available at: https://finnsementti.fi/wp-content/uploads/Ykkossementti_ktt_2021-01-21.pdf.
- Finnsementti Oy. 2023. Käyttöturvallisuustiedote CEM III/B 42,5 L-LH/SR Parainen. [Cited 6 Dec 2023]. Available at: https://finnsementti.fi/wp-content/uploads/KolmosBertta_ktt_fi_29042022.pdf.
- Fitz, L. Elliot, M. 2016. More Than Square. *Structure Magazine*. pp. 39-41. [Cited 26 Nov 2023]. Available at: <https://www.structuremag.org/?p=9872>.
- Greenspec. [Cited 6 Nov 2023]. Available at: <https://www.greenspec.co.uk/building-design/rammed-earth/>
- Guerra, B. C. Shahi, S. Mollaei, A. Skaf, N. Weber, O. Leite, F. Haas, C. 2021. Circular economy applications in the construction industry: A global scan of trends and opportunities. *Journal of Cleaner Production*, Volume 324. ISSN 0959-6526. <https://doi.org/10.1016/j.jclepro.2021.129125>.
- Holopainen, K. 2022. Uusiomateriaaleista suljetun maan tekniikalla valmistettu meluseinäkoerakenne. Master's thesis. Master's programme in Geoen지니어ing. Aalto University. Espoo, Finland. 89 p.
- Hogan-O'Neill, W.J. 2021. *Prefabricated and Modular Architecture – Aligning Design with Manufacture and Assembly*. The Crowood Press Ltd. 176 p. ISBN 978-1-78500-807-8.
- Iskhakov, I. Ribakov, Y. 2021. Structural phenomenon based theoretical model of concrete tensile behaviour at different stress-strain conditions. *Journal of Building Engineering*. Vol. 33. ISSN 2352-7102. <https://doi.org/10.1016/j.jobbe.2020.101594>.
- Jaquin, P. 2012. 'History of earth building techniques', in M.R. Hall, R. Lindsay, M. Krayenhoff (eds). *Modern Earth Buildings*. Woodhead Publishing. pp. 307-323. ISBN 978-0-85709-026-3
- Jaquin, P. Augarde, C. 2012. *Earth building*. Watford, United Kingdom: IHS BRE Press. 100 p. ISBN 978-1-84806-192-7.
- Jaquin, P. Augarde, C. Gallipoli, D. Toll, D.G. 2009. The strength of unstabilised rammed earth materials. *Geotechnique*. Vol. 59. Issue 5. pp. 487-490. ISSN 0016-8505. <https://doi.org/10.1680/geot.2007.00129>.
- JP Concrete. [Cited 28 Nov 2023]. Available at: [Interlocking Concrete Blocks For Retaining Walls - JP Concrete](#).

Kariyawasam, K.K.G.K.D. Jayasinghe, C. 2016. Cement stabilized rammed earth as a sustainable construction material. *Construction and Building Materials*. Vol. 105. pp. 519-527. ISSN 0950-0618. <https://doi.org/10.1016/j.conbuildmat.2015.12.189>.

Kiertomaa Oy. [Cited 21 Oct 2023]. Available at: <https://www.kiertomaa.fi/kiertomaa-oy/>.

Kitio, V. Ngungui, J. 2015. Interlocking Stabilized Soil Blocks (ISSB). *Urban Energy Technical Note 20*. UN-Habitat. 4 p.

Mehta, P. K. Monteiro, P. J. 2014. *Concrete: microstructure, properties and materials*. McGraw-Hill Education, 2014. ISBN 978-0-07-179787-0.

Miller, S. A. Habert, G. Myers, R. J. Harvey, J. T. 2021. Achieving net zero greenhouse gas emissions in the cement industry via value chain mitigation strategies. *One Earth*. Vol. 4. Issue 10. pp. 1398-1411. ISSN 2590-3322. <https://doi.org/10.1016/j.oneear.2021.09.011>.

Minke, G. 2006. *Building with earth: Design and technology of a sustainable architecture*. Berlin, Germany: Birkhauser. 199 p. ISBN-13:978-3-7643-7477-8.

Narloch, P. Woyciechowski, P. Kotowski, J. Gawriuczenkow, I. Wojcik, E. 2020. The Effect of Soil Mineral Composition on the Compressive Strength of Cement Stabilized Rammed Earth. *Materials*. 13(2). 324 p. <https://doi.org/10.3390/ma13020324>.

Poundfield Precast – A PPG Company. [Cited 28 Nov 2023]. Available at: [Precast Interlocking Concrete Blocks | Betaloc® XL | Poundfield Precast](#).

Pylkkänen, K. Nurmikolu, A. 2015. *Routa ja routiminen ratarakenteessa. Liikenneviraston tutkimuksia ja selvityksiä. Liikennevirasto*. Helsinki. ISBN 978-952-317-089-6.

Schuldyakov, K.V. Kramar, L. Y. Trofimov, L. Y. 2016. The properties of slag cement and its influence on the structure of the hardened cement paste. *Procedia Engineering*. Vol. 150. pp. 1433-1439. ISSN 1877-7058. <https://doi.org/10.1016/j.proeng.2016.07.202>.

SFS-EN 12390-3:2019:en. 2019. *Testing hardened concrete. Part 3: Compressive strength of test specimens*. Helsinki: Finnish standards association. 20 p.

SFS-EN 13242+A1. 2008. *Aggregates for unbound and hydraulically bound materials for use in civil engineering work and road construction*. Helsinki: Finnish standards association. 42 p.

SFS-EN 13286-2:en. 2011. *Unbound and hydraulically bound mixtures. Part 2: Test methods for laboratory reference density and water content. Proctor compaction*. Helsinki: Finnish standards association. 30 p.

SFS-EN 13791:2019:en. 2019. *Assessment of in-situ compressive strength in structures and precast concrete components*. Helsinki: Finnish standards association. 38 p.

SFS-EN 197-1:en. 2012. *Cement. Part 1: Composition, specifications and conformity criteria for common cements*. Helsinki: Finnish standards association. 39 p.

SFS-EN 933-1:en. 2012. *Tests for geometrical properties of aggregates. Part 1: Determination of particle size distribution. Sieving method*. Helsinki: Finnish standards association. 19 p.

- SFS-EN ISO 17892-3:en. 2015. Geotechnical investigation and testing. Laboratory testing of soil. Part 3: Determination of particle density. Helsinki: Finnish standards association. 19 p.
- SFS-EN 196-1:2016:en. 2016. Methods of testing cement. Part 1: Determination of strength. Helsinki: Finnish standards association. 33 p.
- SFS-EN ISO 14688-1. 2018. Geotechnical investigation and testing. Identification and classification of soil. Part 1: Identification and description (ISO 14688-1:2017). Helsinki: Finnish standards association. 29 p.
- SFS-EN 12697-31:2019:en. 2019. Bituminous mixtures. Test methods. Part 31: Specimen preparation by gyratory compactor. Helsinki: Finnish standards association. 23 p.
- SFS-EN 12504-4:2021:en. 2021. Testing concrete in structures. Part 4: Determination of ultrasonic pulse velocity. Helsinki: Finnish standards association. 18 p.
- SFS-EN 13286-41:2021:en. 2021. Unbound and hydraulically bound mixtures. Part 41: Test method for the determination of the compressive strength of hydraulically bound mixtures. Helsinki: Finnish standards association. 12 p.
- SFS 5884:2022. 2022. Betonimurskeen maa- ja viherrakennuskäytön laadunvalvontajärjestelmä. Helsinki: Finnish standards association. 26 p.
- Sivakrishna, A. Adesina, A. Awoyera, P.O. Rajesh Kumar, K. 2020. Green concrete: A review of recent developments. *Materials Today: Proceedings*, Volume 27, part 1. ISSN 2214-7853. <https://doi.org/10.1016/j.matpr.2019.08.202>.
- Solismaa, S. Torppa, A. Kuva, J. Heikkilä, P. Hyvönen, S. Juntunen, P. Benzaazoua, M. Kauppila, T. 2021. Substitution of Cement with Granulated Blast Furnace Slag in Cemented Paste Backfill: Evaluation of Technical and Chemical Properties. *Minerals*. 11, 1068. <https://doi.org/10.3390/min11101068> .
- Stora Enso. 2023. Kuvaus jätteen rinnakkaispoltoista Stora Enso Varkauden kattila K6:lla. [Cited 18 Oct 2023]. Available at: <https://www.ymparisto.fi/sites/default/files/documents/Liite%20%20J%C3%A4tteen%20rinnakkaispolto%20kattila%20K6%202022.pdf> .
- Teittinen, T. 2019. Uusiomaarakentamisen ympäristövaikutusindikaattorit ja päästölaskenta tie- ja katurakentamisessa. Master's thesis. Water and Environmental Engineering. Aalto University. Espoo, Finland. 84 p.
- Tellus Design. 2017. Elite Precast Concrete Limited – Reference guide for designing retaining walls using interlocking concrete blocks. Shropshire, United Kingdom. 19 p.
- Turun Seudun Energiantuotanto Oy. [Cited 17 Oct 2023]. Available at: <https://tset.fi/tuotanto-ja-operointi/laitoksen-esittely/>
- Törnqvist, J. Jauhiainen, P. 2001. ICT-koe tien rakennekerros materiaalien deformaatioherkkyyden määrittämisessä. *Tiehallinto. Tiehallinnon selvityksiä 63/2001*. Helsinki, Suomi. 11 p. [Cited 18 Oct 2023]. Available at: <https://www.doria.fi/bitstream/handle/10024/139036/4240tie.pdf?sequence=1&isAllowed=y> .
- United Nations Environment Programme. 2023. *Building Materials and the Climate: Constructing a New Future*. ISBN 978-92-807-4084-8.

Uygunogly, T. Topcu, I.B. Gencil, O. Brostow, W. 2012. The effect of fly ash content and types of aggregates on the properties of pre-fabricated concrete interlocking blocks (PCIBs). *Construction and Building Materials*. Vol. 30. pp. 180-187. ISSN 0950-0618.

Venkatarama Reddy, B.V. Prasanna Kumar, P. 2010. Embodied energy in cement stabilised rammed earth walls. *Energy and Buildings*. Vol. 42. Issue 3. pp. 380-385. ISSN 0378-7788.
<https://doi.org/10.1016/j.enbuild.2009.10.005>.

Walker, P. Keable, R. Marton, J. Maniatidis, V. 2005. *Rammed Earth – Design and construction guidelines*. IHS BRE Press. 156 p. ISBN-13:978-1860817342.

Wallenius, A. Al-Neshawy, F. Punkki, J. 2023. 'Assessment procedure of determining compressive strength of hardened reinforced concrete structures', in *Proceedings of the International Conference on Non-Destructive Evaluation of Concrete in Nuclear Applications – NDE NucCon*. Aalto University publication series SCIENCE+TECHNOLOGY, no. 3, vol. 2023, Aalto University. pp. 127-136. ISBN 978-952-64-1140-8.

Wayu, A. 2023. Technical properties of fine-grained sand from Nilsjä quarry and its use in earth construction. Master's thesis draft. Master's programme in Geoengineering. Aalto University. Espoo, Finland.

Winnefeld, F. Leemann, A. German, A. Lothenbach, B. 2022. CO₂ storage in cement and concrete by mineral carbonation. *Current Opinion in Green and Sustainable Chemistry*. Vol. 38. ISSN 2452-2236.
<https://doi.org/10.1016/j.cogsc.2022.100672>.

Zhang, Y. Korkiala-Tanttu, L. K. Borén, M. 2019. Assessment for Sustainable Use of Quarry Fines as Pavement Construction Materials: Part II-Stabilization and Characterization of Quarry Fine Materials. *Materials*. Vol. 12. No. 15. 2450. <https://doi.org/10.3390/ma12152450>

Attachments

Attachment 1: Laboratory test results for quality control of the crushed concrete (Kiertomaa Oy). 6 pages.

Attachment 2: Laboratory test results for quality control of the crushed rock (Kiertomaa Oy). 4 pages.

Attachment 3: Technical data sheet of CEM I from FinnSementti. 1 page.

Attachment 4: Technical data sheet of CEM III/B from FinnSementti. 1 page.

Attachment 5: Laboratory test results for quality control of the ashes from Naantali power plant. 16 pages.

Attachment 6: Laboratory test results for quality control of the fly ash from Stora Enso power plant in Varkaus. 11 pages.

Attachment 7: Charts of the modified Proctor tests. 4 pages.

Attachment 8: Charts of the UCT tests. 16 pages.



Laboratoriopalvelut

PANK-hyväksytty testausorganisaatio

Laboratoriopalveluita vuodesta 1951

RAKEISUUSTUTKIMUS

Asiakas	Kiertomaa Oy	Kunta	Turku
Projekti	Kiertomaa Oy	Materiaali	BeM II
Urakoitsija	Kivikolmio Oy	Lajite	0/63
Paikka	Saramäki	Diaarinro	135/2022/1
Yhteyshenkilö	Jussi Kortesoja	Kasa	

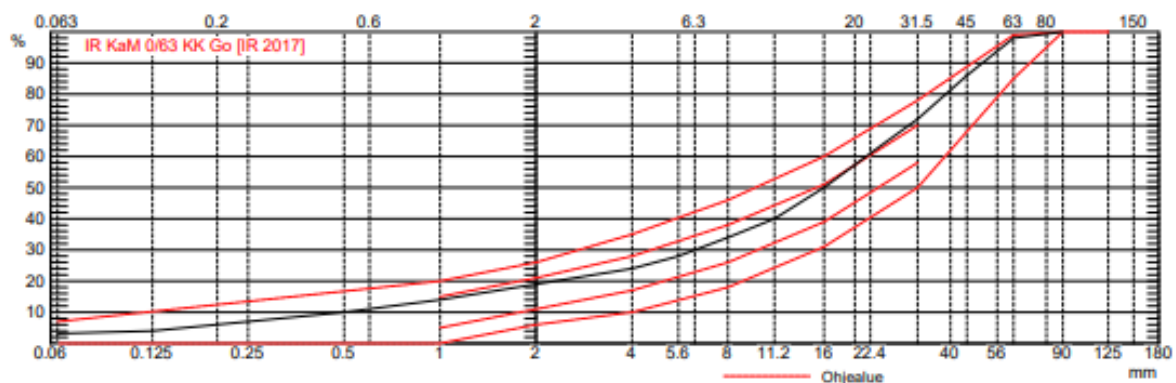
Näytetunnus	1
Näytteenottopvm	20.10.2022
Näytteenottaja	Urakoitsija

Seulontatapa	Pesuseulonta (SFS-EN 933-1:2012)
E-moduli [MPa]	280

Kokeen nimi (Menetelmä) [Yksikkö]	Tulos
Vesipitoisuus (SFS-EN 1097-5:2008) [%]	11.5

Seulat mm	Ohjealue min	max	Läpäisy %
90	100	100	100
63	85	99	98
45			86
31.5	50	78	72
22.4			61
16	31	60	50
11.2			40
8	18	46	34
5.6			28
4	10	35	24
2	6	26	19
1	0	20	14
0.5			10
0.25			7
0.125			4
0.063	0.0	7.0	3.2

* Poikkeaa ohjeesulalta



Huom! Testaustulos koskee ainoastaan testattua näytettä.

Jakelu	
--------	--

Päiväys 21.10.2022

Allekirjoitus

Juha Lindberg

Lindberg Juha

Raision aluelaboratorio
Pajakatu 5
21280 Raisio
juha.lindberg@mitta.fi
0400 223 983


Laboratoriopalvelut

PANK-hyväksytty testausorganisaatio

Laboratoriopalveluita vuodesta 1951

RAKEISUUSTUTKIMUS

Asiakas	Kiertomaa Oy	Kunta	Turku
Projekti	Kiertomaa Oy	Materiaali	BeM II
Urakoitsija	Kivikolmio Oy	Lajite	0/63 BeM
Paikka	Saramäki	Diaarinro	135/2022/2
Yhteyshenkilö	Jussi Kortesoja	Kasa	

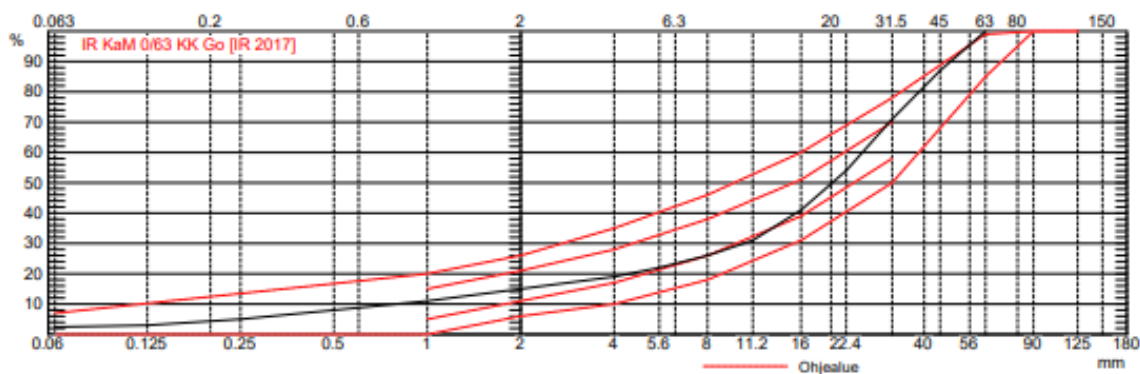
Näytetunnus	2
Näytteenottopvm	24-26.10.2022
Näytteenottaja	Urakoitsija

Seulontatapa	Pesuseulonta (SFS-EN 933-1:2012)
E-moduuli [MPa]	280

Kokeen nimi (Menetelmä) [Yksikkö]	Tulos
Vesipitoisuus (SFS-EN 1097-5:2008) [%]	9.8

Seulat mm	Ohjealue min	max	Läpäisy %
63	85	99	100 *
45			87
31.5	50	78	71
22.4			54
16	31	60	41
11.2			31
8	18	46	26
5.6			22
4	10	35	19
2	6	26	15
1	0	20	11
0.5			8
0.25			5
0.125			3
0.063	0.0	7.0	2.4

* Poikkeaa ohjeseulalta



Huom! Testaustulos koskee ainoastaan testattua näytettä.

Jakelu	
--------	--

Päiväys 31.10.2022

Allekirjoitus

Lindberg Juha

 Raision aluelaboratorio
 Pajakatu 5
 21280 Raisio
 juha.lindberg@mitta.fi
 0400 223 983


**Karkean uusiokiviaineksen
osa-aineiden luokittelutesti**

SFS-EN 933-11+AC

tilaaja	Kiertomaa Oy, Jussi Kortesoja
näyte näytteenottaja	BeM 0/63 Kiertomaa, Saramäki Kivikolmio Oy
työnumero	22-2270

Osa-aineiden osuudet raekoossa 4-63 mm

	osa-aine	[cm ³ /kg]	vaatimus (843/2017)
<i>kelluvat</i>	FL	7,2	≤ 10 cm ³ /kg

	osa-aine	[%]	
<i>kellumattomat</i>			
muut (metalli, puu, kumi, muovi,...)	X	0,2	≤ 1 p-%
betoni, betonituotteet, laasti, betoniharkot	Rc	89	
kiviaines	Ru	8,9	
tiilet, kaakelit, kellumaton vaahtobetoni	Rb	2,2	≤ 30 p-%
bitumiset materiaalit	Ra	0,0	
lasi	Rg	0,0	
	yht.	100	

kuivauslämpötila, T [°C]:	105
---------------------------	-----

Testaustulos koskee ainoastaan testattua näytettä.

Oulussa 7.11.2022

Tuija Nykyri


Laboratoriopalvelut

PANK-hyväksytty testausorganisaatio

Laboratoriopalveluita vuodesta 1951

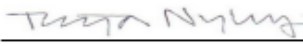
TUTKIMUSSELOSTUS

Asiakas	Kiertomaa Oy	Kunta	
Projekti	Saramäki	Materiaali	BeM
Urakoitsija		Lajite	0/63
Paikka	Kiertomaa, Saramäki	Diaarinro	22-2270
Yhteyshenkilö	Jussi Kortesoja	Kasa	

Näytetunnus	1	Näyteenottaja	Kivikolmio Oy
-------------	---	---------------	---------------

Kokeen nimi	Menetelmä	Yksikkö	Tulos	Luokka
Kiintotiheys	SFS-EN 1097-6	Mg/m ³	2,39	

Jakelu	jussi.kortesoja@kiertomaa.fi
--------	------------------------------

Päiväys 08.11.2022 Allekirjoitus 
Tuija Nykyri

Mitta Oy
Typpitie 1
90120 Oulu
etunimi.sukunimi@mitta.fi

Tapio Mattila, puh. 040 - 8490302

16.12.2022

Kiertomaa Oy
Jussi Kortesoja

Tilauksenne 14.11.2022

BETONIMURSKEEN PURISTUSLUJUUS

- Näytteet** 1 kpl, BeM 0/63 mm, Saramäki BeM II (Tampereen yliopiston työnnumero (GeoLa/188/2022). Näyte on toimitettu Tampereen yliopistolle 14.11.2022. Näytteenotto ja näytteen edustavuus ovat tilaajan vastuulla.
- Näytteiden esikäsittely** Kuivaamattomasta näytteestä seulottiin < 22,4 mm materiaalia koekappaleiden valmistusta varten.
- Testausmenetelmät** Koekappaleet (Ø 100 mm, korkeus 100 mm) valmistettiin kiertotiivistyslaitteella työpaineella 820 kPa ja 160 kierros määrää käyttäen. 17.11.2022 valmistetut koekappaleet säilytettiin muovipussiin suljettuina tiiviissä muovilaukossa puristus hetken asti. Puristusnopeutena käytettiin 2,5 kN/s.
- Tulokset** Tulokset on esitetty oheisessa taulukossa. Testit tehtiin 17.11.-16.12.2022 välisenä aikana. Koekappaleiden vesipitoisuus oli puristushetkellä 14,4-15,0 % ja kuivairtotiheys 1,79-1,81 g/cm³.

Taulukko 1. BeM < 22,4 mm puristuslujuus.

Näyte	Puristuslujuus [MPa]			
	7 vrk (24.11.2022)		28 vrk (15.12.2022)	
	yksittäiset	keski-arvo	yksittäiset	keski-arvo
GeoLa/188/2022	0,89;0,83;0,70	0,81	0,97;1,14;1,07;0,76	0,98

Tulokset pätevät ainoastaan testatuille näytteille. Testausselostuksen saa kopioida ainoastaan kokonaisuudessaan.

Laboratorioteknikko


Tapio Mattila

JAKELU:

Asiakas
Tampereen yliopisto

Tulostettu 16.12.2022

PANK-hyväksytty testausorganisaatio


Laboratoriopalvelut

PANK-hyväksytty testausorganisaatio

Laboratoriopalveluita vuodesta 1951

TUTKIMUSSELOSTUS

Asiakas	Kiertomaa Oy	Kunta	Turku
Projekti	Saramäki BeM	Materiaali	BeM
Urakoitsija		Lajite	0/63
Paikka	Saramäki	Diiaarinro	22-2270
Yhteyshenkilö	Jussi Kortesoja	Kasa	

Näytetunnus	1	Näytteenottaja	Kivikolmio Oy	
Kokeen nimi	Menetelmä	Yksikkö	Tulos	Luokka
Los Angeles-luku	SFS-EN 1097-2:2011		35 (35.2)	LA ₃₅



Kuva 1

Los Angeles-luku	LA ₁₅	LA ₂₀	LA ₂₅	LA ₃₀	LA ₃₅	LA ₄₀	LA ₄₅	LA ₅₀	LA ₆₀
Jakelu	jussi.kortesoja@kiertomaa.fi								

Päiväys 09.11.2022

Allekirjoitus

Tuija Nykyri

 Mitta Oy
 Typpitie 1
 90120 Oulu
 etunimi.sukunimi@mitta.fi


Laboratoriopalvelut

PANK-hyväksytty testausorganisaatio

Laboratoriopalveluita vuodesta 1951

TUTKIMUSSELOSTUS

Asiakas	Kiertomaa Oy	Kunta	Turku
Projekti	Kiertomaa Oy	Materiaali	KaM
Urakoitsija	Terrawise Oy	Lajite	0/16
Paikka	Kiertomaa, Saramäki	Diaarinro	21-0138
Yhteyshenkilö	Päivi Laakso	Kasa	

Näytetunnus	1	Näytteenottopvm	02.02.2021
		Näytteenottaja	Terrawise Oy

Kokeen nimi	Menetelmä	Yksikkö	Tulos	Luokka
Kiintotiheys, näennäinen	SFS-EN 1097-6:2014	Mg/m ³	2.71	
Kuulamyllyarvo	SFS-EN 1097-9:2014	%	20.3	A _N 30
- Kuulamyllyarvo 1		%	20.9	
- Kuulamyllyarvo 2		%	19.6	
Los Angeles-luku	SFS-EN 1097-2:2011		29 (28.7)	LA ₃₀



Kuva 1

Kuulamylly	A _N 7	A _N 10	A _N 14	A _N 19	A _N 30	
Los Angeles-luku	LA ₁₅	LA ₃₀	LA ₄₅	LA ₆₀	LA ₇₅	LA ₉₀

Jakelu	
--------	--

Päiväys 10.02.2021

Allekirjoitus

Marko Hyvönen

 PL 157
 00521 Helsinki
 Puhelin 08 5356 000
 etunimi.sukunimi@mitta.fi

Tutkimusseloste



PANK-hyväksytty testausorganisaatio

Työnumero 23-490

Petrografinen kuvaus (SFS-EN 932-3:2022)	
Tilaaaja	Kiertomaa Oy, Jussi Kortesoja
Näyte	Saramäki, Lohkare, Turku
Näytteenottaja	Urakoitsija, 28.03.2023
Kivilaji	Kvartsisyeniitti

Mineraalikoostumus		
Mineraali	Prosenttiosuus (til-%)	Raekoko (mm)
Kalimaasälpä	62	0.5-12.0
Kvartsi	16	<0.1-6.0
Biotiitti	10	<0.1-3.0
Plagioklaasi	8	0.3-5.0
Muut mineraalit	4	<0.1-4.0

Mineraalien %-osuus laskettu pistelaskurilla

Kuvaus

Aksessoriset mineraalit	→ Granaatti (3 %), Serisiitti, Kloriitti, Muskoviitti, Zirkoni
Tekstuuri	→ Karkearakeinen, Hypidiomorfisgranulaarinen
Suuntautuneisuus	→ Heikosti suuntautunut
Huokoisuus	→ Ei havaittu
Muuttuneisuus	→ Biotiitti→Kloriitti Plagioklaasi→Serisiitti
Rapautumisaste	→ Rp0, Rapautumaton
Kiderajat	→ Suorat ja terävät
Väri	→ Punertavan harmaa
Simpukan kuoret	→ Ei havaittu

Kiviaineksen mineraloginen soveltuvuus			
Käyttökohde	Standardi	Soveltuvuus	Vaadittavat lisätestit
Sitomattomat	SFS-EN 13242	Soveltuu	
Asfaltti	SFS-EN 13043	Soveltuu	
Raidesepeli	SFS-EN 13450	Soveltuu	

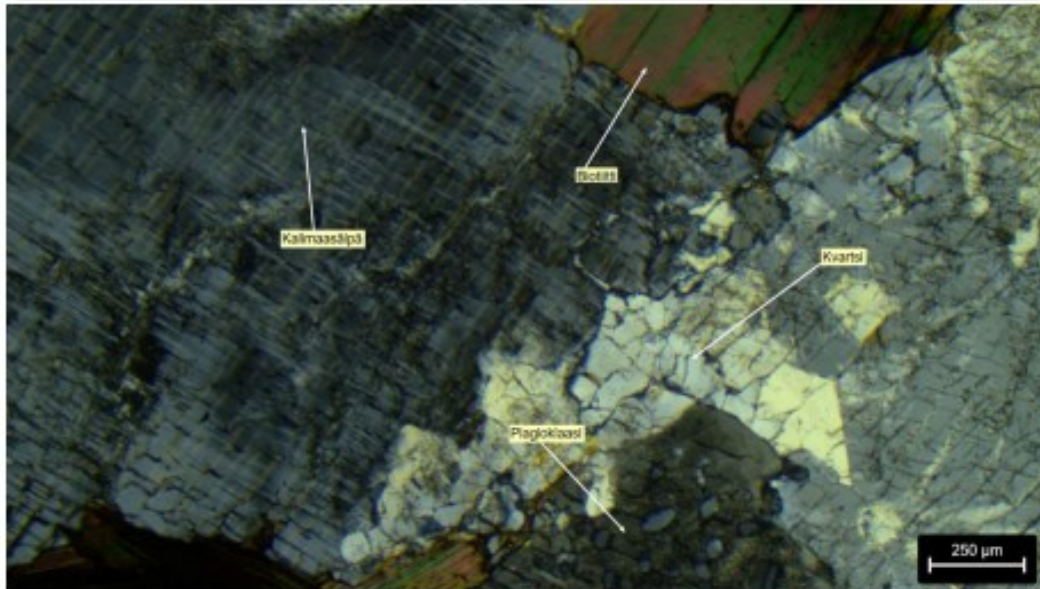
Tutkimusseloste



PANK-hyväksytty testausorganisaatio

Kivilaji CE merkintään

Kvartsisyeniitti kalliomurske



Oulussa 28.04.2023

Lauri Herukka
Geologiharjoittelija

(Petrografinen kuvaus koskee ainoastaan tutkittua näytettä)


Laboratoriopalvelut

PANK-hyväksytty testausorganisaatio

Laboratoriopalveluita vuodesta 1951

RAKEISUUSTUTKIMUS, KESKIAARVO

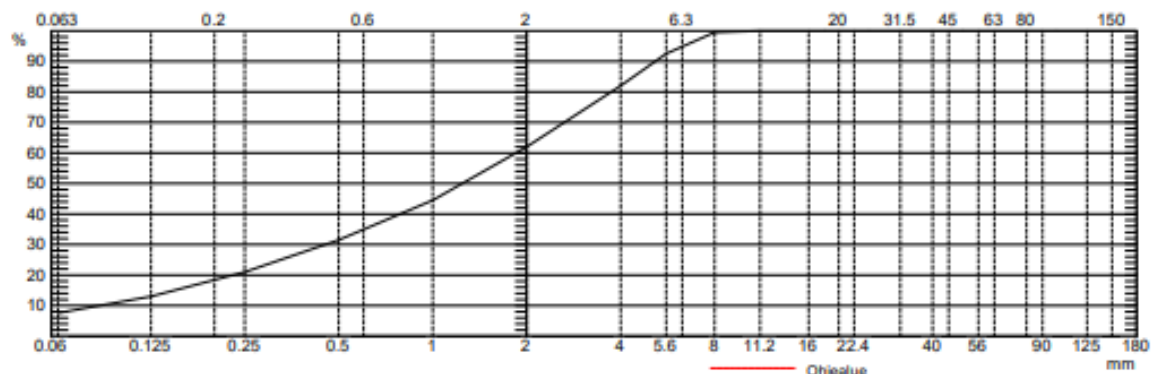
Asiakas	TerraWise	Kunta	Turku
Projekti	Kiertomaa	Materiaali	KaM
Urakoitsija	MREA Oy	Lajite	0/8
Paikka	Saramäki	Diariinro	58/2021
Yhteyshenkilö		Kasa	

Näytteenottoväli	24.5.2021 - 24.5.2021
Näytteitä	2

Seulontatapa	Pesuseulonta (SFS-EN 933-1:2012)
Puhtaus	f ₈

Kokeen nimi (Menetelmä) [Yksikkö]	Keskiarvo	Suurin
Vesipitoisuus (SFS-EN 1097-5:2008) [%]	0.60	0.70

Seulat mm	Ohjealue		Läpäisy %
	min	max	
11.2			100
8			100
5.6			93
4			82
2			62
1			45
0.5			32
0.25			21
0.125			13
0.063			7.5



Huomi! Testaustulos koskee ainoastaan testattua näytettä.

Jakelu	
--------	--

Päiväys 26.05.2021

Allekirjoitus

Lindberg Juha

 Raision aluelaboratorio
 Pajakatu 5
 21280 Raisio
 juha.lindberg@mitta.fi
 0400 223 983

Cement 5/2022

Ykkös

SEMENTTI

Portlandcement
CEM I 42,5 R

Ykkössementti is a specialty made cement and its for chemical properties are tailored for special applications and dry products. Ykkössementti is manufactured at the Parainen plant.

Cement properties	Requirements (SFS-EN 197-1)
Strength 2 d	≥ 20 MPa
Strength 28 d	$\geq 42,5$ MPa and $\leq 62,5$ MPa
Initial setting time	≥ 60 min
Soundness	≤ 10 mm
Loss on ignition	$\leq 5\%$
Insoluble residue	$\leq 5\%$
SO ₃	$\leq 4,0\%$
Chloride content	$\leq 0,10\%$
Cr6+	≤ 2 mg/kg

Cement composition	Requirements (SFS-EN 197-1)
Cement clinker	$\geq 95\%$ and $\leq 100\%$

FINNSEMENTTI
A CRH COMPANY

Finnsementti Oy
FI-21600 Parainen, Tel. +358 201 206 200
info@finnsementti.fi, name.surname@finnsementti.fi
semnet.fi, finnsementti.fi



Cement 9/2023



Blast furnace cement
CEM III/B 42,5 L – LH/SR

KolmosBertta is a blast furnace slag cement. As a LH and SR grade cement, it is suitable for use in concrete applications requiring sulphate resistance and low heat of hydration. Thanks to its low heat of hydration (270 J/g), KolmosBertta is ideal for massive concrete structures. Thanks to the high blast furnace slag mix, KolmosBertta is Finnsementti's most environmentally friendly cement, currently.

KolmosBertta is suitable for use in concrete alone or in combination with other binders, which gives the concrete manufacturer wide possibilities to implement various applications.

Cement properties	Requirements (SFS-EN 197-1)
Strength 7 d	≥ 16 MPa
Strength 28 d	≥ 42,5 MPa and ≤ 62,5 MPa
Initial setting time	≥ 60 min
Soundness	≤ 10 mm
Loss on ignition	≤ 5%
Insoluble residue	≤ 5%
SO ₃	≤ 4,0%
Chloride content	≤ 0,10%
Cr6+	≤ 2 mg/kg
Heat of hydration	≤ 270 J/g
Cement composition	Requirements (SFS-EN 197-1)
Cement clinker	≥ 20% and ≤ 34%
GGBFS	≥ 66% and ≤ 80%

FINNSEMENTTI
A CRH COMPANY

Finnsementti Oy
FI-21600 Parainen, Tel. +358 201 206 200
info@finnsementti.fi, name.surname@finnsementti.fi
semnet.fi, finnsementti.fi





TUTKIMUSTODISTUS

1(8)

Tilaus: 2207692

Pvm: 3.1.2023

Turun Seudun Energiantuotanto Oy
 Satu Viranko
 Satamatie 16
 21100 Naantali



Tilauksen nimi: **MARA- ja Kaatopaikkakelpoisuus, pohjatuikka**
 Näyte: 22HY0448 NA4 pohjatuikka
 Näytteenottoaika: 28.11.2022
 Näyte saapui: 15.12.2022 Näytteenottaja: Janne Sinervo
 Analysointi aloitettu: 19.12.2022

Määrittäminen	Yksikkö	Tutkimustulos	Laatuvaatimus/ Raja-arvo	Laatusuositus/ Ohjearvo	Menetelmä
Kuiva-aine	%	100,0			SFS-EN 14346
DOC	mg/kg	59	800		CEN/TR 16192:2020, SFS-EN 1484:1997*
Hehkutushäviö kuiva-aineessa	%	< 0,1			SFS-EN 15169
TOC, kuiva-aineessa	%	< 0,1	5 %		Sis. men. P- LAB-KRKK- 402
pH		13	Vähintään 6,0		SFS-EN 16192
Fenoli-indeksi, alihankinta	mg/kg	<0,10			ISO 14402 7
Öljypitoisuus (C10-C21)	mg/kg	< 50			SFS-EN 14039 mod.
Öljypitoisuus (C21-C40)	mg/kg	< 50			SFS-EN 14039
Öljypitoisuus (C10-C40)	mg/kg	< 50	2500		SFS-EN 14039
BTEX-yhdisteiden summa	mg/kg	< 1,0			Laskennalli- nen
Bentseeni	mg/kg	< 0,01			SFS-EN ISO 22155:2016
Tolueeni	mg/kg	< 0,01			SFS-EN ISO 22155:2016
Ksyleeni	mg/kg	< 0,01			SFS-EN ISO 22155:2016
Etyylibentseeni	mg/kg	< 0,01			SFS-EN ISO 22155:2016
Naftaleeni	mg/kg	< 0,05			SFS-EN 17503 mod.

*Akreditoitu menetelmä. Akkreditointi ei koske lausuntoa. Tulokset pätevät vain testatuille näytteille. Raporttia ei saa kopioida osittain ilman testauslaboratorion lupaa. Analyysien mittausepävarmuudet ovat saatavilla pyydettyäessä. Mittausepävarmuutta ei ole huomioitu lausunnossa verrattaessa tuloksia laatuvaatimuksiin.



TUTKIMUSTODISTUS

2(8)

Tilaus: 2207692

Pvm: 3.1.2023

Turun Seudun Energiantuotanto Oy
 Satu Viranko
 Satamatie 16
 21100 Naantali



Asenaftyleeni	mg/kg	< 0,05			SFS-EN 17503 mod.
Asenaftteeni	mg/kg	< 0,05			SFS-EN 17503 mod.
Fluoreeni	mg/kg	< 0,05			SFS-EN 17503 mod.
Fenantreeni	mg/kg	< 0,05			SFS-EN 17503 mod.
Antraseeni	mg/kg	< 0,05			SFS-EN 17503 mod.
Fluoranteeni	mg/kg	< 0,05			SFS-EN 17503 mod.
Pyreeni	mg/kg	< 0,05			SFS-EN 17503 mod.
Bents(a)antraseeni	mg/kg	< 0,05			SFS-EN 17503 mod.
Kryseeni	mg/kg	< 0,05			SFS-EN 17503 mod.
Bentso(b)fluoranteeni	mg/kg	< 0,05			SFS-EN 17503 mod.
Bentso(k)fluoranteeni	mg/kg	< 0,05			SFS-EN 17503 mod.
Bentso(a)pyreeni	mg/kg	< 0,05			SFS-EN 17503 mod.
Indeno(1,2,3-cd)pyreeni	mg/kg	< 0,05			SFS-EN 17503 mod.
Dibentso(a,h)antraseeni	mg/kg	< 0,05			SFS-EN 17503 mod.
Bentso(g,h,i)peryleeni	mg/kg	< 0,05			SFS-EN 17503 mod.
PAH-yhdisteiden summa	mg/kg	< 0,5	150		SFS-EN 17503 mod.
PCB-28	mg/kg	< 0,002			SFS-EN 17322 mod.
PCB-52	mg/kg	< 0,002			SFS-EN 17322 mod.
PCB-101	mg/kg	< 0,002			SFS-EN 17322 mod.
PCB-118	mg/kg	< 0,002			SFS-EN 17322 mod.

*Akkreditoitu menetelmä. Akkreditointi ei koske lausuntoa. Tulokset pätevät vain testatuille näytteille. Raportilla ei saa kopioida osittain ilman testauslaboratorion lupaa. Analyysin mittausepävarmuudet ovat saatavilla pyydettäessä. Mittausepävarmuutta ei ole huomioitu lausunnona verrattaessa tuloksia laatuvaatimuksiin.



TUTKIMUSTODISTUS

3(8)

Tilaus: 2207692

Pvm: 3.1.2023

Turun Seudun Energiantuotanto Oy
 Satu Viranko
 Satamatie 16
 21100 Naantali



PCB-138	mg/kg	< 0,002			SFS-EN 17322 mod.
PCB-153	mg/kg	< 0,002			SFS-EN 17322 mod.
PCB-180	mg/kg	< 0,002			SFS-EN 17322 mod.
PCB-yhdisteiden summa	mg/kg	< 0,05			SFS-EN 17322 mod.
Arseeni, liukoinen (As)	mg/kg	< 0,010	2		CEN/TR 16192:2020, SFS-EN ISO 17294- 2:2016, mod. ICP-M- S*
Barium, liukoinen (Ba)	mg/kg	2,6	100		CEN/TR 16192:2020, SFS-EN ISO 17294- 2:2016, mod. ICP-M- S*
Kadmium, liukoinen (Cd)	mg/kg	< 0,010	1		CEN/TR 16192:2020, SFS-EN ISO 17294- 2:2016, mod. ICP-M- S*
Kromi, liukoinen (Cr)	mg/kg	0,25	10		CEN/TR 16192:2020, SFS-EN ISO 17294- 2:2016, mod. ICP-M- S*

*Akkreditoitu menetelmä. Akkreditointi ei koske lausuntoa. Tulokset pätevät vain testatuille näytteille. Raporttia ei saa kopioida osittain ilman testauslaboratorion lupaa. Analyysien mittausepävarmuudet ovat saatavilla pyydettyäessä. Mittausepävarmuutta ei ole huomioitu lausunnossa verrattaessa tuloksia laatuvaatimuksiin.



TUTKIMUSTODISTUS

4(8)

Tilaus: 2207692

Pvm: 3.1.2023

Turun Seudun Energiantuotanto Oy
 Satu Viranko
 Satamatie 16
 21100 Naantali



Kupari, liukoinen (Cu)	mg/kg	< 0,20	50		CEN/TR 16192:2020, SFS-EN ISO 17294- 2:2016, mod. ICP-M- S*
Elohopea, liukoinen (Hg)	mg/kg	< 0,010	0,2		CEN/TR 16192:2020, SFS-EN ISO 17294- 2:2016, mod. ICP-M- S*
Molybdeeni, liukoinen (Mo)	mg/kg	0,79	10		CEN/TR 16192:2020, SFS-EN ISO 17294- 2:2016, mod. ICP-M- S*
Nikkeli, liukoinen (Ni)	mg/kg	< 0,050	10		CEN/TR 16192:2020, SFS-EN ISO 17294- 2:2016, mod. ICP-M- S*
Lyijy, liukoinen (Pb)	mg/kg	< 0,050	10		CEN/TR 16192:2020, SFS-EN ISO 17294- 2:2016, mod. ICP-M- S*
Antimoni, liukoinen (Sb)	mg/kg	< 0,050	0,7		CEN/TR 16192:2020, SFS-EN ISO 17294- 2:2016, mod. ICP-M- S*

*Akkreditoitu menetelmä. Akkreditointi ei koske lausuntoa. Tulokset pätevät vain testatuille näytteille. Raporttia ei saa kopioida osittain ilman testauslaboratorion lupaa. Analyysien mittausepävarmuudet ovat saatavilla pyydettäessä. Mittausepävarmuutta ei ole huomioitu lausunnossa verrattaessa tuloksia laatuvaatimuksiin.



TUTKIMUSTODISTUS

5(8)

Tilaus: 2207692

Pvm: 3.1.2023

Turun Seudun Energiantuotanto Oy
 Satu Viranko
 Satamatie 16
 21100 Naantali



Seleeni, liukoinen (Se)	mg/kg	< 0,050	0,5		CEN/TR 16192:2020, SFS-EN ISO 17294- 2:2016, mod. ICP-M- S*
Vanadiini, liukoinen (V)	mg/kg	< 0,010			CEN/TR 16192:2020, SFS-EN ISO 17294- 2:2016, mod. ICP-M- S*
Sinkki, liukoinen (Zn)	mg/kg	0,40	50		CEN/TR 16192:2020, SFS-EN ISO 17294- 2:2016, mod. ICP-M- S*
Kaksivaiheinen ravistelutesti		Tehty			SFS-EN 12457-3
Kloridi (Cl-)	mg/kg	< 500	15000		CEN/TR 16192:2020, SFS-EN ISO 10304- 1:2009*
Fluoridi (F-)	mg/kg	< 9	150		CEN/TR 16192:2020, SFS-EN ISO 10304- 1:2009*
Sähkönjohtavuus	mS/m	1000			SFS-EN 27888:1994 (Sis. men. 080)
Haihdutusjäännös, TDS	mg/kg	43000	60000		SFS-EN 15126 mod.
Hapon neutralointikapasiteetti (ANC)	mol H+ / kg	6,0	Aina tutkittava ja arvioitava		CEN/TS 15364:2006, mod.

*Akkreditoitu menetelmä. Akkreditointi ei koske lausuntoa. Tulokset pätevät vain testatuille näytteille. Raporttia ei saa kopioida osittain ilman testaustalouden lupaa. Analyysien mittaustapa- ja menetelmät ovat saatavilla pyydettäessä. Mittaustapa- ja menetelmien ei ole huomioitu lausunnossa verrattaessa tuloksia laatuvaatimuksiin.



TUTKIMUSTODISTUS

6(8)

Tilaus: 2207692

Pvm: 3.1.2023

Turun Seudun Energiantuotanto Oy
 Satu Viranko
 Satamatie 16
 21100 Naantali



Sulfaatti (SO4)	mg/kg	15000	20000		CEN/TR 16192:2020, SFS-EN ISO 10304- 1:2009*
-----------------	-------	-------	-------	--	--

*Akkreditoitu menetelmä. Akkreditointi ei koske lausuntoa. Tulokset pätevät vain testatuille näytteille. Raporttia ei saa kopioida osittain ilman testauslaboratorion lupaa. Analyysien mittausepävarmuudet ovat saatavilla pyydettäessä. Mittausepävarmuutta ei ole huomioitu lausunnossa verrattaessa tuloksia laatuvaatimuksiin.



TUTKIMUSTODISTUS

7(8)

Tilaus: 2207692

Pvm: 3.1.2023

Turun Seudun Energiantuotanto Oy
 Satu Viranko
 Satamatie 16
 21100 Naantali



Lausunto Näytemateriaali täyttää hyötykäyttökelpoisuuden vaatimukset tehtyjen määritysten osalta kun se käytetään päälystetyissä väylärakenteissa tai teollisuus- ja varastorakennusten pohjarakenteessa tai stabilointiaineena edellä mainituissa maarakentamiskohteissa. Se ei kuitenkaan sovellu käytettäväksi peitettynä kenttärakenteisiin näytteen liukoisten molybdeeni- ja sulfaattipitoisuuksien vuoksi, eikä se sovellu peitettynä väylärakenteisiin, päälystettynä kenttärakenteisiin eikä tuhkamursketeihin sen liukoisen sulfaattipitoisuuden vuoksi. (VNa 843/2017)

Valtioneuvoston asetuksessa 843/2017 kloridille, sulfaatille ja fluoridille asetettuja raja-arvoja ei sovelleta rakenteeseen, joka täyttää kaikki seuraavat edellytykset: sijaitsee enintään 500 m etäisyydellä merestä, rakenteen läpi suotautuvan veden purkautumissuunta on mereen sekä rakenteen ja meren välillä ei ole talousvedenottoon käytettäviä kaivoja (VNa 843/2017).

Lopullisen päätöksen jätteiden hyödyntämisestä maanrakentamisessa tekee paikallinen ympäristöviranomaisen.

Näytemateriaali voidaan liukoisuustestin tulosten perusteella tehtyjen määritysten osalta loppusijoittaa vaarattoman jätteen kaatopaikalle (VNa 331/2013).

Näytteen ANC on kohtalainen.

Lausunto perustuu lainsäädännön (VNa 331/2013) raja-arvoihin ja tehtyihin määrittäisiin eikä siinä oteta huomioon näytemateriaalin jäteluokitusta. Ympäristöviranomaisen tekee lopullisen päätöksen näytemateriaalin loppusijoittamisesta.

Raportilla näkyvissä olevat raja-arvot: vaarattoman jätteen kaatopaikka (VNa 331/2013).

SGS Finland Oy

Anu Villberg
 Kemisti

Tämä tutkimustodistus on allekirjoitettu sähköisesti.

Tuloksia koskevat tiedustelut

Elintarvikkeet, rehut,
 maanparannusaineet ja
 vedet

Eeva Luoma, Laatupäällikkö, puh. +358 50 464 7567,
 eeva.luoma@sgs.com

*Akkreditoitu menetelmä. Akkreditointi ei koske lausuntoa. Tulokset pätevät vain testatuille näytteille. Raporttia ei saa kopioida osittain ilman testauslaboratorion lupaa. Analyysien mittausepävarmuudet ovat saatavilla pyydettyäessä. Mittausepävarmuutta ei ole huomioitu lausunnossa verrattaessa tuloksia laatuvaatimuksiin.



TUTKIMUSTODISTUS

8(8)

Tilaus: 2207692
Pvm: 3.1.2023

Turun Seudun Energiantuotanto Oy
Satu Viranko
Satamatie 16
21100 Naantali



Metallianalytiikka Anu Villberg, Kemisti, puh. +358 43 850 1146,
anu.villberg@sgs.com
Ympäristöanalytiikka Elinnoora Koskinen, Chemist, +358 9 225 286 20,
elinnoora.koskinen@sgs.com

Lisätiedot Hiilivetytulosten mittausepävarmuus:
>C10-C21, >C21-<C40 ja >C10-<C40: 50-300 mg/kg ± 35 %, 300-1000 mg/kg ± 18 %, yli
1000 mg/kg ± 13 %.

PAH-yhdisteiden mittausepävarmuus: 0,05-0,5 mg/kg ± 39 %, 0,5-2,0 mg/kg ± 33 % ja yli 2,0
mg/kg ± 20 %.

Yksittäisten PCB-yhdisteiden mittausepävarmuus on ± 50 %.

Yksittäisten bensiinihiilivetyjen (BTEX) mittausepävarmuus: 0,01-0,05 mg/kg ± 50 %, 0,051-
0,5 mg/kg ± 30 %, yli 0,51 mg/kg ± 20 %.

Liukoisten metallien analyysien (ICP-MS) epävarmuusarvio: < 0,5 mg/kg ± 50 %, 0,5-5
mg/kg ± 20 % ja yli 5 mg/kg ± 10 %.

DOC- ja TOC-määntysten mittausepävarmuus on ± 20 %.

Kuiva-ainemäärityksen mittausepävarmuus on $\pm 1,9$ suht.-%.

IC-määntysten mittausepävarmuudet ovat: Fluoridi: ± 50 %, kloridi: ± 25 %, sulfaatti: ± 25 %.

Laboratoriot

7 SGS Finland Oy, Kotka (akkreditoitu testauslaboratorio T156, akkreditointivaatimus SFS-
EN ISO/IEC 17025)

Jakelu satu.viranko@turkuenergia.fi

Laskutus Turun Seudun Energiantuotanto Oy, Satamatie 16, 21100 Naantali

Yritys on antanut tämän dokumentin palvelujen yleisten toimitusehtojensa mukaisesti, jotka ovat saatavilla osoitteessa
<https://www.sgs.com/en/terms-and-conditions>. Toimitusehdot sisältävät rajoituksia yrityksen vahingonkorvausvastuuseen, hyvityksiin
ja lain valintaan. Tämän dokumentin haltijan tulee huomioida, että informaatio tässä dokumentissa kuvaa tilanteen sellaisena kuin
yhtiö on sen työsuorituksensa aikana todennut asiakkaan mahdollisten ohjeiden mukaisesti. Yrityksen vastuu rajoittuu yrityksen
asiakkaseen eikä tämä dokumentti estä kaupan osapuolia käyttämästä kaupan asiakirjojen mukaisia oikeuksia ja velvoitteita. Tämän
dokumentin sisällön tai ulkomuodon luvaton muuttaminen, väärentäminen tai vääristely on lainvastaista ja tekijä voidaan asettaa
syyttäneeseen lain ankarimman tulkinnan mukaisesti.

*Akkreditoitu menetelmä. Akkreditointi ei koske lausuntoa. Tulokset pätevät vain testatuille näyttille. Raporttia ei saa kopioida osittain ilman
testauslaboratorion lupaa. Analyysien mittausepävarmuudet ovat saatavilla pyydettyinä. Mittausepävarmuutta ei ole huomioitu
lausunnossa verrattaessa tuloksia laatuvaatimuksiin.



TUTKIMUSTODISTUS

1(8)

Tilaus: 2207691

Pvm: 3.1.2023

Turun Seudun Energiantuotanto Oy
 Satu Viranko
 Satamatie 16
 21100 Naantali



Tilauksen nimi: **MARA- ja Kaatopaikkakelpoisuus, lentotuhka**
 Näyte: 22HY0447 NA4 lentotuhka
 Näytteenottoaika: 28.11.2022
 Näyte saapui: 15.12.2022 Näytteenottaja: Janne Sinervo
 Analysointi aloitettu: 19.12.2022

Määrittäminen	Yksikkö	Tutkimustulos	Laatuvaatimus/ Raja-arvo	Laatusuositus/ Ohjearvo	Menetelmä	
Kuiva-aine	%	100,0			SFS-EN 14346	
DOC	mg/kg	96	1000		CEN/TR 16192:2020, SFS-EN 1484:1997*	
Hekikutushäviö kuiva-aineessa	%	0.49	10 %		SFS-EN 15169	
TOC, kuiva-aineessa	%	0.24	6 %		Sis. men. P- LAB-KRKK- 402	
Tuhka kuiva-aineessa	%	99.5			SFS-EN 13039	
pH		13			SFS-EN 16192	
Fenoli-indeksi, alihankinta	mg/kg	0,10			ISO 14402	7
Öljypitoisuus (C10-C21)	mg/kg	< 50			SFS-EN 14039 mod.	
Öljypitoisuus (C21-C40)	mg/kg	< 50			SFS-EN 14039	
Öljypitoisuus (C10-C40)	mg/kg	< 50			SFS-EN 14039	
BTEX-yhdisteiden summa	mg/kg	< 1,0			Laskennallinen	
Bentseeni	mg/kg	< 0,01			SFS-EN ISO 22155:2016	
Tolueneeni	mg/kg	0,02			SFS-EN ISO 22155:2016	
Ksyleeni	mg/kg	< 0,01			SFS-EN ISO 22155:2016	
Etyyliibentseeni	mg/kg	< 0,01			SFS-EN ISO 22155:2016	

*Akkreditoitu menetelmä. Akkreditointi ei koske lausuntoa. Tulokset pätevät vain testatuille näytteille. Raporttia ei saa kopioida osittain ilman testauslaboratorion lupaa. Analyysien mittausepävarmuudet ovat saatavilla pyydettyessä. Mittausepävarmuutta ei ole huomioitu lausunnossa verrattaessa tuloksia laatuvaatimuksiin.

SGS Finland Oy | Lepolantie 9, FI-03600 Karkkila, Finland
 t. +358 9 2252 860, www.sgs.fi

Member of SGS Group
 Business ID 0634247-4



TUTKIMUSTODISTUS

2(8)

Tilaus: 2207691

Pvm: 3.1.2023

Turun Seudun Energiantuotanto Oy
 Satu Viranko
 Satamatie 16
 21100 Naantali



Naftaleeni	mg/kg	0,11			SFS-EN 17503 mod.
Asenaftyleeni	mg/kg	< 0,05			SFS-EN 17503 mod.
Asenaftteeni	mg/kg	< 0,05			SFS-EN 17503 mod.
Fluoreeni	mg/kg	< 0,05			SFS-EN 17503 mod.
Fenantreeni	mg/kg	< 0,05			SFS-EN 17503 mod.
Antraseeni	mg/kg	< 0,05			SFS-EN 17503 mod.
Fluoranteeni	mg/kg	< 0,05			SFS-EN 17503 mod.
Pyreeni	mg/kg	< 0,05			SFS-EN 17503 mod.
Bents(a)antraseeni	mg/kg	< 0,05			SFS-EN 17503 mod.
Kryseeni	mg/kg	< 0,05			SFS-EN 17503 mod.
Bentso(b)fluoranteeni	mg/kg	< 0,05			SFS-EN 17503 mod.
Bentso(k)fluoranteeni	mg/kg	< 0,05			SFS-EN 17503 mod.
Bentso(a)pyreeni	mg/kg	< 0,05			SFS-EN 17503 mod.
Indeno(1,2,3-cd)pyreeni	mg/kg	< 0,05			SFS-EN 17503 mod.
Dibentso(a,h)antraseeni	mg/kg	< 0,05			SFS-EN 17503 mod.
Bentso(g,h,i)peryleeni	mg/kg	< 0,05			SFS-EN 17503 mod.
PAH-yhdisteiden summa	mg/kg	< 0,5			SFS-EN 17503 mod.
PCB-28	mg/kg	< 0,002			SFS-EN 17322 mod.
PCB-52	mg/kg	< 0,002			SFS-EN 17322 mod.
PCB-101	mg/kg	< 0,002			SFS-EN 17322 mod.

*Akkreditoitu menetelmä - Akkreditointi ei koske lausuntoa. Tulokset pätevät vain testatuille näytteille. Raporttia ei saa kopioida osittain ilman testaustalouden lupaa. Analyysien mittausepävarmuudet ovat saatavilla pyydettyessä. Mittausepävarmuutta ei ole huomioitu lausunnossa verrattaessa tuloksia laatuvaatimuksiin.



TUTKIMUSTODISTUS

3(8)

Tilaus: 2207691

Pvm: 3.1.2023

Turun Seudun Energiantuotanto Oy
 Satu Viranko
 Satamatie 16
 21100 Naantali



PCB-118	mg/kg	< 0,002			SFS-EN 17322 mod.
PCB-138	mg/kg	< 0,002			SFS-EN 17322 mod.
PCB-153	mg/kg	< 0,002			SFS-EN 17322 mod.
PCB-180	mg/kg	< 0,002			SFS-EN 17322 mod.
PCB-yhdisteiden summa	mg/kg	< 0,05			SFS-EN 17322 mod.
Arseeni, liukoinen (As)	mg/kg	0,031	25		CEN/TR 16192:2020, SFS-EN ISO 17294- 2:2016, mod. ICP-M- S*
Barium, liukoinen (Ba)	mg/kg	12	300		CEN/TR 16192:2020, SFS-EN ISO 17294- 2:2016, mod. ICP-M- S*
Kadmium, liukoinen (Cd)	mg/kg	< 0,010	5		CEN/TR 16192:2020, SFS-EN ISO 17294- 2:2016, mod. ICP-M- S*
Kromi, liukoinen (Cr)	mg/kg	2,6	70		CEN/TR 16192:2020, SFS-EN ISO 17294- 2:2016, mod. ICP-M- S*

*Akkreditoitu menetelmä. Akkreditointi ei koske lausuntoa. Tulokset pätevät vain testatuille näytteille. Raporttia ei saa kopioida osittain ilman testauslaboratorion lupaa. Analyysien mittausepävarmuudet ovat saatavilla pyydettäessä. Mittausepävarmuutta ei ole huomioitu lausunnossa verrattaessa tuloksia lastuvaatimuksiin.



TUTKIMUSTODISTUS

4(8)

Tilaus: 2207691

Pvm: 3.1.2023

Turun Seudun Energiantuotanto Oy
 Satu Viranko
 Satamatie 16
 21100 Naantali



Kupari, liukoinen (Cu)	mg/kg	< 0,20	100		CEN/TR 16192:2020, SFS-EN ISO 17294-2:2016, mod. ICP-M-S*
Elohopea, liukoinen (Hg)	mg/kg	< 0,010	2		CEN/TR 16192:2020, SFS-EN ISO 17294-2:2016, mod. ICP-M-S*
Molybdeeni, liukoinen (Mo)	mg/kg	3,4	30		CEN/TR 16192:2020, SFS-EN ISO 17294-2:2016, mod. ICP-M-S*
Nikkeli, liukoinen (Ni)	mg/kg	< 0,050	40		CEN/TR 16192:2020, SFS-EN ISO 17294-2:2016, mod. ICP-M-S*
Lyijy, liukoinen (Pb)	mg/kg	0,32	50		CEN/TR 16192:2020, SFS-EN ISO 17294-2:2016, mod. ICP-M-S*
Antimoni, liukoinen (Sb)	mg/kg	< 0,050	5		CEN/TR 16192:2020, SFS-EN ISO 17294-2:2016, mod. ICP-M-S*

*Akkreditoitu menetelmä. Akkreditointi ei koske lausuntoa. Tulokset pätevät vain testatuille näytteille. Raporttia ei saa kopioida osittain ilman testauslaboratorion lupaa. Analyysien mittausepävarmuudet ovat saatavilla pyydettyessä. Mittausepävarmuutta ei ole huomioitu lausunnossa verrattaessa tuloksia laatuvaatimuksiin.



TUTKIMUSTODISTUS

5(8)

Tilaus: 2207691

Pvm: 3.1.2023

Turun Seudun Energiantuotanto Oy
 Satu Viranko
 Satamatie 16
 21100 Naantali



Seleeni, liukoinen (Se)	mg/kg	0,32	7		CEN/TR 16192:2020, SFS-EN ISO 17294- 2:2016, mod. ICP-M- S*
Vanadiini, liukoinen (V)	mg/kg	0,013			CEN/TR 16192:2020, SFS-EN ISO 17294- 2:2016, mod. ICP-M- S*
Sinkki, liukoinen (Zn)	mg/kg	0,96	200		CEN/TR 16192:2020, SFS-EN ISO 17294- 2:2016, mod. ICP-M- S*
Yksivaiheinen ravistelutesti		Tehty			SFS-EN 12457-2
Kloridi (Cl-)	mg/kg	17000	25000		CEN/TR 16192:2020, SFS-EN ISO 10304- 1:2009*
Fluoridi (F-)	mg/kg	< 9	500		CEN/TR 16192:2020, SFS-EN ISO 10304- 1:2009*
Sähkönjohtavuus	mS/m	1500			SFS-EN 27888:1994 (Sis. men. 080)
Haihdutusjäännös, TDS	mg/kg	81000	100000		SFS-EN 15126 mod.
Hapon neutralointikapasiteetti (ANC)	mol H+ / kg	8,6	Aina tutkittava ja arvioitava		CEN/TS 15364:2006, mod.

*Akkreditoitu menetelmä. Akkreditointi ei koske lausuntoa. Tulokset pätevät vain testatuille näytteille. Raporttia ei saa kopioida osittain ilman testauslaboratorion lupaa. Analyysien mittausepävarmuudet ovat saatavilla pyydettyessä. Mittausepävarmuutta ei ole huomioitu lausunnossa verrattaessa tuloksia laatuvaatimuksiin.



TUTKIMUSTODISTUS

6(8)

Tilaus: 2207691

Pvm: 3.1.2023

Turun Seudun Energiantuotanto Oy
 Satu Viranko
 Satamatie 16
 21100 Naantali



Sulfaatti (SO4)	mg/kg	18000	50000		CEN/TR 16192:2020, SFS-EN ISO 10304- 1:2009*
-----------------	-------	-------	-------	--	--

*Akkreditoitu menetelmä. Akkreditointi ei koske lausuntoa. Tulokset pätevät vain testatuille näytteille. Raporttia ei saa kopioida osittain ilman testauslaboratorion lupaa. Analyysien mittausepävarmuudet ovat saatavilla pyydettyessä. Mittausepävarmuutta ei ole huomioitu lausunnossa verrattaessa tuloksia laatuvaatimuksiin.


TUTKIMUSTODISTUS

7(8)

Tilaus: 2207691
Pvm: 3.1.2023

Turun Seudun Energiantuotanto Oy
Satu Viranko
Satamatie 16
21100 Naantali



Lausunto Näyttemateriaali ei täytä hyötykäyttökelpoisuuden vaatimuksia missään maanrakentamiskohteessa näytteen liukoisen kloridipitoisuuden vuoksi. Lisäksi näytteen liukoiset kromi-, molybdeeni- ja sulfaattipitoisuudet ylittävät tietyille maanrakentamiskohteille asetetut raja-arvot. (VNa 843/2017)

Valtioneuvoston asetuksessa 843/2017 kloridille, sulfaatille ja fluoridille asetettuja raja-arvoja ei sovelleta rakenteeseen, joka täyttää kaikki seuraavat edellytykset: sijaitsee enintään 500 m etäisyydellä merestä, rakenteen läpi suotautuvan veden purkautumissuunta on mereen sekä rakenteen ja meren välillä ei ole talousvedenottoon käytettäviä kaivoja (VNa 843/2017).

Lopullisen päätöksen jätteiden hyödyntämisestä maanrakentamisessa tekee paikallinen ympäristöviranomaisen.

Näyttemateriaalia ei voida liukoisuustestin tulosten perusteella tehtyjen määritysten osalta loppusijoittaa vaarattoman jätteen kaatopaikalle sen liukoisen kloridipitoisuuden ja liuenneiden aineiden kokonaismäärän (TDS) vuoksi (VNa 331/2013).

Näyttemateriaali voidaan liukoisuustestin tulosten perusteella tehtyjen määritysten osalta loppusijoittaa vaarallisen jätteen kaatopaikalle (VNa 331/2013).

Näytteen ANC on kohtalainen.

Lausunto perustuu lainsäädännön (VNa 331/2013) raja-arvoihin ja tehtyihin määrittelyihin eikä siinä oteta huomioon näyttemateriaalin jäteluokitusta. Ympäristöviranomaisen tekee lopullisen päätöksen näyttemateriaalin loppusijoittamisesta.

Raportilla näkyvissä olevat raja-arvot: vaarallisen jätteen kaatopaikka (VNa 331/2013).

SGS Finland Oy

Anu Villberg
Kemisti

Tämä tutkimustodistus on allekirjoitettu sähköisesti.

Tuloksia koskevat tiedustelut

Elintarvikkeet, rehut,
maanparannusaineet ja
vedet

Eeva Luoma, Laatuspäälikkö, puh. +358 50 464 7567,
eeva.luoma@sgs.com

*Akkreditoitu menetelmä. Akkreditointi ei koske lausuntoa. Tulokset pätevät vain testatuille näytteille. Raporttia ei saa kopioida osittain ilman testauslaboratorion lupaa. Analyysien mittauspävarmuudet ovat saatavilla pyydettäessä. Mittauspävarmuutta ei ole huomioitu lausunnossa verrattaessa tuloksia laatuvaatimuksiin.

**TUTKIMUSTODISTUS**

8(8)

Tilaus: 2207691

Pvm: 3.1.2023

Turun Seudun Energiantuotanto Oy
 Satu Viranko
 Satamatie 16
 21100 Naantali



Metallianalytiikka	Anu Villberg, Kemisti, puh. +358 43 850 1146, anu.villberg@sgs.com
Ympäristöanalytiikka	Ellinora Koskinen, Chemist, +358 9 225 286 20, ellinora.koskinen@sgs.com

Lisätiedot Hiilivetytulosten mittausepävarmuus:
 >C10-C21, >C21-<C40 ja >C10-<C40: 50-300 mg/kg ± 35 %, 300-1000 mg/kg ± 18 %, yli
 1000 mg/kg ± 13 %.

PAH-yhdisteiden mittausepävarmuus: 0,05-0,5 mg/kg ± 39 %, 0,5-2,0 mg/kg ± 33 % ja yli 2,0
 mg/kg ± 20 %.

Yksittäisten PCB-yhdisteiden mittausepävarmuus on ± 50 %.

Yksittäisten bensiinihiilivetyjen (BTEX) mittausepävarmuus: 0,01-0,05 mg/kg ± 50 %, 0,051-
 0,5 mg/kg ± 30 %, yli 0,51 mg/kg ± 20 %.

Liukoisten metallien analyysien (ICP-MS) epävarmuusarvio: < 0,5 mg/kg ± 50 %, 0,5–5
 mg/kg ± 20 % ja yli 5 mg/kg ± 10 %.

DOC- ja TOC-määritysten mittausepävarmuus on ± 20 %.

Kuiva-ainemäärityksen mittausepävarmuus on $\pm 1,9$ suht.-%.

IC-määritysten mittausepävarmuudet ovat: Fluoridi: ± 50 %, kloridi: ± 25 %, sulfaatti: ± 25 %.

Laboratoriot

7 SGS Finland Oy, Kotka (akkreditoitu testauslaboratorio T156, akkreditointivaatimus SFS-
 EN ISO/IEC 17025)

Jakelu satu.viranko@turkuenergia.fi

Laskutus Turun Seudun Energiantuotanto Oy, Satamatie 16, 21100 Naantali

Yritys on antanut tämän dokumentin palvelujen yleisten toimitusehtojensa mukaisesti, jotka ovat saatavilla osoitteessa
<https://www.sgs.com/en/terms-and-conditions>. Toimitusehdot sisältävät rajoituksia yrityksen vahingonkorvausvastuuseen, hyvityksiin
 ja lain valintaan. Tämän dokumentin haltijan tulee huomioida, että informaatio tässä dokumentissa kuvaa tilanteen sellaisena kuin
 yhtiö on sen työsuorituksensa aikana todennut asiakkaan mahdollisten ohjeiden mukaisesti. Yrityksen vastuu rajoittuu yrityksen
 asiakkaaseen eikä tämä dokumentti estä kaupan osapuolia käyttämästä kaupan asiakirjojen mukaisia oikeuksia ja velvoitteita. Tämän
 dokumentin sisällön tai ulkomuodon luvaton muuttaminen, väärentäminen tai vääristely on lainvastaista ja tekijä voidaan asettaa
 syytteeseen lain ankarimman tulkinnan mukaisesti.

*Akkreditoitu menetelmä. Akkreditointi ei koske lausuntoa. Tulokset pätevät vain testatuille näytteille. Raporttia ei saa kopioida osittain ilman
 testauslaboratorion lupaa. Analyysien mittausepävarmuudet ovat saatavilla pyydettyessä. Mittausepävarmuutta ei ole huomioitu
 lausunnoissa verrattaessa tuloksia laatuvaatimuksiin.



Tutkimusno EUFI05-00012935
 Asiakasno YB0001291
 4503306666

Stora Enso Oyj / Varkaus
 Susanna Kiiskinen
 PL 169
 78201 VARKAUS
 FINLAND
 s-posti: susanna.kiiskinen@storaenso.com

Tilauksen kuvaus

Stora Enso Varkaus, tuhkan kaatopaikkakelpoisuus

Näyttenumero	693-2022-00006685
Näytteen nimi	K6 Lentotuhka 7-14.2.2022
Näytteen kuvaus	Tuhka
Matriisi	Tuhka
Näytteenottopäivä	
Vastaanottopäivä	21.02.2022
Analysointi aloitettu	21.02.2022
Näytteenottaja	Asiakas

Analyytit	Testikoodi	Yksikkö	Tulokset
Fysikaalis-kemialliset tutkimukset			
Kuiva-ainepitoisuus	YBC15	%	99,6
Hekikutushäviö (550 °C)YBC11		% ka	5,5
Orgaaninen kokonaishiiliYBB32 (TOC) *		% ka	4,4
pH 1:10	YBC07		12,5
ANC, pH 12 +	YBC07	moles H+/kg ka	0,54
ANC, pH 11 +	YBC07	moles H+/kg ka	1,4
ANC, pH 10 +	YBC07	moles H+/kg ka	1,9
ANC, pH 9 +	YBC07	moles H+/kg ka	2,4
ANC, pH 8 +	YBC07	moles H+/kg ka	2,9
ANC, pH 7 +	YBC07	moles H+/kg ka	3,4
ANC, pH 6 +	YBC07	moles H+/kg ka	4,4
ANC, pH 5 +	YBC07	moles H+/kg ka	5,4
ANC, pH 4 +	YBC07	moles H+/kg ka	6,5
Kuiva-ainepitoisuus *	RZDRY	%	100
Alkuaineanalyysit			
Elohopea (Hg) *	YBHG1	mg/kg ka	0,73
Arseeni (As) *	YB15M	mg/kg ka	13
Barium (Ba)	YB15N	mg/kg ka	1200



Näyttenumero	693-2022-00006685
Näytteen nimi	K8 Lentotuhka
Näytteen kuvaus	7-14.2.2022 Tuhka
Matriisi	Tuhka
Näytteenottopäivä	
Vastaanottopäivä	21.02.2022
Analysointi aloitettu	21.02.2022
Näytteenottaja	Asiakas

Analysit	Testikoodi	Yksikkö	Tulokset
Alkuaineanalyytit			
Lyijy (Pb) *	YB15P	mg/kg ka	160
Kromi (Cr) *	YB15Q	mg/kg ka	76
Nikkeli (Ni) *	YB15S	mg/kg ka	51
Antimoni (Sb)	YB15U	mg/kg ka	23
Kadmium (Cd) *	YB15W	mg/kg ka	6,1
Koboltti (Co)	YB15Z	mg/kg ka	17
Molybdeeni (Mo)	YB161	mg/kg ka	11
Vanadiini (V)	YB165	mg/kg ka	59
Kupari (Cu) *	YB167	mg/kg ka	180
Sinkki (Zn) *	YB16F	mg/kg ka	1100
Mikroaaltohajotus	YBE30		tehty
PAH			
Asenafteni *	RZP34	mg/kg ka	<0,01
Asenaftyleeni *	RZP34	mg/kg ka	0,070
Antraseeni *	RZP34	mg/kg ka	0,013
Bentso(a)antraseeni *	RZP34	mg/kg ka	0,014
Bentso(b)fluoranteeni *	RZP34	mg/kg ka	0,057
Bentso(k)fluoranteeni *	RZP34	mg/kg ka	0,011
Bentso(a)pyreeni *	RZP34	mg/kg ka	<0,01
Bentso(g,h,i)peryleeni *	RZP34	mg/kg ka	<0,01
Dibentso(a,h)antraseeni *	RZP34	mg/kg ka	<0,01
Fenantreeni *	RZP34	mg/kg ka	0,89
Fluoreeni *	RZP34	mg/kg ka	<0,01
Fluoranteeni *	RZP34	mg/kg ka	0,40
Kryseeni *	RZP34	mg/kg ka	0,054
Indeno(1,2,3-cd)pyreeni *	RZP34	mg/kg ka	<0,01
Naftaleeni *	RZP34	mg/kg ka	1,5
Pyreeni *	RZP34	mg/kg ka	0,068
Summa 16 EPA-PAH (upper bound) *	RZP34	mg/kg ka	3,2
L/S2, 2-valih rav.testi SFS-EN 12457-3			



Näyttenumero	693-2022-00006685
Näytteen nimi	K6 Lentotuhka
Näytteen kuvaus	7-14.2.2022 Tuhka
Matriisi	Tuhka
Näytteenottopäivä	
Vastaanottopäivä	21.02.2022
Analysointi aloitettu	21.02.2022
Näytteenottaja	Asiakas

Analyytit	Testikoodi	Yksikkö	Tulokset
L/S2, 2-vaih rav.testi SFS-EN 12457-3			
pH L/S=2 *	YBJ21		12,7
Sähkönjohtavuus L/S=2YBJ31		mS/m	2200
Arseeni (As) L/S=2 *	YB0GQ	mg/kg ka	<0,002
Barium (Ba) L/S=2 *	YB0GR	mg/kg ka	0,86
Kadmium (Cd) L/S=2 *	YB0H1	mg/kg ka	<0,001
Kromi (Cr) L/S=2 *	YB0GT	mg/kg ka	0,19
Kupari (Cu) L/S=2 *	YB0H3	mg/kg ka	0,019
Elohopea (Hg) L/S=2 *	YB0H0	mg/kg ka	<0,001
Molybdeeni (Mo) L/S=2 *	YB0H4	mg/kg ka	2,7
Nikkeli (Ni) L/S=2 *	YB0GU	mg/kg ka	<0,002
Lyijy (Pb) L/S=2 *	YB0GS	mg/kg ka	0,021
Antimoni (Sb) L/S=2 *	YB0GY	mg/kg ka	<0,002
Seleeni (Se) L/S=2 *	YB0H6	mg/kg ka	0,075
Vanadiini (V) L/S=2 *	YB0GV	mg/kg ka	<0,002
Sinkki (Zn) L/S=2 *	YB0HB	mg/kg ka	0,25
Kloridi L/S=2 *	YB0QB	mg/kg ka	3900
Fluoridi L/S=2 *	YB0QC	mg/kg ka	5,6
Sulfaatti L/S=2 *	YB0QA	mg/kg ka	7800
DOC L/S=2 *	YBJ01	mg/kg ka	21
TDS L/S=2 *	YBJ41	mg/kg ka	20000
L/S10 kum., 2-vaih. rav.testi SFS-EN 12457-3			
pH L/S=8 *	YBJ22		12,6
Sähkönjohtavuus L/S=8YBJ32		mS/m	990
Arseeni (As) L/S=10 (Kum.) *	YB0NH	mg/kg ka	<0,01
Barium (Ba) L/S=10 (Kum.) *	YB0NI	mg/kg ka	2,7
Kadmium (Cd) L/S=10 (Kum.) *	YB0NQ	mg/kg ka	<0,005
Kromi (Cr) L/S=10 (Kum.) *	YB0NJ	mg/kg ka	1,2
Kupari (Cu) L/S=10 (Kum.) *	YB0P0	mg/kg ka	<0,05



Tutkimustodistus AR-22-YB-009512-01
Päivämäärä 16.03.2022

Sivu 4/11

Näyttenumero	693-2022-00006685
Näytteen nimi	K6 Lentotuhka
Näytteen kuvaus	7-14.2.2022 Tuhka
Matriisi	Tuhka
Näytteenottopäivä	
Vastaanottopäivä	21.02.2022
Analysointi aloitettu	21.02.2022
Näytteenottaja	Asiakas

Analyytit	Testikoodi	Yksikkö	Tulokset
L/S10 kum., 2-vaih. rav.testi SFS-EN 12457-3			
Elohopea (Hg) L/S=10 (Kum.) *	YB0NP	mg/kg ka	<0,004
Molybdeeni (Mo) L/S=10 (Kum.) *	YB0NS	mg/kg ka	5,5
Nikkeli (Ni) L/S=10 (Kum.) *	YB0NL	mg/kg ka	<0,01
Lyijy (Pb) L/S=10 (Kum.) *	YB0NK	mg/kg ka	0,24
Antimoni (Sb) L/S=10 (Kum.) *	YB0NN	mg/kg ka	<0,01
Seleen (Se) L/S=10 (Kum.) *	YB0NT	mg/kg ka	0,18
Vanadiini (V) L/S=10 (Kum.) *	YB0NM	mg/kg ka	0,014
Sinkki (Zn) L/S=10 (Kum.) *	YB0P3	mg/kg ka	0,55
Kloridi L/S=10 (Kum.) *	YB0QE	mg/kg ka	4800
Fluoridi L/S=10 (Kum.) *	YB0QF	mg/kg ka	19
Sulfaatti L/S=10 (Kum.) *	YB0QD	mg/kg ka	28000
DOC L/S=10 (Kum.) *	YBJ02	mg/kg ka	67
TDS L/S=10 (Kum.) *	YBJ42	mg/kg ka	54000
PCDD/F -yhdisteet			
2,3,7,8-TetraCDD *	RZP39	pg/g ka	1,2
1,2,3,7,8-PentaCDD *	RZP39	pg/g ka	2,6
1,2,3,4,7,8-HeksaCDD *	RZP39	pg/g ka	<2
1,2,3,6,7,8-HeksaCDD *	RZP39	pg/g ka	<2
1,2,3,7,8,9-HeksaCDD *	RZP39	pg/g ka	<2
1,2,3,4,6,7,8-HeptaCDD *	RZP39	pg/g ka	<4
OktaCDD *	RZP39	pg/g ka	<5
2,3,7,8-TetraCDF *	RZP39	pg/g ka	18
1,2,3,7,8-PentaCDF *	RZP39	pg/g ka	3,2
2,3,4,7,8-PentaCDF *	RZP39	pg/g ka	2,8
1,2,3,4,7,8-HeksaCDF *	RZP39	pg/g ka	<2
1,2,3,6,7,8-HeksaCDF *	RZP39	pg/g ka	<2
2,3,4,6,7,8-HeksaCDF *	RZP39	pg/g ka	<2
1,2,3,7,8,9-HeksaCDF *	RZP39	pg/g ka	<2



Tutkimustodistus AR-22-YB-009512-01
Päivämäärä 16.03.2022

Sivu 5/11

Näyttenumero	693-2022-00006685
Näytteen nimi	K6 Lentotuhka
Näytteen kuvaus	7-14.2.2022 Tuhka
Matriisi	Tuhka
Näytteenottopäivä	
Vastaanottopäivä	21.02.2022
Analysointi aloitettu	21.02.2022
Näytteenottaja	Asiakas

Analyytit	Testikoodi	Yksikkö	Tulokset
PCDD/F -yhdisteet			
1,2,3,4,6,7,8-HeptaCDFRZP39 *		pg/g ka	<2
1,2,3,4,7,8,9-HeptaCDFRZP39 *		pg/g ka	<2
OktaCDF *	RZP39	pg/g ka	<5
I-TEQ (NATO/CCMS) alaraja *	RZP39	mg/kg ka	0,0000060
I-TEQ (NATO/CCMS) sis. 1/2 LOQ *	RZP39	mg/kg ka	0,0000067
I-TEQ (NATO/CCMS) yläraja *	RZP39	mg/kg ka	0,0000074
WHO 1998-PCDD/F TEQ alaraja *	RZP39	mg/kg ka	0,0000073
WHO(1998)-PCDD/F TEQ incl. 1/2 LOQ *	RZP39	mg/kg ka	0,0000080
WHO 1998-PCDD/F TEQ yläraja *	RZP39	mg/kg ka	0,0000087
WHO(2005)-PCDD/F TEQ alaraja *	RZP39	mg/kg ka	0,0000067
WHO(2005)-PCDD/F TEQ sis. 1/2 LOQ *	RZP39	mg/kg ka	0,0000074
WHO(2005)-PCDD/F TEQ yläraja *	RZP39	mg/kg ka	0,0000081
PCB 77 *	RZP38	pg/g ka	9,0
PCB 81 *	RZP38	pg/g ka	<4
PCB 105 *	RZP38	pg/g ka	5,1
PCB 114 *	RZP38	pg/g ka	<4
PCB 118 *	RZP38	pg/g ka	13
PCB 123 *	RZP38	pg/g ka	<4
PCB 126 *	RZP38	pg/g ka	<4
PCB 156 *	RZP38	pg/g ka	<4
PCB 157 *	RZP38	pg/g ka	<4
PCB 167 *	RZP38	pg/g ka	<4
PCB 169 *	RZP38	pg/g ka	<4
PCB 189 *	RZP38	pg/g ka	<4
WHO(2005)-PCB TEQ alaraja *	RZP38	mg/kg ka	0,0000000 14
WHO(2005)-PCB TEQ sis. 1/2 LOQ *	RZP38	mg/kg ka	0,0000026



Näyttenumero	693-2022-00006685
Näytteen nimi	K6 Lentotuhka
Näytteen kuvaus	7-14.2.2022 Tuhka
Matriisi	Tuhka
Näytteenottopäivä	
Vastaanottopäivä	21.02.2022
Analysointi aloitettu	21.02.2022
Näytteenottaja	Asiakas

Analyysit	Testikoodi	Yksikkö	Tulokset
PCDD/F -yhdisteet			
WHO(2005)-PCB TEQ yläraja *	RZP38	mg/kg ka	0,0000052

*Menetelmä on akkreditoitu.

Kommentti

Näyttemäärä 6,6 kg

ALLEKIRJOITUS

16.03.2022



Hanne Korva, Analyysipalvelupäällikkö

HanneKorva@eurofins.fi +358 406784084

Tutkimustodistus on sähköisesti hyväksytty.



Menetelmätiedot

Testikoodi	Parametrin nimi	Menetelmän mittauserävarmuus	Menetelmän määrittäysraja	Akkreditoitu	Menetelmä	Laboratorio
Fysikaalis-kemialliset tutkimukset						
YBC15	Kuiva-ainepitoisuus	<25:±0.5%yks. >25:±2%	0,2	Ei	SFS-EN 15934:2012	YB
YBC11	Hehkutushäviö (550 °C)	<4:±0.2%yks.ka >4:±5%	0,2	Ei	SFS-EN 15169:2007	YB
YBB32	Orgaaninen kokonaishili (TOC)	<1.5:±0.3%yks.ka >1.3:±20%	0,5	Kyllä	SFS-EN 13137:2001	YB
YBC07	pH 1:10	± 0.3 pH yks.		Ei	CEN/TS 15364:2006	YB
YBC07	ANC, pH 12 +	± 20%	0,01	Ei	CEN/TS 15364:2006	YB
YBC07	ANC, pH 11 +	± 20%	0,01	Ei	CEN/TS 15364:2006	YB
YBC07	ANC, pH 10 +	± 20%	0,01	Ei	CEN/TS 15364:2006	YB
YBC07	ANC, pH 9 +	± 20%	0,01	Ei	CEN/TS 15364:2006	YB
YBC07	ANC, pH 8 +	± 20%	0,01	Ei	CEN/TS 15364:2006	YB
YBC07	ANC, pH 7 +	± 20%	0,01	Ei	CEN/TS 15364:2006	YB
YBC07	ANC, pH 6 +	± 20%	0,01	Ei	CEN/TS 15364:2006	YB
YBC07	ANC, pH 5 +	± 20%	0,01	Ei	CEN/TS 15364:2006	YB
YBC07	ANC, pH 4 +	± 20%	0,01	Ei	CEN/TS 15364:2006	YB
RZDRY	Kuiva-ainepitoisuus	5%(<30%) 1,5%(>30%)	3	Kyllä	SFS 3008; SFS-ISO 11465; SFS-EN 15934	RZ
Alkuaineanalyysit						
YBHG1	Elohopea (Hg)	<0.2:±0.03mg/kgka >0.2:±15%	0,04	Kyllä	EPA 3051A; SFS-ISO 16772:en (2007)	YB
YB15M	Arseeni (As)	<10:±1.5mg/kgka >10:±15%	3	Kyllä	EPA 3051A; SFS-EN ISO 11885:2009	YB
YB15N	Barium (Ba)	<5:±0.75mg/kgka >5:±15%	1	Ei	EPA 3051A; SFS-EN ISO 11885:2009	YB
YB15P	Lyijy (Pb)	<10:±1.6mg/kgka >10:±16%	2	Kyllä	EPA 3051A; SFS-EN ISO 11885:2009	YB
YB15Q	Kromi (Cr)	<8.5:±1.5mg/kgka >8.5:±18%	2	Kyllä	EPA 3051A; SFS-EN ISO 11885:2009	YB
YB15S	Nikkeli (Ni)	<5:±0.9mg/kgka >5:±18%	1	Kyllä	EPA 3051A; SFS-EN ISO 11885:2009	YB
YB15U	Antimoni (Sb)	<10:±2.0mg/kgka >10:±20%	2	Ei	EPA 3051A; SFS-EN ISO 11885:2009	YB
YB15W	Kadmium (Cd)	<1.4:±0.20mg/kgka >1.4:±14%	0,3	Kyllä	EPA 3051A; SFS-EN ISO 11885:2009	YB
YB15Z	Koboltti (Co)	<6:±0.9mg/kgka >6:±15%	1	Ei	EPA 3051A; SFS-EN ISO 11885:2009	YB
YB161	Molybdeeni (Mo)	<5:±0.9mg/kgka >5:±18%	1	Ei	EPA 3051A; SFS-EN ISO 11885:2009	YB
YB165	Vanadiini (V)	<10:±1.7mg/kgka >10:±17%	2	Ei	EPA 3051A; SFS-EN ISO 11885:2009	YB
YB167	Kupari (Cu)	<10:±1.6mg/kgka >10:±16%	2	Kyllä	EPA 3051A; SFS-EN ISO 11885:2009	YB
YB16F	Sinkki (Zn)	<12:±2.0mg/kgka >12:±17%	3	Kyllä	EPA 3051A; SFS-EN ISO 11885:2009	YB
YBE30	Mikroaaltohajotus			Ei	EPA 3051A	YB
PAH						
RZP34	Asenafteeni	38%	0,01	Kyllä	SFS-EN 15527	RZ



PAH						
RZP34	Asenaityfeeni	30%	0,01	Kyllä	SFS-EN 15527	RZ
RZP34	Antraseeni	25%	0,01	Kyllä	SFS-EN 15527	RZ
RZP34	Bentso(a)antraseeni	18%	0,01	Kyllä	SFS-EN 15527	RZ
RZP34	Bentso(b)fluoranteeni	34%	0,01	Kyllä	SFS-EN 15527	RZ
RZP34	Bentso(k)fluoranteeni	41%	0,01	Kyllä	SFS-EN 15527	RZ
RZP34	Bentso(a)pyreeni	27%	0,01	Kyllä	SFS-EN 15527	RZ
RZP34	Bentso(g,h,i)peryleneeni	32%	0,01	Kyllä	SFS-EN 15527	RZ
RZP34	Dibentso(a,h)antraseeni	27%	0,01	Kyllä	SFS-EN 15527	RZ
RZP34	Fenanitreeni	27%	0,01	Kyllä	SFS-EN 15527	RZ
RZP34	Fluoreeni	23%	0,01	Kyllä	SFS-EN 15527	RZ
RZP34	Fluoranteeni	23%	0,01	Kyllä	SFS-EN 15527	RZ
RZP34	Kryseeni	42%	0,01	Kyllä	SFS-EN 15527	RZ
RZP34	Indeno(1,2,3-cd)pyreeni	22%	0,01	Kyllä	SFS-EN 15527	RZ
RZP34	Naftaleeni	35%	0,01	Kyllä	SFS-EN 15527	RZ
RZP34	Pyreeni	24%	0,01	Kyllä	SFS-EN 15527	RZ
RZP34	Summa 16 EPA-PAH (upper bound)		0,16	Kyllä	SFS-EN 15527	RZ
L/S2, 2-valh rav.testi SFS-EN 12457-3						
YBJ21	pH L/S=2	± 0.3 pH yks.		Kyllä	SFS-EN ISO 10523:2012.	YB
YBJ31	Sähköjohtavuus L/S=2	<15:±3mS/m >15:±20%	5	Kyllä	SFS-EN 27888:1994	YB
YB0GQ	Arseeni (As) L/S=2	<0.01:±0.002mg/kgka >0.01:±20%	0,002	Kyllä	SFS-EN ISO 17294-2:2016; SFS-EN 12457-3:02	YB
YB0GR	Barium (Ba) L/S=2	<0.065:±0.01mg/kgka >0.065:±15%	0,01	Kyllä	SFS-EN ISO 17294-2:2016; SFS-EN 12457-3:02	YB
YB0H1	Kadmium (Cd) L/S=2	<0.007:±0.001mg/kgka >0.007:±14%	0,001	Kyllä	SFS-EN ISO 17294-2:2016; SFS-EN 12457-3:02	YB
YB0GT	Kromi (Cr) L/S=2	<0.013:±0.002mg/kgka >0.013:±15%	0,002	Kyllä	SFS-EN ISO 17294-2:2016; SFS-EN 12457-3:02	YB
YB0H3	Kupari (Cu) L/S=2	<0.05:±0.01mg/kgka >0.05:±20%	0,01	Kyllä	SFS-EN ISO 17294-2:2016; SFS-EN 12457-3:02	YB
YB0H0	Elohopea (Hg) L/S=2	<0.006:±0.001mg/kgka >0.006:±17%	0,001	Kyllä	SFS-EN ISO 17294-2:2016; SFS-EN 12457-3:02	YB
YB0H4	Molybdeeni (Mo) L/S=2	<0.013:±0.002mg/kgka >0.013:±15%	0,002	Kyllä	SFS-EN ISO 17294-2:2016; SFS-EN 12457-3:02	YB
YB0GU	Nikkeli (Ni) L/S=2	<0.013:±0.002mg/kgka >0.013:±15%	0,002	Kyllä	SFS-EN ISO 17294-2:2016; SFS-EN 12457-3:02	YB
YB0GS	Lyijy (Pb) L/S=2	<0.005:±0.001mg/kgka >0.005:±20%	0,001	Kyllä	SFS-EN ISO 17294-2:2016; SFS-EN 12457-3:02	YB
YB0GY	Antimoni (Sb) L/S=2	<0.01:±0.002mg/kgka >0.01:±20%	0,002	Kyllä	SFS-EN ISO 17294-2:2016; SFS-EN 12457-3:02	YB
YB0H6	Seleeni (Se) L/S=2	<0.056:±0.01mg/kgka >0.056:±18%	0,01	Kyllä	SFS-EN ISO 17294-2:2016; SFS-EN 12457-3:02	YB
YB0GV	Vanadiini (V) L/S=2	<0.013:±0.002mg/kgka >0.013:±15%	0,002	Kyllä	SFS-EN ISO 17294-2:2016; SFS-EN 12457-3:02	YB
YB0HB	Sinkki (Zn) L/S=2	<0.05:±0.01mg/kgka >0.05:±20%	0,01	Kyllä	SFS-EN ISO 17294-2:2016; SFS-EN 12457-3:02	YB
YB0QB	Kloridi L/S=2	<75:±9mg/kgka >75:±12%	10	Kyllä	SFS-EN ISO 10304-1:2009	YB
YB0QC	Fluoridi L/S=2	<5:±0.75mg/kgka >5:±15%	1	Kyllä	SFS-EN ISO 10304-1:2009	YB



L/S2, 2-vaih rav.testi SFS-EN 12457-3						
YB0QA	Sulfaatti L/S=2	<75:±9mg/kgka >75:±12%	10	Kyllä	SFS-EN ISO 10304-1:2009	YB
YBJ01	DOC L/S=2	<50:±8mg/kgka >50:±16%	10	Kyllä	SFS-EN 1484:1997	YB
YBJ41	TDS L/S=2	± 13%	250	Kyllä	SFS-EN 15216:2008	YB
L/S10 kum., 2-vaih. rav.testi SFS-EN 12457-3						
YBJ22	pH L/S=8	± 0.3 pH yks.		Kyllä	SFS-EN ISO 10523:2012.	YB
YBJ32	Sähkönjohtavuus L/S=8	<15:±3mS/m >15:±20%	5	Kyllä	SFS-EN 27888:1994	YB
YB0NH	Arseeni (As) L/S=10 (Kum.)	<0.05:±0.01mg/kgka >0.05:±20%	0,01	Kyllä	SFS-EN ISO 17294-2:2016; SFS-EN 12457-3:02	YB
YB0NI	Barium (Ba) L/S=10 (Kum.)	<0.25:±0.05mg/kgka >0.25:±20%	0,05	Kyllä	SFS-EN ISO 17294-2:2016; SFS-EN 12457-3:02	YB
YB0NQ	Kadmium (Cd) L/S=10 (Kum.)	<0.025:±0.005mg/kgka >0.025:±20%	0,005	Kyllä	SFS-EN ISO 17294-2:2016; SFS-EN 12457-3:02	YB
YB0NJ	Kromi (Cr) L/S=10 (Kum.)	<0.05:±0.01mg/kgka >0.05:±20%	0,01	Kyllä	SFS-EN ISO 17294-2:2016; SFS-EN 12457-3:02	YB
YB0P0	Kupari (Cu) L/S=10 (Kum.)	<0.23:±0.05mg/kgka >0.23:±22%	0,05	Kyllä	SFS-EN ISO 17294-2:2016; SFS-EN 12457-3:02	YB
YB0NP	Elohopea (Hg) L/S=10 (Kum.)	<0.02:±0.004mg/kgka >0.02:±20%	0,004	Kyllä	SFS-EN ISO 17294-2:2016; SFS-EN 12457-3:02	YB
YB0NS	Molybdeeni (Mo) L/S=10 (Kum.)	<0.062:±0.01mg/kgka >0.062:±16%	0,01	Kyllä	SFS-EN ISO 17294-2:2016; SFS-EN 12457-3:02	YB
YB0NL	Nikkeli (Ni) L/S=10 (Kum.)	<0.056:±0.01mg/kgka >0.056:±18%	0,01	Kyllä	SFS-EN ISO 17294-2:2016; SFS-EN 12457-3:02	YB
YB0NK	Lyijy (Pb) L/S=10 (Kum.)	<0.025:±0.005mg/kgka >0.025:±20%	0,005	Kyllä	SFS-EN ISO 17294-2:2016; SFS-EN 12457-3:02	YB
YB0NN	Antimoni (Sb) L/S=10 (Kum.)	<0.05:±0.01mg/kgka >0.05:±20%	0,01	Kyllä	SFS-EN ISO 17294-2:2016; SFS-EN 12457-3:02	YB
YB0NT	Seleeni (Se) L/S=10 (Kum.)	<0.2:±0.04mg/kgka >0.2:±20%	0,04	Kyllä	SFS-EN ISO 17294-2:2016; SFS-EN 12457-3:02	YB
YB0NM	Vanadiini (V) L/S=10 (Kum.)	<0.067:±0.01mg/kgka >0.067:±15%	0,01	Kyllä	SFS-EN ISO 17294-2:2016; SFS-EN 12457-3:02	YB
YB0P3	Sinkki (Zn) L/S=10 (Kum.)	<0.25:±0.05mg/kgka >0.25:±20%	0,05	Kyllä	SFS-EN ISO 17294-2:2016; SFS-EN 12457-3:02	YB
YB0QE	Kloridi L/S=10 (Kum.)	<300:±45mg/kgka >300:±15%	50	Kyllä	SFS-EN ISO 10304-1:2009	YB
YB0QF	Fluoridi L/S=10 (Kum.)	<20:±4mg/kgka >20:±20%	5	Kyllä	SFS-EN ISO 10304-1:2009	YB
YB0QD	Sulfaatti L/S=10 (Kum.)	<300:±45mg/kgka >300:±15%	50	Kyllä	SFS-EN ISO 10304-1:2009	YB
YBJ02	DOC L/S=10 (Kum.)	<200:±40mg/kgka >200:±20%	50	Kyllä	SFS-EN 1484:1997	YB
YBJ42	TDS L/S=10 (Kum.)	± 14%	1250	Kyllä	SFS-EN 15216:2008	YB
PCDD/F -yhdisteet						
RZP39	2,3,7,8-TetraCDD	35%	1	Kyllä	EPA 1613; SFS-ISO 13914; SFS-EN 16190	RZ
RZP39	1,2,3,7,8-PentaCDD	35%	2	Kyllä	EPA 1613; SFS-ISO 13914; SFS-EN 16190	RZ
RZP39	1,2,3,4,7,8-HeksaCDD	35%	2	Kyllä	EPA 1613; SFS-ISO 13914; SFS-EN 16190	RZ
RZP39	1,2,3,6,7,8-HeksaCDD	35%	2	Kyllä	EPA 1613; SFS-ISO 13914; SFS-EN 16190	RZ
RZP39	1,2,3,7,8,9-HeksaCDD	35%	2	Kyllä	EPA 1613; SFS-ISO 13914; SFS-EN 16190	RZ



PCDD/F -yhdisteet						
RZP39	1,2,3,4,6,7,8-HeptaCDD	35%	4	Kyllä	EPA 1613; SFS-ISO 13914; SFS-EN 16190	RZ
RZP39	OktaCDD	35%	8	Kyllä	EPA 1613; SFS-ISO 13914; SFS-EN 16190	RZ
RZP39	2,3,7,8-TetraCDF	35%	1	Kyllä	EPA 1613; SFS-ISO 13914; SFS-EN 16190	RZ
RZP39	1,2,3,7,8-PentaCDF	35%	2	Kyllä	EPA 1613; SFS-ISO 13914; SFS-EN 16190	RZ
RZP39	2,3,4,7,8-PentaCDF	35%	2	Kyllä	EPA 1613; SFS-ISO 13914; SFS-EN 16190	RZ
RZP39	1,2,3,4,7,8-HeksaCDF	35%	2	Kyllä	EPA 1613; SFS-ISO 13914; SFS-EN 16190	RZ
RZP39	1,2,3,6,7,8-HeksaCDF	35%	2	Kyllä	EPA 1613; SFS-ISO 13914; SFS-EN 16190	RZ
RZP39	2,3,4,6,7,8-HeksaCDF	35%	2	Kyllä	EPA 1613; SFS-ISO 13914; SFS-EN 16190	RZ
RZP39	1,2,3,7,8,9-HeksaCDF	35%	2	Kyllä	EPA 1613; SFS-ISO 13914; SFS-EN 16190	RZ
RZP39	1,2,3,4,6,7,8-HeptaCDF	35%	4	Kyllä	EPA 1613; SFS-ISO 13914; SFS-EN 16190	RZ
RZP39	1,2,3,4,7,8,9-HeptaCDF	35%	4	Kyllä	EPA 1613; SFS-ISO 13914; SFS-EN 16190	RZ
RZP39	OktaCDF	35%	8	Kyllä	EPA 1613; SFS-ISO 13914; SFS-EN 16190	RZ
RZP39	I-TEQ (NATO/CCMS) alaraja			Kyllä	EPA 1613; SFS-ISO 13914; SFS-EN 16190	RZ
RZP39	I-TEQ (NATO/CCMS) sis. 1/2 LOQ		0,0000021	Kyllä	EPA 1613; SFS-ISO 13914; SFS-EN 16190	RZ
RZP39	I-TEQ (NATO/CCMS) yläraja		0,0000041	Kyllä	EPA 1613; SFS-ISO 13914; SFS-EN 16190	RZ
RZP39	WHO 1998-PCDD/F TEQ alaraja			Kyllä	EPA 1613; SFS-ISO 13914; SFS-EN 16190	RZ
RZP39	WHO(1998)-PCDD/F TEQ incl. 1/2 LOQ		0,0000026	Kyllä	EPA 1613; SFS-ISO 13914; SFS-EN 16190	RZ
RZP39	WHO 1998-PCDD/F TEQ yläraja		0,0000051	Kyllä	EPA 1613; SFS-ISO 13914; SFS-EN 16190	RZ
RZP39	WHO(2005)-PCDD/F TEQ alaraja			Kyllä	EPA 1613; SFS-ISO 13914; SFS-EN 16190	RZ
RZP39	WHO(2005)-PCDD/F TEQ sis. 1/2 LOQ		0,0000023	Kyllä	EPA 1613; SFS-ISO 13914; SFS-EN 16190	RZ
RZP39	WHO(2005)-PCDD/F TEQ yläraja		0,0000047	Kyllä	EPA 1613; SFS-ISO 13914; SFS-EN 16190	RZ
RZP38	PCB 77	35%	4	Kyllä	EPA 1668; SFS-ISO 13914; SFS-EN 16190	RZ
RZP38	PCB 81	35%	4	Kyllä	EPA 1668; SFS-ISO 13914; SFS-EN 16190	RZ
RZP38	PCB 105	35%	4	Kyllä	EPA 1668; SFS-ISO 13914; SFS-EN 16190	RZ
RZP38	PCB 114	35%	4	Kyllä	EPA 1668; SFS-ISO 13914; SFS-EN 16190	RZ
RZP38	PCB 118	35%	4	Kyllä	EPA 1668; SFS-ISO 13914; SFS-EN 16190	RZ
RZP38	PCB 123	35%	4	Kyllä	EPA 1668; SFS-ISO 13914; SFS-EN 16190	RZ
RZP38	PCB 126	35%	4	Kyllä	EPA 1668; SFS-ISO 13914; SFS-EN 16190	RZ
RZP38	PCB 156	35%	4	Kyllä	EPA 1668; SFS-ISO 13914; SFS-EN 16190	RZ



PCDD/F -yhdisteet						
RZP38	PCB 157	35%	4	Kyllä	EPA 1668; SFS-ISO 13914; SFS-EN 16190	RZ
RZP38	PCB 167	35%	4	Kyllä	EPA 1668; SFS-ISO 13914; SFS-EN 16190	RZ
RZP38	PCB 169	35%	4	Kyllä	EPA 1668; SFS-ISO 13914; SFS-EN 16190	RZ
RZP38	PCB 189	35%	4	Kyllä	EPA 1668; SFS-ISO 13914; SFS-EN 16190	RZ
RZP38	WHO(2005)-PCB TEQ aliraja			Kyllä	EPA 1668; SFS-ISO 13914; SFS-EN 16190	RZ
RZP38	WHO(2005)-PCB TEQ sis. 1/2 LOG		0,00000026	Kyllä	EPA 1668; SFS-ISO 13914; SFS-EN 16190	RZ
RZP38	WHO(2005)-PCB TEQ yliraja		0,00000052	Kyllä	EPA 1668; SFS-ISO 13914; SFS-EN 16190	RZ

Laboratorio		
RZ	Eurofins Environment Testing Finland (Lahti)	SFS-EN ISO/IEC 17025:2017 FINAS T039
YB	Eurofins Ahma - Oulu	SFS-EN ISO/IEC 17025:2017 FINAS T131

Jakelu : FPPaivalab.varkaus@storaenso.com

Huomautukset

Tutkimustodistuksen osittainen kopioiminen on sallittu vain laboratorion kirjallisella luvalla. Testaustulokset koskevat vain vastaanotettua ja tutkittua näytettä. Mahdollinen lausunto ei kuulu akkreditoinnin piiriin.

QF 0-3 mm

